



# Cobalt catalyst supports for Fischer-Tropsch synthesis

FATIMA PARDO-TARIFA

Doctoral Thesis in Chemical Engineering  
KTH Royal Institute of Technology  
School of Chemical Science and Engineering  
Department of Chemical Engineering  
Stockholm, Sweden 2017

**Cobalt catalyst supports for Fischer-Tropsch synthesis**  
FATIMA PARDO-TARIFA

TRITA-CHE Report 2017:38

ISSN 1654-1081

ISBN 978-91-7729-548-8

Akademisk avhandling som med tillstånd av Kungliga Tekniska högskolan i Stockholm framlägges till offentlig granskning för avläggande av teknologie doktorsexamen, torsdagen den 26 oktober 2017 kl. 10:00 i sal L1, Drottning Kristinas väg 30, Kungliga Tekniska högskolan, Stockholm.

Fakultetsopponent: Professor Olga Guerrero, University of Málaga, Málaga, Spain.

© Fatima Pardo-Tarifa 2017

Tryck: Universitetservice US-AB

*To the authors that inspire me on the long road to freedom*

*(Violeta Parra, Mercedes Sosa, Nelson Mandela, Cat Stevens, Simone de Beauvoir,...)*

*Because to be free is not simply to get rid of the chains, but to live in a way  
that respects and increases the freedom of others and ourselves  
Because freedom, like any other virtue, does not exist in a vacuum,  
it must be worked and practiced to exist at all  
Because life is based in moments,  
and there is no time to make bad ones  
Because all that we have before dying,  
are memories of the good feelings  
For that and more, let's free our mind and heart,  
let's do all we can with our lives, because we just have this one,  
and is running, is running at high speed, and there is no time to wait until  
tomorrow, life is happening now, now while we are angry, sad  
and complaining about ourselves and others  
Let's just smile! Smile, because a smile has beauty,  
health, grace, is a dance,  
is a flower in a garden, is light, and is life... Give life!*

*Fatima Pardo-Tarifa*



## Abstract

In the Fischer-Tropsch (FT) synthesis, CO and H<sub>2</sub> (synthesis gas) are converted into hydrocarbons that can be further upgraded to high-quality fuels and chemicals. Different carbon sources such as natural gas, coal and biomass can be used as feed-stocks for the synthesis gas. In commercial applications, supported cobalt catalysts are commonly used in the Fischer-Tropsch synthesis, especially when the synthesis gas emanates from natural gas and when the desired final product is diesel. The activity and selectivity of a cobalt catalyst is dependent on several parameters, one of them being the support.

The present thesis is focused on the design, synthesis and characterization of alumina and silica materials with non-conventional morphology, and evaluation of their feasibility as cobalt supports in the FT synthesis. Nanoparticles of alumina and mesoporous silica have been synthesized by non-conventional techniques, i.e water-in-oil microemulsion and the atrane route. The effects of incorporating promoters, such as Ce and Zr, have also been studied.

Ce- and Zr-alumina nanoparticles were synthesized by coprecipitation in water-in-oil microemulsion are demonstrated. The obtained product is amorphous alumina with highly dispersed promoters, resulting in strong cobalt-support interactions and low cobalt reducibility. By increasing the calcination temperature of the Ce-promoted support, crystalline CeO<sub>2</sub> is obtained which apparently increases the cobalt reducibility and thereby the catalytic activity (per gram catalyst). The small pore size of the materials may induce diffusion limitations on the reactants arrival and/or result in very small cobalt particles, which favour methane over long-chain hydrocarbons.

Successful preparations of pore expanded mesoporous silicas with 1D, 2D and 3D pore structures via the atrane route, combined with the addition of swelling agents, at mild conditions have been demonstrated. The advantage of this method is that pore expansion can be achieved at mild conditions and there is no need for a post-synthesis process using an autoclave system.

In larger silica support pores, larger cobalt particles will be formed and the weaker the cobalt-support interactions will be. This generally results in a higher cobalt reducibility for larger-pore supports and thereby a higher catalytic activity. However, for 1D and 2D silica materials, also the pore length is an important parameter governing the catalytic performance as diffusion limitations on reactant arrival may be present at shorter diffusion distances than in materials with 3D porous structures.

**Keywords:** Silica, alumina, zirconium, cerium, mesoporous materials, nanoparticles, microemulsion, atrane route, cobalt catalyst, Fischer-Tropsch synthesis.

## Sammanfattning

Titel: Bärare för kobaltkatalysator i Fischer-Tropsch-syntes

I Fischer-Tropsch-reaktionen omvandlas CO och H<sub>2</sub> (syntesgas) till kolväten som kan uppgraderas till bränslen och kemikalier av hög kvalitet. Olika kolkällor såsom naturgas, kol eller biomassa kan användas som råvaror till syntesgasen. I industriell skala används vanligen koboltkatalysatorer i Fischer-Tropsch-reaktionen, speciellt om syntesgasen framställts från naturgas och när diesel är önskad slutprodukt. Koboltkatalysatorns aktivitet och selektivitet är beroende av många parametrar varav en är bärarmaterialet som kobolten är dispergerad över.

Denna avhandling beskriver design, tillverkning och karakterisering av material bestående av aluminium- eller kiseloxid med icke-konventionella strukturer, och utvärdering av deras lämplighet som bärarmaterial till koboltkatalysatorer i Fischer-Tropsch-reaktionen. Nanopartiklar av aluminiumoxid samt mesoporös kisel-dioxid har tillverkats med icke-konventionella tekniker (i mikroemulsion samt genom "the atrane route"). Effekterna av att inkludera promotorer såsom Ce och Zr har också studerats.

Nanopartiklar av aluminiumoxid promoterade med Ce eller Zr syntetiserades genom samutfällning i en "vatten-i-olja"-mikroemulsion demonstreras. De erhållna materialen består av amorf aluminiumoxid i vilken promotorn är väl dispergerad, vilket resulterar i en stark interaktion mellan kobolt och bärarmaterialen och därmed i en låg reducerbarhet av kobolten. Genom att öka kalcineringstemperaturen för det Ce-promoterade bärarmaterialet kristalliseras större partiklar av ceriumoxid ut. Detta leder till att koboltens reducerbarhet ökas och därmed även den katalytiska aktiviteten (räknat per gram katalysator). Bärarmaterialen har relativt små pordiametrar vilket kan leda till masstransportbegränsningar eller till väldigt små koboltpartiklar, vilket i sin tur resulterar i att metan favoriseras framför längre kolväten.

Porexpanderade mesoporösa kiseloxider med 1D-, 2D- och 3D-porstrukturer syntetiserades via "the atrane route". Denna tillverkningsprocess möjliggör porexpansion (genom tillsats av svällmedel)

vid milda betingelser och eliminerar behovet av en separat porexpansionsprocess i autoklav.

Ju större porerna i kiseloxidmaterialen är, desto större blir koboltpartiklarna i katalysatorn och desto svagare blir interaktionen mellan kobolt och bärrmaterial. Detta resulterar i en högre reducerbarhet av kobolten för bärrmaterial med större porer, och även i en högre katalytisk aktivitet. Dock bör beaktas att för kiseloxidmaterial med 1D- och 2D-porstrukturer så är även porlängden en viktig reglerparameter för den katalytiska aktiviteten och selektiviteten eftersom masstransportbegränsningar kan föreligga vid mycket kortare diffusionsavstånd än i material med 3D-struktur.

## Resumen

Título: Soportes de catalizadores de cobalto para la síntesis de Fischer-Tropsch

En la síntesis de Fischer-Tropsch (FT), CO y H<sub>2</sub> (gas de síntesis) se convierten en hidrocarburos que a su vez pueden ser convertidos a combustibles líquidos y productos químicos de alta calidad. Diferentes fuentes de carbono como el gas natural, el carbón y la biomasa pueden utilizarse como reservas de alimentación para la obtención del gas de síntesis. En aplicaciones comerciales, los catalizadores de cobalto soportados se usan comúnmente en la síntesis de Fischer-Tropsch, especialmente cuando el gas de síntesis emana del gas natural y cuando el producto final deseado es diesel. La actividad y selectividad de un catalizador de cobalto depende de varios parámetros, siendo uno de ellos el soporte.

La presente tesis está centrada en el diseño, síntesis y caracterización de materiales de alúmina y sílice con morfología no convencional y evaluación de su viabilidad como soportes de cobalto en la síntesis de FT. Se han sintetizado nanopartículas de alúmina y sílice mesoporosa mediante técnicas no convencionales, es decir, microemulsión de agua en aceite y por la ruta de atramos. También se han estudiado los efectos que pueda tener la incorporación de promotores, tales como Ce y Zr.

Los resultados muestran que ha sido posible la obtención de nanopartículas de alumina con Ce- y con Zr, sintetizadas por el método de co-precipitación en microemulsión de agua-en-aceite. El producto obtenido es alúmina amorfa con promotores altamente dispersos, lo que resulta resulta en fuertes interacciones de cobalto con el soporte y una baja reducibilidad de cobalto. Al aumentar la temperatura de calcinación del soporte promovido con Ce, se obtiene CeO<sub>2</sub> cristalino que aparentemente aumenta la capacidad de reducción del cobalto y por tanto la actividad catalítica (por gramo de catalizador). Los materiales poseen tamaños de poro pequeño y pueden inducir a la limitada difusión de los gases reactantes al sitio activo del catalizador y/o dar lugar a partículas de cobalto muy

pequeñas, lo que favorece la producción de metano sobre los hidrocarburos de cadena larga.

Esta tesis también presenta una síntesis generalizada de sílices mesoporosas con poros expandidos y estructuras de poros 1D, 2D y 3D (Dimensiones) a través de la ruta de atranos. La ventaja de este método es que la expansión de poros se obtiene condiciones moderadas.

Naturalmente, cuanto más grandes sean los poros de los soportes de sílice, más grandes serán las partículas de cobalto formadas y más débiles serán las interacciones de cobalto-soporte. Esto generalmente da lugar a una mayor capacidad de reducción de cobalto para soportes de poros más grandes y por lo tanto una actividad catalítica más alta. Las sílices con estructuras porosas 3D presentaron los resultados catalíticos más exitosos, resultado atribuido a su estructura.

## List of appended papers

The work presented in this thesis is based on the following publications. The papers are appended at the end of the thesis, and are referred to in the text using Roman numerals.

- I. R. Suárez, L. Lopez, J. Barrientos, **F. Pardo**, M. Boutonnet, S. Järås  
*Catalytic conversion of biomass-derived synthesis gas to fuels*  
Catalysis 27 (2015) 62-143, The Royal Society of Chemistry.
- II. **F. Pardo-Tarifa**, S. Cabrera, M. Sanchez-Dominguez, M. Boutonnet.  
*Ce-promoted Co/Al<sub>2</sub>O<sub>3</sub> catalysts for Fischer–Tropsch synthesis*  
International Journal of Hydrogen Energy 42 (2017) 9754-9765.
- III. **F. Pardo-Tarifa**, S. Cabrera, M. Sanchez-Dominguez, R. Andersson, M. Boutonnet  
*Synthesis and characterization of novel Zr-Al<sub>2</sub>O<sub>3</sub> nanoparticles prepared by microemulsion method and its use as cobalt catalyst support for CO hydrogenation reaction*  
Synthesis and Catalysis 2 (2017) 2-9.
- IV. **F. Pardo-Tarifa**, V. Montes, M. Claire, S. Cabrera, H. Kusar, A. Marinas, M. Boutonnet  
*Silica with 3-Dimensional mesocellular pore structure used as support for cobalt Fischer-Tropsch catalyst.*  
Synthesis and Catalysis 3 (2017) 2-11.
- V. **F. Pardo-Tarifa**, S. Cabrera, R. Andersson, H. Kusar, M. Boutonnet  
*Zr incorporation on 3D mesocellular foam MCF silica potential for cobalt Fischer-Tropsch catalyst.*  
(To be submitted).

### Contributions to the publications:

- I. I have contributed to the introduction and conclusion sections by discussions with all the authors. I wrote the section “*Fischer-Tropsch catalysts*”.
- II. I am the main author of this paper.
- III. I am the main author of this paper.
- IV. I am the main author of this paper.
- V. I am the main author of this paper.

## Conference contributions

*(Presenting author in bold)*

## Oral presentations

**F. Pardo**, S. Cabrera, A. Marinas, V. Montes, M. Boutonnet

*Characterization of cobalt deposited on mesoporous materials with several pore diameters: The formation of metal-support species*

Metrics Meeting UBIOCHEM III, Palermo, Italy, January, 24-25, 2013

**F. Pardo**, S. Cabrera, S. Järås, A. Marinas, V. Montes, M. Boutonnet

*Cobalt on ordered mesoporous supports for Fischer-Tropsch Synthesis*

Catalysis for Renewable Sources: Fuel, energy, chemicals. Lund, Sweden, July, 22-28, 2013

**Awarded for being the best oral presentation**

**F. Pardo**, V. Montes, S. Cabrera, A. Marinas, M. Boutonnet

*Synthesis of silicas with spherical structure used as support for cobalt Fischer-Tropsch catalysts*

Metrics Meeting UBIOCHEM III Valencia, Spain, September, 24-25, 2013

## Poster presentations

**F. Pardo**, S. Cabrera, S. Järås, M. Boutonnet

*Cobalt supported on pore expanded MCM-41 for Fischer-Tropsch Application*

Syngas Convention Cape Town, South Africa, April, 1-4, 2012

**F. Pardo**, S. Cabrera, S. Järås, M. Boutonnet.

*Synthesis of PEMCM-41: On the reduction of cobalt-silicate formation*

EFCATS Summer School “School in catalysis”, Verbania, Italy, September 11-17, 2012

**F. Pardo**, S. Cabrera, S. Järås, A. Marinas, V. Montes, M. Boutonnet  
*Synthesis of spherical shape silicas as support for cobalt based catalysts potential for Fischer Tropsch Synthesis*

8<sup>th</sup> International Conference on Environmental Catalysis, Asheville, USA,  
August 24-27, 2014

**F. Pardo-Tarifa**, M. Sanchez-Dominguez, S. Cabrera, M. Boutonnet  
*Synthesis of Ce-doped Alumina Nanoparticles in water-in-oil W/O Microemulsions system*

European Conference in Colloidal Science, Limassol, Cyprus, September 7-12, 2014

J. Barrientos, **F. Pardo-Tarifa**, M. Boutonnet, S. Järås  
*Liquid and gas Fischer-Tropsch fuel production from olive industry waste: Fuel from waste*

KTH Energy Dialogue, Stockholm, Sweden, November 20<sup>th</sup>, 2014

***Awarded with the first prize for the best poster presentation***

**F. Pardo-Tarifa**, S. Cabrera, M. Boutonnet.

*Novel porous and non-porous nanoparticles used as supports for cobalt Fischer-Tropsch catalysts*

V NanoAndes School, San José, Costa Rica. November, 23-27, 2015

***Awarded for being the second best poster presentation.***

# Contents

<b>Part I: Introduction .....</b>	<b>1</b>
<b>Chapter 1 .....</b>	<b>3</b>
<b>Setting the scene.....</b>	<b>3</b>
1.1 Scope of the work .....	4
1.2 Thesis outline.....	5
<b>Chapter 2.....</b>	<b>7</b>
<b>Conversion to synthetic fuels (Paper I).....</b>	<b>7</b>
2.1 Gas-to-liquid (GTL) .....	8
2.2 Synthesis gas production for Fischer-Tropsch applications .....	9
2.3 Fischer-Tropsch synthesis.....	9
<b>Chapter 3.....</b>	<b>13</b>
<b>Fischer-Tropsch catalysts (Paper I) .....</b>	<b>13</b>
3.1 Cobalt catalysts .....	13
3.2 Cobalt catalyst preparation .....	15
3.3 Effects of cobalt catalyst parameters on the activity and selectivity in Fischer-Tropsch synthesis.....	16
3.4 Cobalt supports .....	17
3.5 Promoters .....	18
3.6 Effect of the support in Fischer-Tropsch synthesis.....	20
3.7 Strong metal-support interaction.....	20
3.8 New materials as Fischer-Tropsch catalyst supports.....	21

<b>Part II: Experimental.....</b>	<b>29</b>
<b>Chapter 4.....</b>	<b>31</b>
<b>Support and catalyst preparation (Papers II-V).....</b>	<b>31</b>
4.1 Support synthesis.....	31
4.2 Conventional supports .....	31
4.3 Non-conventional supports.....	31
4.4 Catalyst preparation .....	36
<b>Chapter 5.....</b>	<b>37</b>
<b>Catalyst characterization.....</b>	<b>37</b>
5.1 N <sub>2</sub> physisorption .....	37
5.2. X-ray Diffraction (XRD).....	37
5.3 H <sub>2</sub> chemisorption.....	37
5.4 Transmission electron microscopy (TEM).....	38
5.5 Temperature programmed reduction (TPR).....	38
<b>Chapter 6.....</b>	<b>41</b>
<b>Fischer-Tropsch experiments.....</b>	<b>41</b>
6.1 Set-up and experimental procedure.....	41
6.2 Product analysis and data treatment .....	43
<b>Part III: Results and discussions .....</b>	<b>45</b>
<b>Chapter 7.....</b>	<b>47</b>
<b>Co/Al<sub>2</sub>O<sub>3</sub> catalysts promoted with Ce and Zr for</b>	
<b>Fischer-Tropsch synthesis(Papers II and III) .....</b>	<b>47</b>
7.1 Microemulsion vs. impregnation method.....	47
7.2 Synthesis of Al <sub>2</sub> O <sub>3</sub> , Zr-Al <sub>2</sub> O <sub>3</sub> and Ce-Al <sub>2</sub> O <sub>3</sub> by water-	
in-oil microemulsion method.....	48
7.3 Characterization of the nanoparticle supports .....	49
7.4 Catalytic activity in the Fischer-Tropsch reaction.....	61

7.5 Conclusions.....	64
<b>Chapter 8.....</b>	<b>66</b>
<b>Ordered mesoporous silicas as support for cobalt</b>	
<b>Fischer-Tropsch catalyst (Paper IV) .....</b>	<b>66</b>
8.1 Synthesis approach.....	66
8.2 Characterization of the materials.....	68
8.3 Catalytic activity .....	77
8.4 Conclusions .....	78
<b>Chapter 9.....</b>	<b>80</b>
<b>Mesoporous silicas promoted with Zr as potential</b>	
<b>support for cobalt Fischer-Tropsch catalysts</b>	
<b>(Paper V) .....</b>	<b>80</b>
9.1 Characterization of the materials .....	81
9.2 Conclusions .....	89
<b>Chapter 10 .....</b>	<b>90</b>
<b>Final conclusions .....</b>	<b>90</b>
<b>Acknowledgements .....</b>	<b>94</b>
<b>Nomenclature .....</b>	<b>98</b>
<b>References.....</b>	<b>100</b>



# **Part I: Introduction**



# Chapter 1

## Setting the scene

This thesis is a result of a joint project between the department of Chemical Engineering at KTH Royal Institute of technology, Stockholm, Sweden and the Institute of Natural Gas at UMSA Universidad Mayor de San Andrés, La Paz, Bolivia. The project was financially supported by the Swedish International Development Cooperation Agency, SIDA. The mission of SIDA is to reinforce research capacity through education and funding research projects in developing countries. This project was aimed at increasing technology expertise at Bolivian universities.

Bolivia is rich in natural resources, such as minerals, natural gas, and forests. Still, the country is one of the poorest on the South American continent. The lack of technical knowledge and specialized education therefore hinder the domestic industry from adding value to the natural resources. Bolivia has the second largest natural gas reserve in Latin America and its economy relies mostly on the export of this raw material to the neighbouring countries. Paradoxically, while the country is a huge energy exporter of natural gas (>80% of its total production), the energy import of diesel is increasing every year as the country develops. Additionally, the diesel is subsidized since 1997 with 0.53 US cents per liter to the final consumer, making it a large expense for the government. To reduce the diesel import dependence, make use the available natural gas as well as develop the country, the government, industries, and academia are focusing their resources on the development of local technical knowledge and implementation of this knowledge for converting natural gas to diesel, i.e. the gas-to-liquid (GTL) process. In the GTL process natural gas is converted to heavy hydrocarbons which can be used as fuel, i.e. diesel or gasoline or chemicals among others. The GTL process implies the conversion of natural gas to synthesis gas ( $H_2 + CO$ ), thereafter the synthesis gas is converted to long-chain liquid hydrocarbons via Fischer-Tropsch synthesis, and subsequently the FT products are upgraded to

obtain the final products. Commercial Fischer-Tropsch synthesis in a GTL plant is performed with cobalt-based catalysts.

## 1.1 Scope of the work

New explorations of catalyst design aim to make an affordable, highly active and selective, as well as stable catalyst. Some of the most important variables include the selection of the metal precursor, metal loading, support characteristics, promoters, preparation and catalyst activation method. The cobalt-support characteristics and/or promoters may influence the physicochemical properties of the deposited cobalt particle such as: particle size, degree of reduction, dispersion, metal-support interaction among others; and as a consequence the performance of the final catalyst in the Fischer-Tropsch reaction.

The general aim of this work was to study, on one hand, the relationship between the synthesis method and the structure of cobalt supports with non-conventional morphology; and on the other hand, the relationship of the support structure and composition with the final cobalt catalysts and their influence on the Fischer-Tropsch reaction at low temperature. In addition, two kinds of promoters modified the support: one, structural promoter, which is obtained by changing the structure of the support and two, chemical promoter, obtained by the addition of Zr or Ce to the alumina or silica support. In particular, concerning the structural promoter, the morphology of the supports, i.e.  $\text{Al}_2\text{O}_3$  nanoparticles and ordered mesoporous  $\text{SiO}_2$  were investigated in order to evaluate their influence on the final cobalt catalyst. Concerning the incorporation of chemical, i.e. Ce and Zr, two methods of promoter incorporation were evaluated: one, impregnation of the promoter on commercial alumina and two, co-precipitation of promoter and the support precursor. The effect of promoter and method of incorporation was investigated in the performance of the final cobalt catalyst.

The work included in this thesis was mainly conducted at the Division of Chemical Technology at KTH Royal Institute of Technology, Stockholm,

Sweden while some of the data analysis and writing was done at the Natural Gas Institute at Universidad Mayor de San Andrés (UMSA), La Paz, Bolivia. In addition, two research stays were included: one at the department of Organic Chemistry at Córdoba University, Spain, where part of the characterization of the mesoporous silica was performed; and another at the Research Center for Advanced Materials (CIMAV) in Monterrey, Mexico, where I prepared nanoparticles using the water-in-oil microemulsion method.

## **1.2 Thesis outline**

Following this introduction, chapter 2 presents the synthesis of fuels through the Gas-to-Liquid (GTL) process, with focus on Fischer-Tropsch synthesis. Chapter 3 provides a background on the Fischer-Tropsch catalysts with a particular focus on cobalt catalysts, especially on the alumina and silica supports and promoters with non-conventional morphology and synthesis methods. The second part of this thesis explains how supports were synthesized and structurally characterized. The physicochemical characterization of the cobalt catalyst on those supports is also presented. The Fischer-Tropsch reactor set-up and catalytic tests are also explained in this section. The third part of the thesis corresponds to the results, discussion and conclusions of the investigation.



## Chapter 2

### Conversion to synthetic fuels (Paper I)

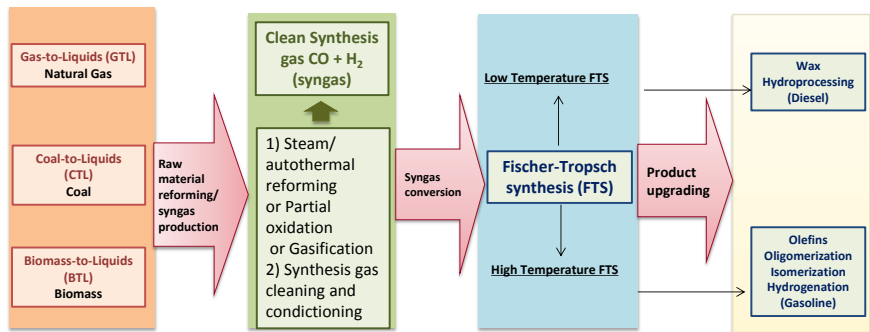


**Figure 2.1:** Main steps for producing Fischer-Tropsch products: syngas generation, gas purification, Fischer-Tropsch synthesis and product upgrading.

Different feedstocks can be converted into synthetic fuels, where liquid fuels are the preferred ones. The process is named according to the feedstock: gas-to liquid (GTL), biomass-to-liquid (BTL) and coal-to-liquid (CTL).<sup>1-3</sup> If the conversion is performed via Fischer-Tropsch synthesis (FT), the raw material is first converted into synthesis gas which is a mixture of CO and H<sub>2</sub>, and the synthesis gas is subsequently reacted to form hydrocarbons<sup>4,6</sup>.

The general process is divided into three main steps: synthesis gas manufacturing; Fischer-Tropsch synthesis; and product upgrading (see **Figure 2.1**). The first step is dependent on the feedstock. The second step the synthesis gas is converted into a variety of hydrocarbons with different chain lengths, which will depend on the catalyst and the process parameters<sup>7, 8</sup>. Some of the FT products can be directly used for food, cosmetics and medical applications. If high quality fuels are required, Fischer-Tropsch wax is hydrocracked. Hydrocracking is a selective process,

in which heavy hydrocarbons are broken down to lighter products, such as naphtha, kerosene and diesel oil, in the presence of  $H_2$ <sup>8,9</sup>.

## 2.1 Gas-to-liquid (GTL)

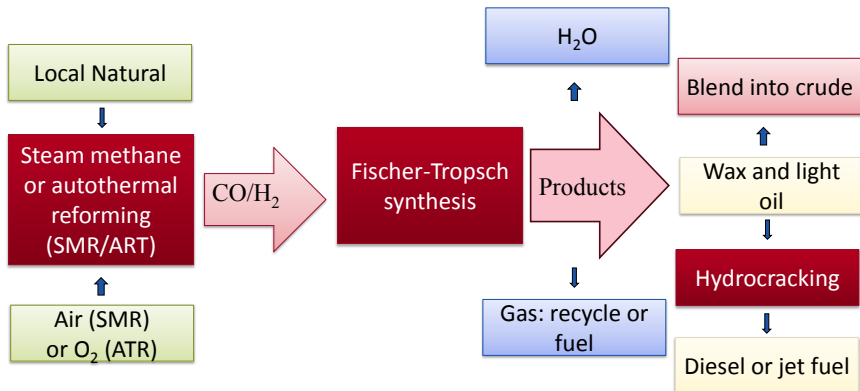


**Figure 2.2:** Diagram of the GTL process

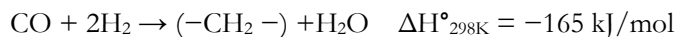
The GTL process is shown in **Figure 2.2**. It is a very attractive option for making natural gas reserves more economically feasible. The chemical or cryogenic conversion of this natural gas into an easily transportable liquid is usually chosen when the reserves are localized in remote areas (>3000 km) and the costs of a gas pipeline is too high. The cryogenic process is a condensation of natural gas into liquid (LNG). A chemical conversion of the natural gas produces methanol, dimethyl ether (DME) or hydrocarbons via the Fischer-Tropsch reaction<sup>9</sup>.

## 2.2 Synthesis gas production for Fischer-Tropsch applications

The natural gas which mainly contains methane may be transformed to synthesis gas through several processes; however the predominant commercial technology is steam methane reforming (SMR). SMR catalyses the reaction between methane and steam to obtain hydrogen and carbon monoxide. Partial oxidation (POX) is an alternative technology which combines methane and oxygen exothermally to obtain synthesis gas. The two technologies produce synthesis gas with different H<sub>2</sub>/CO ratios, about 3-5 with the SMR process (which can be lowered with the addition of CO<sub>2</sub>) and about 1.6-1.9 with the POX process. Partial oxidation can be performed both catalytically and non-catalytically. A third alternative is autothermal reforming (ATR) which is seen as a hybrid between the two previous processes in a single reactor<sup>10</sup>.

## 2.3 Fischer-Tropsch synthesis

The Fischer-Tropsch synthesis is an exothermic reaction between H<sub>2</sub> and CO (syngas) which produces water and a wide variety of hydrocarbons (gas, liquid and waxes). The FT products are mainly n-paraffins and  $\alpha$ -olefins and, to a lesser extent, branched hydrocarbons and oxygenates. The reaction is described as follows:

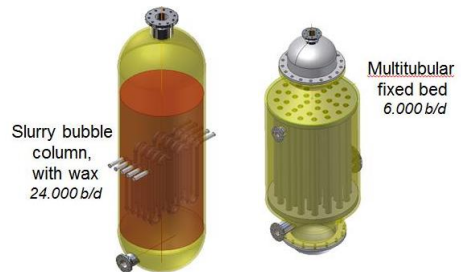


The product selectivity depends on the employed catalysts and the operating parameters of the reaction, such as reaction temperature, pressure and feed composition<sup>11</sup>. The FT industry mainly uses iron-based catalysts for coal-to-liquids (CTL) and cobalt-based catalysts for GTL application. The Fischer-Tropsch reaction is operated at high pressures (usually P=20-45 bar) and there are currently two operated modes: high-temperature FT (HTFT) and low-temperature FT (LTFT). The HTFT process operates at temperatures of about 320-350 °C using Fe-based catalysts<sup>12</sup>. The main products are olefins with short-chain length, oxygenates and hydrocarbons

in the gasoline range. The LTFT process operates at temperatures of about 200-250 °C, both Fe- and Co-based catalysts can be employed<sup>12</sup>. The main products are linear long-chain paraffins (middle distillates and waxes). The FT waxes are later hydrocracked to maximize the yield to middle distillates (jet fuel and diesel cut)<sup>13, 14</sup>. The performance of FT technology is highly dependent on the catalyst design and reactor engineering. The LTFT process is commercialized in slurry bubble column reactor and multi-tubular fixed bed reactor (see **Fig. 2.3**).

### Low-temperature FT (LTFT) reactors

- Temperature: 200-250 °C
- Three phase system: gas-liquid-solid
- Products: wax diesel, naphta
- Catalyst: supported cobalt or precipitated iron



### High-temperature FT (HTFT)

- Temperature: 320-350 °C
- Two phase system: gas-solid
- Products: gasoline, chemicals
- Catalyst: fused iron, K-promoted

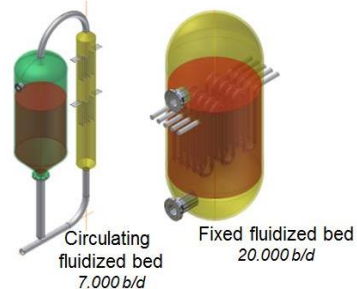


**Figure 2.3:** Overview of the Fischer-Tropsch reactor types presently in use (Adapted from<sup>15</sup>).

Generally the FT reaction is defined as a polymerization reaction in which a hydrocarbon chain increases its length by the insertion of monomers containing one carbon atom. The mechanism can be divided in three steps: chain initiation (monomer formation), chain growth and termination. Two routes can be identified in the FT mechanisms: in the

first, the -CH<sub>2</sub>- is the monomer incorporated into the chain growth; and in the second one, CO and/or enols are the monomers. However, it is commonly accepted that parallel mechanisms can occur on the catalyst surface during FTS<sup>15</sup>. Nevertheless, the mechanistic details concerning CH<sub>2</sub> monomer formation are not agreed upon. Two pathways are proposed for the -CH<sub>2</sub>- monomer formation: the first, known as the direct CO dissociation, CO adsorbs and directly dissociates into C and O atoms. Thereafter, the adsorbed C atoms are hydrogenated and -CH<sub>2</sub>- is formed; in the other pathway called H-assisted CO dissociation, H is bound to CO before it dissociates<sup>16</sup>.

The Fischer-Tropsch products are mainly straight-chain saturated hydrocarbons from methane up to heavy waxes. Independently of the reaction mechanism the FT product distribution can be fairly well approximated by the Anderson-Schulz-Flory (ASF) model. This model has only one assumption: the probability of chain growth ( $\alpha$ ) is independent of the hydrocarbon chain length ( $n$ )<sup>17</sup>. With this assumption the following equations are derived:

$$X_n = \alpha^{n-1} \cdot (1 - \alpha) \quad (2.1)$$

$$\frac{W_n}{n} = \alpha^{n-1} \cdot (1 - \alpha)^2 \quad (2.2)$$

Equation 2.1 relates the probability of chain growth ( $\alpha$ ) and the molar fraction ( $X_n$ ) of hydrocarbons with the same carbon number ( $n$ )<sup>17</sup>. An equivalent expression (equation 2.2) can also be derived in terms of mass fraction ( $W_n$ )<sup>18</sup>. In **Figure 2.4**, the mass fraction of different hydrocarbon groups is plotted against “ $\alpha$ ” according to equation 2.2. Two main regions of the products are typical from HTFT and LTFT operational conditions as shown in **Figure 2.4**<sup>9</sup>. The operation parameters for the Fischer-Tropsch test of the cobalt catalysts studied in this thesis are based on the LTFT process.

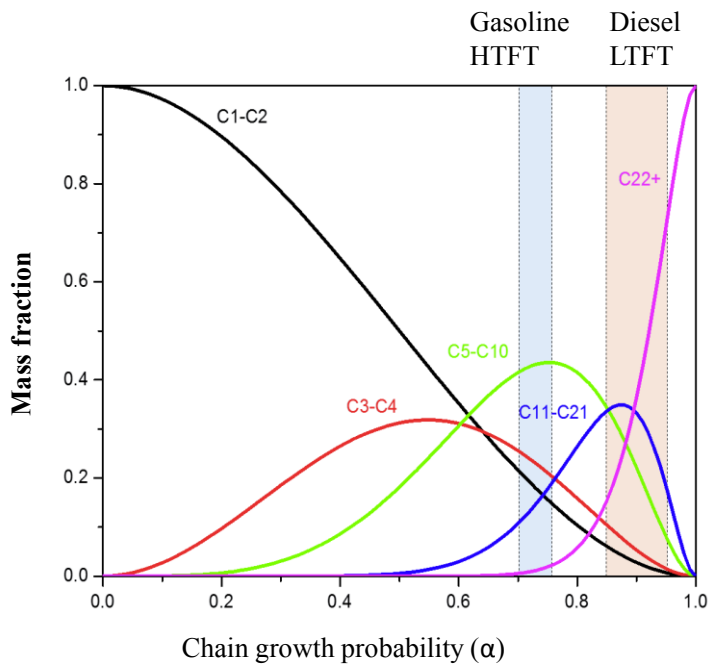


**Figure 2.4:** Anderson-Schulz-Flory FT product distribution as function of the chain growth probability (adapted from<sup>19</sup>)

## Chapter 3

### Fischer-Tropsch catalysts (Paper I)

As mentioned in the previous chapter, the Fischer-Tropsch (FT) process converts synthesis gas or syngas ( $\text{CO} + \text{H}_2$ ) to hydrocarbons with several different molecular weights. The FT reactions include the CO and  $\text{H}_2$  dissociation, hydrogenation and chain growth (carbon coupling) on the surface of the active sites of the catalyst<sup>20</sup>. The active phase consists of metals which can promote CO dissociation with a balanced degree of surface carbon hydrogenation and carbon coupling in order to produce long chain hydrocarbon products. Ni, Fe, Co and Ru are active for CO hydrogenation<sup>21</sup>. The selection of the metal is very important in terms of cost and the desired product. Nickel is very active for hydrogenation, which provokes high selectivity to methane<sup>22</sup>. It also easily forms carbonyls at FTS operating conditions which facilitates atom migration and in this way favours sintering<sup>23</sup>. Ruthenium is the most active metal for FT reactions which produce long-chain hydrocarbons, however it is very expensive and its availability is limited for large scale applications. This leaves the catalyst competition to Fe and Co, which are actually used industrially for producing middle distillate products<sup>23</sup>. Iron catalysts are used for syngas coming from coal or biomass which has a low  $\text{H}_2/\text{CO}$  ratio. Since, iron is highly active for water-gas-shift (WGS) reaction, which can increase the  $\text{H}_2/\text{CO}$  ratio inside the reactor.<sup>24, 25</sup>. The products from Fe catalysts tend to produce mainly linear alpha olefins and a mixture of oxygenates such as alcohols, aldehydes and ketones<sup>26</sup>. The cobalt catalyst is discussed in more detail above.

#### 3.1 Cobalt catalysts

Cobalt-based catalysts are chosen by several companies (see **Table 3.1**) such as Shell, Qatar Petroleum, Sasol, Chevron among others in the Gas-to-Liquid process community for the production of middle distillate fuels via the Low-Temperature Fischer-Tropsch (LTFT) reaction<sup>9, 27, 28</sup>.

**Table 3.1:** Cobalt FT catalysts used and/or patented by FT synthesis companies (Adapted from Paper I and<sup>19, 27, 29, 30</sup>).

Company	Support	Reduction promoter	Structural promoter
Sasol	Y-Al <sub>2</sub> O <sub>3</sub>	Pt	Si
Shell	TiO <sub>2</sub>	-	Mn, V
GTL (Statoil)	NiAl <sub>2</sub> O <sub>4</sub>	Re	-
Nippon Oil	SiO <sub>2</sub>	Ru	Zr
Syntroleum	Y-Al <sub>2</sub> O <sub>3</sub>	Ru	Si, La
BP	ZnO	-	-
Exxon Mobil	TiO <sub>2</sub>	Re	Y-Al <sub>2</sub> O <sub>3</sub>
Conoco Phillips	Y-Al <sub>2</sub> O <sub>3</sub>	Ru, Pt, Re	B
Compact GTL	Al <sub>2</sub> O <sub>3</sub>	Ru, Pt, Re	-

Cobalt-based catalysts are very suitable for wax formation in slurry bubble columns and can operate at high conversion per pass. The advantage of cobalt catalysts is the low activity for the water-gas shift reaction and, the high activity and selectivity to linear paraffins<sup>31</sup>. In addition, it has low activity to oxygenated by-products and finally, has a good availability and relatively low price compared with Ru<sup>32</sup>.

Commercial FT reactors use large amounts of cobalt catalyst and reduce the catalyst cost by dispersing the cobalt on stable high surface area oxides (the support) see **Table 3.1**<sup>33</sup>. The method of deposition is usually by impregnation of an aqueous cobalt solution on the support<sup>33</sup>. In order to increase metal dispersion, reducibility, activity and stability of cobalt-based catalysts, several promoters can be incorporated<sup>12</sup>.

## 3.2 Cobalt catalyst preparation

Incipient wetness impregnation is the most common technique for preparing supported cobalt catalysts. It is based on filling the pore volume of the support with the appropriate concentration of the cobalt salt solution. The impregnation step is followed by drying, calcining in order to decompose the nitrate and obtain supported cobalt oxide. *In situ* reduction transforms the inactive cobalt oxide to active metallic cobalt prior to Fischer-Tropsch synthesis (see **Figure 3.1**).

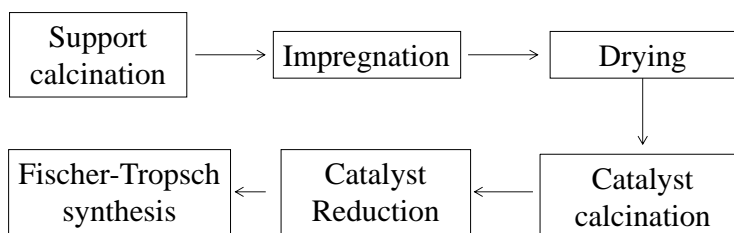


**Figure 3.1:** Catalyst preparation steps.

Each of these steps needs to be optimized in order to prepare a catalyst with high activity and dispersion. The conditions during calcination of the deposited cobalt have a significant influence on the physicochemical characteristics of the final catalyst. For instance, it was found that the catalyst performance is highly dependent on the space velocity of the air and the heating rate<sup>34, 35</sup>. After calcination, the  $\text{Co}_3\text{O}_4$  crystallites are present in aggregates with sizes between 30-700 nm<sup>34, 36</sup>. The reduction step in the catalyst preparation is also very important, since it was reported that the  $\text{H}_2$  flow rate during cobalt oxide reduction should be kept high to avoid high partial pressures of the water produced which may induce metallic cobalt sintering<sup>36</sup>. Reduction temperatures higher than 350 °C result in the diffusion of cobalt ions into the support, forming cobalt aluminate compounds, which are difficult to reduce at low temperature. In addition, sintering of cobalt metal particles has been reported<sup>29</sup>.

### 3.3 Effects of cobalt catalyst parameters on the activity and selectivity in Fischer-Tropsch synthesis

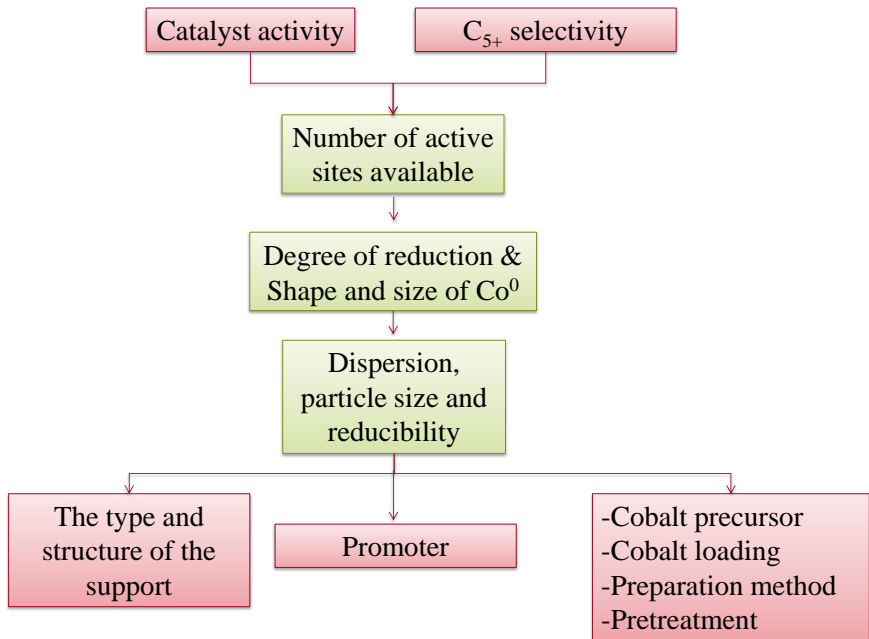


**Figure 3.2:** Factors that influence the activity and selectivity in a cobalt catalyst for Fischer-Tropsch synthesis.

**Figure 3.2** shows a summary of the effect on the performance of the catalyst depending on the catalyst preparation. The catalytic performance, concerning the catalyst activity and selectivity, will be very dependent on number of cobalt active sites, which will be determined by the physicochemical characteristics of the cobalt catalyst, such as: cobalt particle size, degree of reduction and dispersion, among the most important. Indirectly those characteristics are very dependent on several parameters that concern the catalyst preparation, such as chemical composition, support

structure, porosity, promoters, precursors and operating conditions. This thesis is focused on the influence of the support on the cobalt physicochemical characteristics and final performance in Fischer-Tropsch synthesis. Thus, this chapter is focused on the support and oxide promoters of Ce and Zr. In addition, the non-conventional methods of synthesis (microemulsion and *atrans route*) for the supports are discussed.

### 3.4 Cobalt supports

*Conventional supports* such as alumina, silica and titania are the most used industrially for cobalt-based FT catalysts (Table 3.1). The main advantage of these supports is their retention of high surface area after high calcination temperatures (especially in the case of alumina and titania)<sup>28</sup>.

The properties of the support are also an important factor for producing a feasible catalyst. Much work has been done in order to determine the optimal characteristics of the support. Bartholomew and Farrauto have presented some ideal properties<sup>37</sup>:

- moderately high surface area (100-150 m<sup>2</sup>/g)
- low acid-site concentration
- low reactivity with Co to limit metal-support interactions
- high thermal stability during catalyst regeneration
- high strength and attrition resistance

*Non-conventional* supports have been studied in FTS, such as ZrO<sub>2</sub>, carbon-based supports, metallic supports, zeolites, mesoporous oxides, CeO<sub>2</sub> among others<sup>12, 38, 39</sup>.

#### *Al<sub>2</sub>O<sub>3</sub> support*

Gamma alumina,  $\gamma$ -Al<sub>2</sub>O<sub>3</sub>, is mechanically strong and has high surface area which is easily hydrated, in addition it has many acid sites which is not favourable in Fischer-Tropsch synthesis<sup>40</sup>. The decrease in acid sites was reported to increase activity and selectivity to long-chain hydrocarbons due

to an increase in reducibility and bridged type CO adsorption. Therefore, promoters are used in order to increase the stability of the support, and avoid inactive  $\text{CoAl}_2\text{O}_4$  formation<sup>29, 40</sup>.

### *SiO<sub>2</sub> support*

Silica has low hydrothermal stability and can break down in the presence of steam to form cobalt-silicate species that are inactive in the FTS. Similar to alumina, silica supports are also often modified, with stabilizers or promoters such as  $\text{ZrO}_2$ , K,  $\text{TiO}_2$ ,  $\text{CeO}_2$ , among others or by organic solvents to increase the hydrothermal stability<sup>41, 42</sup>. Also, it has been shown that calcination of the support prior to Co deposition can be beneficial<sup>30, 43-47</sup>.

## **3.5 Promoters**

Small cobalt particles usually have strong interaction with the supports  $\text{SiO}_2$ ,  $\text{Al}_2\text{O}_3$  and  $\text{TiO}_2$ . The formed species are reduced at very high temperature. In order to overcome this problem, a number of additives have been investigated for this studied reaction<sup>48</sup>. In general, the additives can be divided into two categories:

- Oxide promoters (stabilize or alter the properties of the support and/or promote the Co)
- Metal promoters (increase reducibility of  $\text{CoO}_x$  and induce favourable interactions with Co).

Metal oxides have been used favourably as promoters for cobalt catalysts; alkali metal oxides, early and late transition metals, noble metals, as well as lanthanide and actinide series oxides. These are used because they may control the surface H/CO ratio through electronic interaction with the metal, increase and facilitate CO dissociation at the promoter-metal interface, and/or lower support acidity (prevents side reactions). There are several reviews that specify the behaviour of these promoters, here we will focus on Zr and Ce promoters, since they have shown good performance in

FTS and no investigation on the proposed synthesis has been done previously<sup>36, 42, 49</sup>.

### **3.5.1 Metal oxide promoters**

These metal oxides can facilitate the dissociation of CO at the promoter-metal interfaces (adlineation sites) and the formation of inactive mixed oxides (between promoter and support) can resist carbon deposition. In addition the CO activity, C<sub>5+</sub> selectivity and the olefin/paraffin ratio increase. The most frequently used promoters are: ZrO<sub>2</sub>, ZnO, Cr<sub>2</sub>O<sub>3</sub>, MnO<sub>2</sub>, TiO<sub>2</sub>. Furthermore, these promoters can control the surface H:CO ratio by decoration of, and electronic interaction with, the Co metal surface which leads to hydrogen-poor olefinic products<sup>50-52</sup>.

#### *Zirconium promoter*

Zirconium is known for increasing the performance of cobalt catalysts when alumina is used as support. The promotion effect is attributed to the increase of active intermediates (-CH<sub>2</sub>-) which enhance the catalyst activity and selectivity to long-chain hydrocarbons. It has also been reported that Zr enhances the cobalt reducibility and consequently the catalyst activity<sup>53-58</sup>.

#### *Cerium promoter*

In the process of CO hydrogenation, CeO<sub>2</sub> can increase the reducibility of the cobalt catalyst. This behaviour is attributed to the defect sites of Ce<sup>4+</sup> and Ce<sup>3+</sup> in the final cerium oxide formed. CeO<sub>2</sub> is beneficial for the Co/SiO<sub>2</sub> or Co/Al<sub>2</sub>O<sub>3</sub> systems, since it seems to increase the selectivity to long-chain hydrocarbons. It was also reported that ceria may favour the dispersion and reducibility of the cobalt catalyst supported on pillared montmorillonite, which resulted in an increase of FTS activity<sup>59, 60</sup>. Additionally, the ceria surface affinity for both H<sub>2</sub> and CO molecules might contribute to the reactivity in FTS when Co/CeO<sub>2</sub> catalyst is used<sup>61</sup>. It was also reported that the addition of cerium to Co/ $\gamma$ -Al<sub>2</sub>O<sub>3</sub> could significantly

decrease the generation rate of CO<sub>2</sub>, CH<sub>4</sub> and C<sub>2</sub>–C<sub>4</sub> while increasing C<sub>5</sub>+ selectivity<sup>62</sup>.

### 3.6 Effect of the support in Fischer-Tropsch synthesis

The support effects in FT reactions concerning the rate and hydrocarbon selectivity are not entirely understood yet. Iglesia et al. <sup>63</sup> reported that the supports SiO<sub>2</sub>, Al<sub>2</sub>O<sub>3</sub>, TiO<sub>2</sub>, ZrO<sub>2</sub> and their modified versions have no influence on the specific FT activity, in contrast a good performance is attributed to the metal dispersion. However, the differences in selectivity were mainly ascribed to diffusion effects of reactants and products on secondary reactions (olefin readsorption). Studies reported that the chemical nature and porosity of the support play a crucial role the intrinsic selectivity in the FT reactions, i.e. explaining different selectivities rather as differences in the intrinsic chain growth probability than in differences in diffusional effects<sup>64</sup>.

It is considered that the support effect has an *indirect* influence on the FT performance. In fact, the physicochemical characteristics of the support, such as the porosity can strongly influence the particle size of the deposited cobalt catalyst and its reducibility especially when the method of the cobalt deposition is impregnation<sup>65</sup>. Even if the conventional supports Al<sub>2</sub>O<sub>3</sub>, SiO<sub>2</sub> and TiO<sub>2</sub> have performed satisfactorily as cobalt-FT catalysts, there is still room for exploring the synthesis of new support materials with enhanced properties. During the past few years, novel carriers such as nanoparticles, ordered mesoporous supports, carbon nanotubes, silicon carbide and zeolites with new chemical compositions have attracted considerable attention for several applications<sup>66, 67</sup>.

### 3.7 Strong metal-support interaction

As mentioned before, active metals are dispersed on oxides in order to increase their surface area, and consequently the number of active sites. However, the interaction between the metal and support must be balanced to achieve a highly active metal dispersion but not too strong metal-support interaction. A strong metal-support interaction may result in the formation

of mixed oxides between the support and the active metal<sup>68, 69</sup>. These undesired species are reduced at temperatures higher than 500 °C, which causes severe sintering of the catalysts that thereafter are considered irreducible or inactive for FT processing. Therefore, the catalyst support can play a major role in the catalyst's behaviour<sup>39, 70</sup>.

Four major effects of metal-support interactions have been identified:

1. Electronic and geometric modification properties of the metal surface by support-derived species deposited on the metal during preparation or during reaction. These modifications may promote or inhibit new catalytic sites. The electronic properties of metal atoms can be modified through a localized charge transfer at the promoter-metal interface.
2. The morphology, electronic and adsorption properties of small metal clusters (<2nm diameter) can change by contact with the support.
3. Inhibition by unreduced metal oxide or metal-support species located near or at metal crystallite surfaces.
4. New reaction pathways catalysed by acid sites in the support.

In summary, very strong metal-support interactions in Co-based Fischer-Tropsch catalysts promote inactive mixed metal oxides, lower the metal activity, and the support may become decorated by metal crystals.

It has been stated that if the Co metal dispersion is lower than 15% then contamination by the support can be avoided and a high extent of reduction (or reducibility, ability to reduce CoOx) can be maintained, about 70-80%. Therefore, the support is central to the productivity of the catalyst in the Fischer-Tropsch synthesis<sup>62, 63</sup>.

### **3.8 New materials as Fischer-Tropsch catalyst supports**

In previous sections, the most common cobalt catalysts were summarized. However, researchers are still developing new methods for synthesis and pre-treatment in order to have a designed material with enhanced properties. During the last decade, novel supports such as ordered

mesoporous oxides, carbon nanotubes, silicon carbide and zeolites have attracted considerable attention.

Comprehensive summaries in this area can be found in Paper I and other publications<sup>25, 27, 29, 31, 39, 46</sup>. In this thesis, nanoparticles and ordered mesoporous material structures will have our attention.

### **3.8.1 Nanoparticle oxides as supports**

The use of nanoparticle oxides as supports for cobalt catalysts used in Fischer-Tropsch synthesis is a relatively new topic and any published paper was found. The nanoparticles prepared and considered in this study have diameters of less than 10 nm and are interesting due to their high surface area per unit mass. In addition, the novel incorporation of highly dispersed promoters i.e. Ce or Zr in Al<sub>2</sub>O<sub>3</sub> makes the material very attractive. Since the nanoparticles are very small it is very probable that they have a high density of edge and corner sites with low coordination on which the interactions with the active metal can increase. To avoid formation of inactive mixed cobalt oxides a promoter can be added in order to stabilize the support oxide. In addition, it is thought that the nanoparticle oxides will maintain a high surface area while a promoter is added. Following this introduction, our main goal is to investigate the effects of the nanoparticle oxide support without and with a promoter on cobalt catalysts and compare the activity and selectivity of the nanoparticle-supported catalysts to cobalt catalysts with more conventional supports.

### **3.8.2 Mesoporous materials in Fischer–Tropsch synthesis**

Ordered mesoporous materials have rapidly developed since 1990 due to their tuneable, large and uniform pore size (1.5 – 50 nm), and large surface area. In the past decades, the methods and techniques of synthesis have been explored. As a consequence, novel mesoporous materials (mostly silica) are emerging together with novel applications in various fields, where the study is particularly based on the relationship between synthesis, structure and application.

Ordered Mesoporous Silica (OMS) has unique properties such as highly ordered pore structures, high specific surface area, as well as tuneable pore size and volume. OMS is of great interest, when used as catalyst support in reactions involving bulky molecules. Its morphology avoids agglomeration of the supported catalyst particles, which results in higher dispersion of the final catalyst<sup>57, 71, 72</sup>. In the Fischer-Tropsch reaction, several mesoporous silicas have been used for cobalt catalyst preparation, the reported results showed that small pores might accumulate the water product from FTS and could oxidize the small metallic cobalt particles ( $\leq 2$  nm)<sup>63, 73-77</sup>. Concerning this topic, numerous studies have been performed on the pore size effect of the support on the cobalt catalyst. The reported results claim that wide pore supports are favourable for FT productivity and higher selectivity to hydrocarbons with more than five carbon atoms ( $S_{C5+}$ ) in the hydrocarbon chain<sup>64, 71, 78-82</sup>.

The pore size of the support will govern the  $Co_3O_4$  particle size. If the support has narrow pores, the deposited cobalt might result in very small particles and their reducibility might be harder and thus it is reflected on the catalytic performance. In contrast, large particles are formed in wider pores<sup>80</sup>. It has also been reported that the selectivity to methane increases when the pore size is small due to mass transport phenomena. The cobalt oxide phases capable of catalysing water-gas shift reaction (increasing the  $H_2/CO$  ratio); and CO diffusion limitation in the catalyst pores results in an increase of the  $H_2/CO$  ratio with and increased fraction of methane as a result. Pore length might also affect the FT performance. Long pores can lead not only to high CO and  $H_2$  concentration gradients inside the catalyst particle, but also to an increase in the  $H_2/CO$  ratio, which results in a higher selectivity to short-chain hydrocarbons. However, internal mass transfer limitations can be present when using new materials with significantly superior activity or when using catalysts with considerably higher selectivity to wax production, which could result in lower diffusion rates. Mesostructured materials based on silica have been synthesized in order to facilitate the diffusion of reactants and products. However, these structures can result in large pore lengths, as in the case of MCM-41 and SBA-15, even when using catalyst pellet sizes which are not expected to present mass-transfer restrictions<sup>80</sup>.

### *Synthesis of ordered mesoporous silicas*

Ordered Mesoporous Silica (OMS) are synthesized with surfactant-template agents to form different structure arrays. The most studied structures are MCM-41 (Mobil composition matter No 41), SBA-15 (Santa Barbara Amorphous type material) and MCM-48 (Mobil composition matter No 48) characterized by their structure: 1-Dimensional (1D) (parallel channels, accessible in one direction), 2-Dimensional (2D) array (parallel and perpendicular channels interconnected between themselves), 3-Dimensional (3D) cubic array (interconnected pores) (see **Figure 3.2**)<sup>72, 83</sup>. The constant research on increasing the pore size of biodegradable silica due to new application in nanomedicine research such as protein or drug delivery, allowed to expand the pores of MCM-41 and SBA-15 silicas by a micelle expander agent<sup>84</sup>. This subject will be discuss in more detail in chapter 8. Furthermore, new researchers found a different kind of silica called Mesoporous cellular silica foams (MCFs)<sup>85</sup>. This type of silica have a different 3D structure pores than MCM-48. It is formed by uniformly large spherical cell pores interconnected with uniform small window pores (see **Figure 3.3**). The average pore size of MCF can be adjusted in the range of 5–50 nm, and the specific surface area of MCF could reach 1000 m<sup>2</sup>/g. The characteristic of this material is the more open porous networks compared with other conventional porous supports. Recently, MCFs have been used as supports in catalysis and it was found that these catalysts exhibited high performance in several catalytic reactions<sup>85-87</sup>.

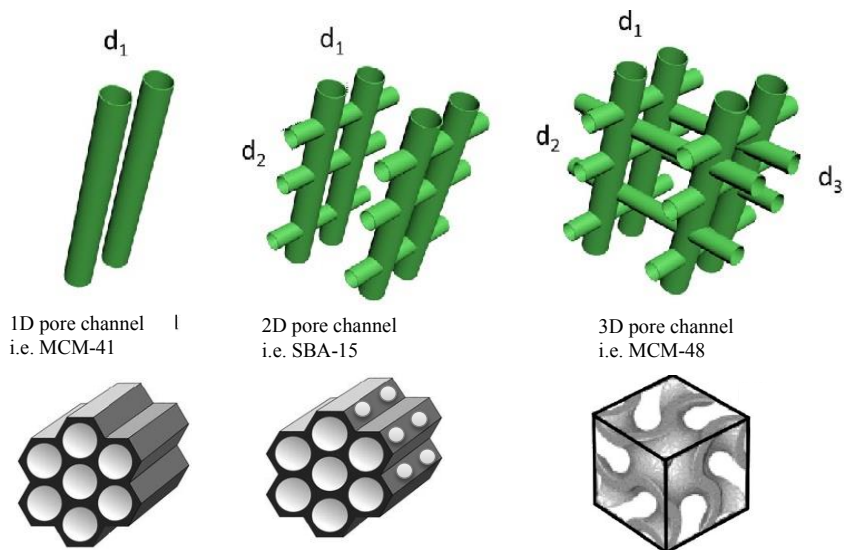
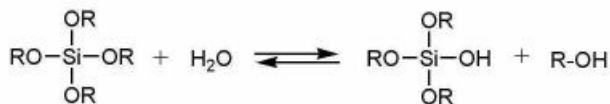


**Figure 3.3:** Schematic representation of silicas with 1D, 2D and 3D pore channel structures (adapted from<sup>78, 88</sup>).

The OMS is formed by a silicon oxide network through polycondensation reactions of a molecular precursor in liquid media; this is the conventional sol-gel synthesis method. Alkoxides are ideal chemical precursors for sol-gel synthesis because they react readily with water (see **Figure 3.4**). The reaction is called hydrolysis, because a hydroxyl ion becomes attached to the silicon atom. Depending on the amount of water and catalyst present, hydrolysis may proceed to completion to silica. Complete hydrolysis often requires an excess of water and/or the use of a hydrolysis catalyst such as acetic acid or hydrochloric acid. Intermediate species including may result as products of partial hydrolysis reactions. Early intermediates result from two partially hydrolysed monomers linked via a siloxane [Si–O–Si] bond. Thus, polymerization is associated with the formation of a 1-, 2-, or 3-dimensional network of siloxane [Si–O–Si] bonds accompanied by the production of H-O-H and R-O-H species. Condensation liberates water or alcohol. This type of reaction can continue to build larger and larger silicon-containing molecules by the process of

polymerization (see **Figure 3.3**). However, a modified version of this technique is the atrane route method developed by Cabrera et al.<sup>89,90</sup>

Step 1: hydrolysis



Step 2: condensation

a) water condensation



b) alcohol condensation



where R is an alkyl chain. For TEOS, R = -CH<sub>2</sub>CH<sub>3</sub>

**Figure 3.4:** Sol-gel reactions

#### *The atrane route*

This method is based on the use of a simple structural directing agent, i.e., cetyltrimethylammonium bromide (CTAB) and a complexing polyalcohol triethanolamine (TEAH<sub>3</sub>). This TEAH<sub>3</sub> forms chelated complexes called atranes, i.e., complexes which include triethanolamine-like ligand species (**Figure 3.5**) with a wide variety of metals (M). The atrane complex is less reactive than a normal organometallic precursor in aqueous solution. Therefore, the hydrolysis and condensation reaction rate of the

inorganic components is slowed down when a metal-atrane complex is used<sup>89-91</sup>. The advantage of synthesizing OMS by this method is that the product results in a more homogeneous ordered material than conventional sol-gel method. In addition, the best advantage was found when mixed ordered mesoporous oxides are desired<sup>90</sup>.

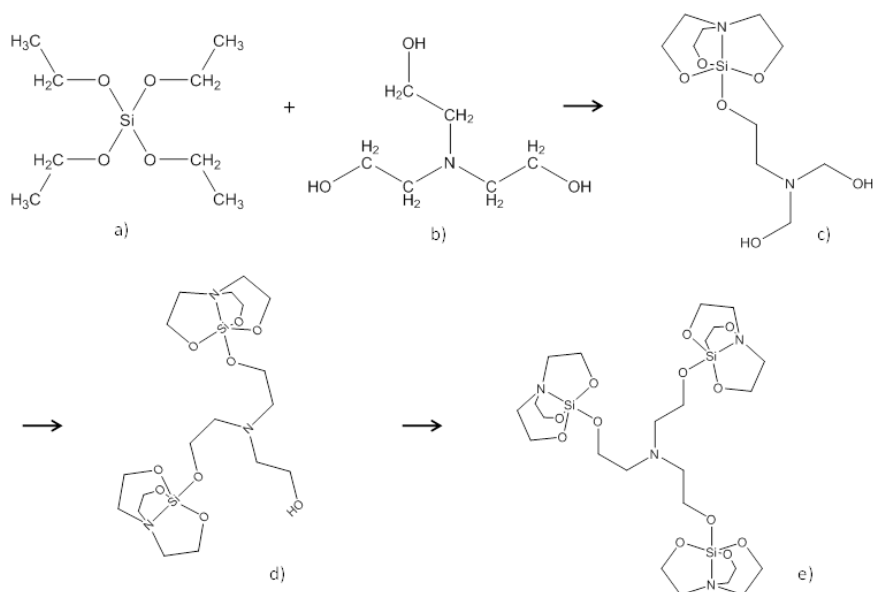


**Figure 3.5** Silatrane oligomer molecular structures: a) Triethylortosilicate precursor (TEOS), b) Triethanolamine TEAH<sub>3</sub> complexing agent c) monomers [Si(TEA)<sub>2</sub>H<sub>2</sub>], d) dimer [Si<sub>2</sub>(TEA)<sub>3</sub>H], e) trimer [Si<sub>3</sub>(TEA)<sub>4</sub>]. For a better understanding of the structures, the hydrogen atoms were eliminated.

As shown previously, the use of mesoporous materials for cobalt catalyst supports have been more studied than nanoparticles, when applied in FTS. However, there is still room for more research on this topic. Based on the studies reported previously, it was found that the pore size of the support is important not only for the cobalt particle size but also for the diffusion limitation on the reactants and products. Herein, it seems very interesting to synthesize silicas with 3D structure by the atrane route.



## **Part II: Experimental**



## Chapter 4

### Support and catalyst preparation (Papers II-V)

#### 4.1 Support synthesis

This section is divided into conventional and non-conventional supports. The first one corresponds to a commercial alumina and its corresponding promoted alumina. The second one refers to alumina synthesized in the form of nanoparticles and ordered mesoporous silicas.

#### 4.2 Conventional supports

A commercial gamma alumina  $\gamma\text{-Al}_2\text{O}_3$  (Versal alumina 250) was dried for 5 h at 80 °C and calcined at 550 °C at a heating rate of 10 °C/min for 6 h in air. This was the support for preparing the  $\text{Co}/\text{Al}_2\text{O}_3$  catalyst. The same alumina was used to prepare the promoted supports.  $\text{Ce-Al}_2\text{O}_3(\text{IM})$  and  $\text{Zr-Al}_2\text{O}_3(\text{IM})$  were prepared by incipient wetness impregnation with  $\text{Ce}(\text{NO}_3)_4 \cdot 6 \text{H}_2\text{O}$  and  $\text{ZrO}(\text{NO}_3)_2$  aqueous solutions, respectively, (molar ratio  $\text{Al}:\text{promoter} = 8$ ) added dropwise to the alumina. IM denotes the impregnation method. The materials were dried at 80 °C for 5 h and calcined at 550 °C.

#### 4.3 Non-conventional supports

The non-conventional supports are referred to the synthesis of alumina nanoparticles and ordered mesoporous silicas. The support was modified by two kinds of promoters: one, structural promoter, which is obtained by changing the pore structure of the support and two, chemical promoter, obtained by the addition of Zr or Ce to the alumina or silica support. In particular, concerning the structural promoter, the morphology of the supports, i.e.  $\text{Al}_2\text{O}_3$  nanoparticles and ordered mesoporous  $\text{SiO}_2$  (with various pore size diameter) were investigated in order to evaluate their influence on the final cobalt catalyst. Concerning the incorporation of

chemical promoters, i.e. Ce and Zr, two methods of promoter incorporation were evaluated: one, impregnation of the promoter on commercial alumina and two, co-precipitation of promoter and the support precursor (Al- or Si-precursor).

### 4.3.1 Nanoparticle supports Ce-Al<sub>2</sub>O<sub>3</sub> and Zr-Al<sub>2</sub>O<sub>3</sub> synthesis

Two types of nanoparticles were prepared, one pure Al<sub>2</sub>O<sub>3</sub>(ME) and the second one promoted alumina nanoparticles (Ce-Al<sub>2</sub>O<sub>3</sub>(ME) and Zr-Al<sub>2</sub>O<sub>3</sub>(ME)). ME denotes the synthesis by microemulsion.

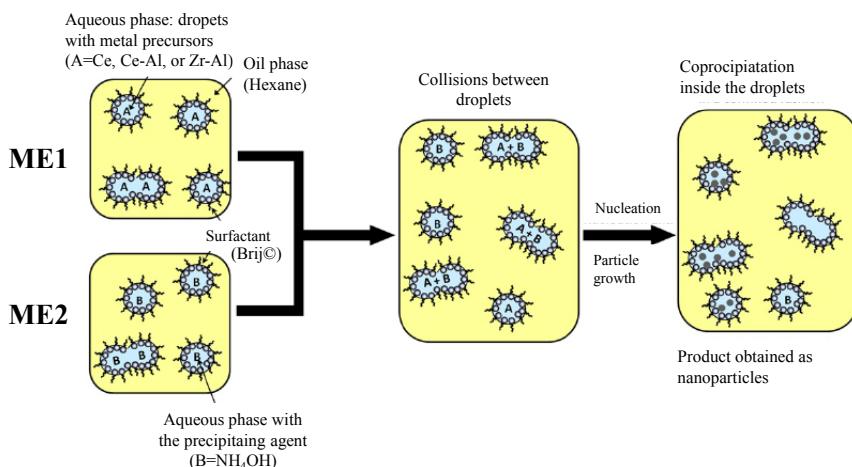


**Figure 4.1:** Main steps for the synthesis of nanoparticles co-precipitated in water-in-oil microemulsion.

In order to synthesize these materials, two water-in-oil microemulsion solutions (microemulsion 1 ME1 and microemulsion 2 ME2) (Table 4.1) were mixed. ME1 contained the metal precursor(s) (Al, Zr and Al or Ce and Al with a molar ratio Al : promoter = 8) while ME2 contained the precipitating agent NH<sub>4</sub>OH. ME2 was added to ME1 dropwise under continuous stirring at 30 °C until pH 9 was reached. The solution was kept at constant conditions for 12 h to complete the reaction. The final solution was destabilized with acetone and the solid product was separated by

centrifugation and washed with acetone and water. The product was freeze-dried in order to avoid particle agglomeration. Afterwards, the product was calcined in air for 6 h at 550 °C (heating rate 10°C/min). The obtained materials were labelled Zr-Al<sub>2</sub>O<sub>3</sub>(ME) and Ce-Al<sub>2</sub>O<sub>3</sub>(ME).

**Table 4.1.** Composition of the water-in-oil W/O microemulsion system.

ME	Phase	Compound(s)	Composition (wt%)
ME1	Oil	Hexane	65.7
	Surfactant	Brij©	26.4
	Aqueous solution	(1 Molar AlCl <sub>3</sub> ·6H <sub>2</sub> O-promoter nitrate molar ratio of Promoter/Al = 1:8)	7.9
ME2	Oil	Hexane	65.7
	Surfactant	Brij©	26.4
	Aqueous solution	(NH <sub>4</sub> OH 38 wt%)	7.9

### 4.3.2 Ordered mesoporous silicas

#### *Synthesis of MCM-41 and pore-expanded MCM-41*

The “Atrane Route” was used to prepare mesoporous silica MCM-41<sup>90</sup>. This method uses cetyltrimethylammonium bromide (CTAB) as a structural directing agent, tetraethyortosilicate (TEOS) as a metal precursor, and 2,2',2"-nitriletriethanol (triethanolamine, TEAH<sub>3</sub>) as a complexing polyalcohol which regulates the hydrolysis rate<sup>83, 89, 90</sup>. The

synthesis of PE-MCM-41 is developed in the same manner as MCM-41, with the difference of adding triisopropylbenzene as a surfactant micelle expander. The main steps for the preparation of MCM-41 and PE-MCM-41 are shown in **Figure 4.2**.

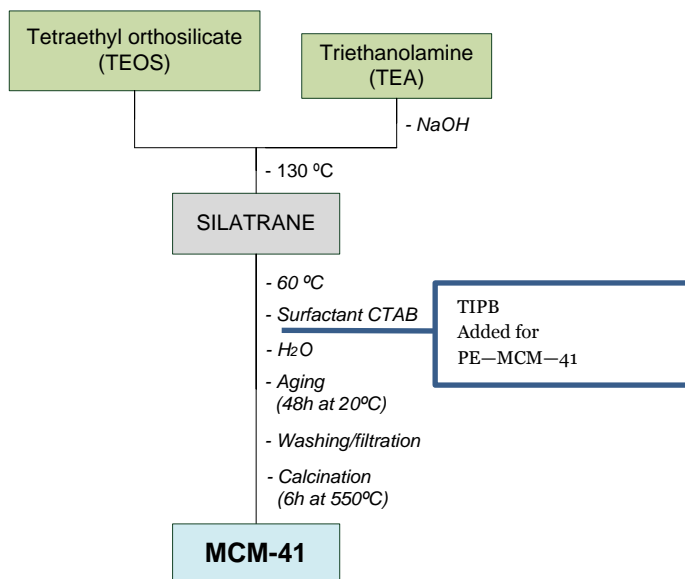


**Figure 4.2:** Main steps for the preparation of MCM-41 and PE-MCM-41 via the “Atrane Route” Elaborated from references<sup>83, 89, 90</sup>.

The molar ratios were 4 TEA : 1 TEOS : 1 NaOH: 0.1 CTAB: 90 H<sub>2</sub>O and 0.05 TIPB for PE-MCM-41 silica.

#### *Synthesis of SBA-15 and pore-expanded SBA-15 silicas*

The SBA-15 was synthesized by dissolving the surfactant P123 ( $M_{av} = 5800$ , EO20-PO70-EO20) in 2 M HCl solution. A homogeneous solution was obtained after stirring at 40 °C for 3 h. Afterwards, the silatrane complex (similar to the one used previously for MCM 41 synthesis), was

added to the solution under vigorous stirring and kept for 12 h at the same conditions. The final product was kept aging for 24 h at room temperature. The pore-expanded SBA-15 (PE-SBA-15) was prepared in the same way as the SBA-15 with the single exception that the swelling agent 1,3,5-trimethylbenzene (TMB) was added to the synthesis solution prior to the addition of the silatrane complex. TMB works as a micelle expander. The final solution was aged at 70 °C for 24 h. The employed molar ratios were: 0.017 P123: 0.0054 TMB: 4.35 HCl: 183 H<sub>2</sub>O: 1 TEOS.

In all the cases, the precipitated solid was separated from the liquid waste by filtration and washed repeatedly with water and ethanol. The materials were dried for 12 h at 70 °C and the organic compounds were removed from the solid by calcination (5 h at 120 °C, then 3 h at 350 °C and 5 h at 550 °C) with a temperature ramp of 5 °C/min in air.

#### *Synthesis of MCF and Zr-MCF silica synthesized by the atrane route*

First, the atrane complexes were prepared as follows: TEOS (tetraethyl orthosilicate Si(OC<sub>2</sub>H<sub>5</sub>)<sub>4</sub>) was added to TEAH<sub>3</sub> (triethanolamine, N(CH<sub>2</sub>-CH<sub>2</sub>-OH)<sub>3</sub>) and heated at 140 °C for 20 min under stirring in order to form silatrane complexes (Zr was also added from Zirconium(IV) tert-butoxide 98 % when required).

The MCF silica was prepared in the same way as SBA-15 with the difference that prior to the addition of the metal-atrane complex the swelling agent 1,3,5-trimethylbenzene (TMB) was added to the synthesis solution as a micelle expander<sup>92</sup>. In order to expand the window pore diameter, NH<sub>4</sub>F was added when required. The final solution was kept at 70 °C for 24 h without agitation.

The employed molar ratios of the reactants in the synthesis were: 0.017P123: 0.0054TMB: 4.35HCl: 0.029NH<sub>4</sub>F: 183H<sub>2</sub>O: 1 TEOS. The molar ratio when Zr and Si were used was Si/Zr=8.

In all the cases, the precipitated solid was separated from the liquid waste by filtration and washed repeatedly with water and ethanol. The material was dried for 12 h at 70 °C and the organic compounds were removed from the solid through calcination (5 h at 120 °C, then 3 h at 350 °C and 5 h at 550 °C).

#### **4.4 Catalyst preparation**

All the described materials were used as supports for preparation of cobalt catalysts. An aqueous solution of  $\text{Co}(\text{NO}_3)_2 \cdot 6\text{H}_2\text{O}$  was impregnated on the supports by the incipient wetness method. After impregnation, the catalysts were dried at 120 °C for 6 h and then calcined at 350°C for 10 h. The total metal loading was 12 wt.% Co.

## Chapter 5

### Catalyst characterization

#### 5.1 N<sub>2</sub> physisorption

N<sub>2</sub> physisorption analyses were carried out using a Micromeritics ASAP 2000 instrument and the Brunauer-Emmett-Teller (BET) method was used to calculate the surface areas. The Barrett-Joyner-Halenda (BJH) method was used to calculate the pore size and pore volume from the desorption isotherm.

#### 5.2. X-ray Diffraction (XRD)

X-ray diffraction (XRD) of the fresh samples was performed on a Siemens D5000 X-ray diffractometer with Cu K $\alpha$  radiation (40 kV, 30 mA). The measurements were recorded from 10° to 90° in the 2 $\theta$  range using a step size of 0.020° and a step time of 12 s for all the samples. The phases were identified by Eva software (version 13.0.0.2, 2007). Crystallite sizes of Co<sub>3</sub>O<sub>4</sub> and CeO<sub>2</sub> were calculated by using the Scherrer equation and by assuming spherical particles<sup>93</sup>. The Co<sup>0</sup> crystallite size was estimated from Co<sub>3</sub>O<sub>4</sub> using the formula  $d(\text{Co}^0) = 0.75 * d(\text{Co}_3\text{O}_4)$ <sup>94,95</sup>.

#### 5.3 H<sub>2</sub> chemisorption

H<sub>2</sub> chemisorption was carried out on a Micromeritics ASAP 2020 instrument. Prior to the analysis, the catalyst sample was reduced with hydrogen. Repeated analyses were made in order to discriminate between the amounts of hydrogen adsorbed via physisorption and chemisorption. The cobalt dispersion (D, %) and the cobalt crystallite size ( $d(\text{Co}^0)$ , nm), was calculated by static hydrogen chemisorption on the reduced catalysts. The measurements were performed on a Micromeritics ASAP 2020 unit at 35 °C, after reducing about 0.15 g of the fresh catalysts using the same conditions as in TPR analysis (H<sub>2</sub> flow at 350 °C (heating rate: 1 °C/min) for 16 h).

## 5.4 Transmission and scanning electron microscopy (TEM)

Transmission electron microscopy (TEM) analysis was performed using a Philips CM300UT-FEG electron microscope with a point resolution of 0.17 nm, information limit of 0.1 nm, which was operated at 200 kV, in which images were acquired with a TVIPS CCD camera. The samples were prepared by immersing a Quantifoil R copper microgrid in fresh catalyst dispersed in ethanol. The morphology of the supports and final catalysts were studied by high resolution-scanning electron microscopy (HR-SEM) using an XHR-SEM Magellan 400 instrument supplied by the FEI Company. The samples were investigated using a low accelerating voltage and no conductive coating.

## 5.5 Temperature programmed reduction (TPR)

The reducibility of the catalysts was investigated by hydrogen temperature-programmed reduction (TPR) <sup>6</sup>. The calcined catalysts (0.15 g) were studied in a Micromeritics Autochem 2910 flowing 5 vol% H<sub>2</sub> in Ar in a range of temperatures from 30 °C to 930 °C (heating rate: 10 °C/min). The H<sub>2</sub> consumption was monitored during the experiment by the difference in thermal conductivity between the inlet and outlet gases. The degree of reduction (DOR, %) was calculated using H<sub>2</sub> TPR of the *in situ* reduced catalysts. Fresh catalyst, 0.15 g, was reduced at 350 °C (1 °C /min) for 16 h in flowing H<sub>2</sub>, then flushed with helium for 30 min. Afterwards, the helium was changed to 5 vol % H<sub>2</sub> in Ar and the temperature was increased from 350 to 930 °C (10 °C /min) and the H<sub>2</sub> consumption was monitored. The TCD was calibrated with Ag<sub>2</sub>O as standard. The DOR was calculated assuming that unreduced cobalt after the reduction pre-treatment was in the form of Co<sup>2+</sup> according to:

$$DOR = 1 - \frac{ATCD \times f}{XCo \div AWCo}$$

where AT<sub>TCD</sub> is the integration of the TCD signal, normalized per mass catalyst; AW<sub>Co</sub> is the atomic weight of Co (58.9 g/mol), f is a calibration

factor correlating the area of the TCD signal and the H<sub>2</sub> consumed; X<sub>Co</sub> is the cobalt loading (12% Co).

The Co<sup>0</sup> particle size was calculated using the formula  $d(\text{Co}^0) = (96/D)*\text{DOR}$ .



## Chapter 6

### 6. Fischer-Tropsch experiments

In this chapter, the equipment and procedures used in the high-pressure catalytic tests are presented (Papers II-IV).

#### 6.1 Set-up and experimental procedure

The FT synthesis was carried out in a down-flow stainless-steel fixed-bed reactor (i.d. 9 mm). The reactor tube was heated by a furnace, regulated by a cascade temperature controller with one sliding thermocouple in the catalyst bed and another one placed in the furnace. This system, together with an aluminum jacket placed outside the reactor, allowed for an even temperature profile along the catalyst bed ( $\pm 1$  °C). The gases were purified from residual contaminants that could poison the catalysts by means of traps upstream the reactor. The reaction products were separated by means of two consecutive traps. The heavy hydrocarbons and most of the water were condensed in the first one kept at 393 K, while lighter HCs were collected in the second one at room temperature. The product gases leaving the traps were depressurized and analysed on-line by means of a gas chromatograph (GC) Agilent 6890. A detailed description of the experimental rig is given in **Figure 6.1**. Usually a catalyst loading between 0.7-2 g (pellet size: 53-90  $\mu\text{m}$ ) diluted with SiC (average pellet size: 75  $\mu\text{m}$ ) was used. The weight ratio between the catalyst and the SiC was 1:5.

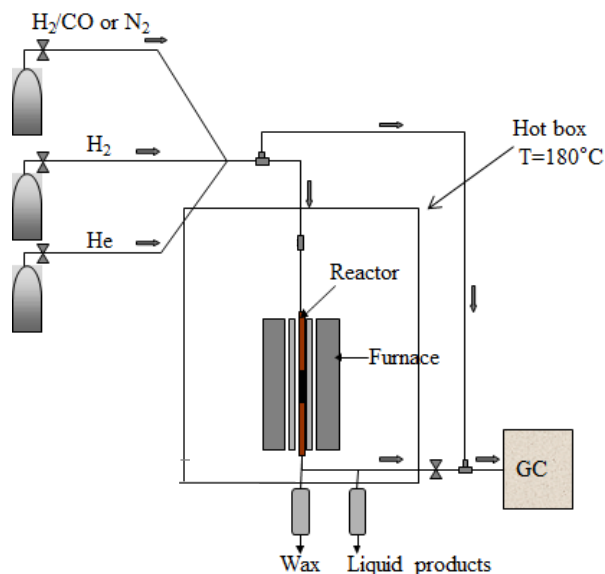


**Figure 6.1:** Simplified scheme of the Fischer-Tropsch reactor

The reference case process conditions were:  $T=483$  K, pressure syngas=20 bar,  $H_2/CO=2.1$ . Prior to catalytic testing, the reactor was pressurized with He and tested for leaks. Subsequently, the system was depressurized to atmospheric pressure and the catalyst was reduced. After reduction, the catalyst was cooled to 453 K and the gas lines were flushed with He for 30 minutes. Then the system was pressurized to 20 bar (or 30 bar, in some cases) in He flow. When the system pressure was stabilized, the flow was switched to the reactant mixture. The syngas contained 3 mol%  $N_2$  as internal standard. Subsequently, the temperature was slowly increased to 483 K (0.15 K/min). In the experimental campaigns of Papers II-V, a first period at higher gas hourly space velocity (GHSV= 2,000-6,000  $Ncm^3/g Co_{cat}, h$ ) was held for 24 h followed by a second period where the space velocity was lowered to reach a higher CO conversion ( $30\pm 3\%$ , for Papers II-V).

## 6.2 Product analysis and data treatment

The heavy hydrocarbons and most of the water were condensed in two traps kept at 120 °C and room temperature, respectively. The product gases leaving the traps were depressurized and analysed on-line with a gas chromatograph (GC), Agilent 6890, equipped with a thermal conductivity detector (TCD) and a flame ionization detector (FID). H<sub>2</sub>, N<sub>2</sub>, CO, CH<sub>4</sub>, and CO<sub>2</sub> were separated by a Carbosieve II packed column and analysed on the TCD. The percentage of CO conversion was calculated by:

$$CO_{conv}(mol\%) = \frac{CO_{in} - CO_{out}}{CO_{in}} \times 100$$

C<sub>1</sub>–C<sub>6</sub> products were separated by an alumina-plot column and quantified on the FID detector, from which it was possible to determine the C<sub>5+</sub> selectivity (S<sub>C5+</sub>). The CO<sub>2</sub>-free S<sub>C5+</sub> (i.e., S<sub>C5+</sub> if excluding CO<sub>2</sub> from the C-atom balance) is defined as follows<sup>97, 98</sup>:

$$S_{C5+} = 100 - (S_{C1} + S_{C2} + S_{C3} + S_{C4})_{CO_2 \text{ free}}$$



## **Part III: Results and discussions**



## Chapter 7

### **Co/Al<sub>2</sub>O<sub>3</sub> catalysts promoted with Ce and Zr for Fischer-Tropsch synthesis (Papers II and III)**

This chapter summarizes the results from papers II and III. Some of the results presented have not been published, but are discussed here in order to give a general context of the study. The effect of zirconium and cerium promotion on the performance of the Co/Al<sub>2</sub>O<sub>3</sub> catalyst was evaluated in the Fischer-Tropsch synthesis (FTS). The cobalt supports: Al<sub>2</sub>O<sub>3</sub>, Ce-Al<sub>2</sub>O<sub>3</sub> and Zr-Al<sub>2</sub>O<sub>3</sub> were prepared by two different methods: precipitation of the metal precursor(s) in water-in-oil microemulsion (denoted by ME) and aqueous impregnation of the promoters on commercial alumina (denoted by IM), as explained in chapter 4. The focus of this study was on the support effect on the physicochemical and catalytic properties of the final cobalt catalyst. The cobalt supports variations were:

- Commercial alumina with structural porosity vs. synthesized alumina nanoparticles with textural porosity.
- Cerium vs. zirconium promoter on alumina.
- Method of promoter incorporation (impregnation vs. co-precipitation)

These supports were impregnated with cobalt, calcined and activated in hydrogen to be tested in Fischer-Tropsch synthesis at close to industrial conditions, as explained in chapters 4 and 6.

#### **7.1 Microemulsion vs. impregnation method**

In general, the most common method for incorporating promoters on a catalyst support is by impregnation of the aqueous metal promoter on the support. However, this method favours a heterogeneous deposition of the promoter and too little study of the dispersion effect on the cobalt catalyst has been reported. The synthesis of promoted alumina by the

microemulsion method has not been investigated before. Thus it seems attractive to explore its development and application. This method is attractive for the synthesis of nanoparticles with more than one component, in our case, the synthesis of bimetallic oxides such as Ce-Al and Zr-Al oxides. The advantage is that the water droplets in the microemulsion work as nanoreactors where the formation of new materials can take place. In this way, the formation of homogeneously mixed oxide particles in the nano-size range can be produced. The advantages of using nanoparticles and promoters for cobalt catalysts have been discussed previously.

## **7.2 Synthesis of Al<sub>2</sub>O<sub>3</sub>, Zr-Al<sub>2</sub>O<sub>3</sub> and Ce-Al<sub>2</sub>O<sub>3</sub> by water-in-oil microemulsion method**

As was explained before, a microemulsion is a system composed of water, oil and surfactant. In order to use it as a confined reactor for the synthesis of materials, it needs to be stable, before, during and after the reaction. Therefore, the proper concentration of the salts, system composition (water, oil and surfactant) and temperature need to be investigated. A stable microemulsion was found at 30 °C with specific water/Brij©/hexane weight ratio of 7.9/26.4/65.7 (see **Table 4.1**). The material synthesized by this method is formed by collision and coalescence of water droplets from ME1 (containing the reactant salts) and ME2 (containing the precipitating agent) (see **Figure 4.1**). In the case of the promoted alumina, the chemical reaction produces oxo-hydroxo metal complexes of the promoter and aluminium. The concentration of these complexes reaches a critical supersaturation which favors the nucleation and formation of very small particles inside the water droplets. These particles will grow by monomer addition of oxo-hydroxo complexes and coalescence.<sup>99</sup>

The main interest of synthesizing these materials by the ME method was to have a good dispersion of the promoter into the alumina support. Since the co-precipitation of the two metals is simultaneous, the purpose is achieved and additionally the particles grow uniformly.

The synthesized materials were compared with commercial alumina Versal 250 impregnated with Ce and Zr promoters. The differences in the physicochemical characteristics from these materials are explained in the following sections.

### **7.3 Characterization of the nanoparticle supports**

Qualitatively, the materials prepared by the microemulsion (ME) have more homogeneous morphology and particle sizes than the corresponding impregnated samples as can be seen in **Figures 7.1** and **7.2**. The nature of the preparation route can be responsible for this difference. In the case of the impregnated supports, i.e. Zr-Al<sub>2</sub>O<sub>3</sub>(IM) and Ce-Al<sub>2</sub>O<sub>3</sub>(IM), particles of several sizes are agglomerated and form pellets of different sizes. However, neither impregnation nor ME supports show any visible changes in the SEM pictures after cobalt impregnation.

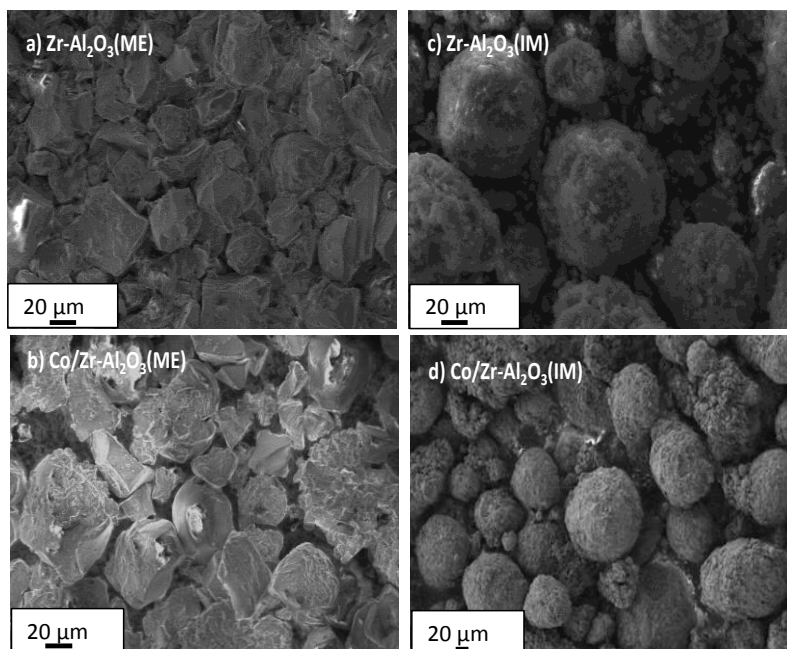


**Figure 7.1:** SEM pictures for a)  $\text{Zr-Al}_2\text{O}_3(\text{ME})$ , b)  $\text{Co/Zr-Al}_2\text{O}_3(\text{ME})$ , c)  $\text{Zr-Al}_2\text{O}_3(\text{IM})$ , d)  $\text{Co/Zr-Al}_2\text{O}_3(\text{IM})$ .

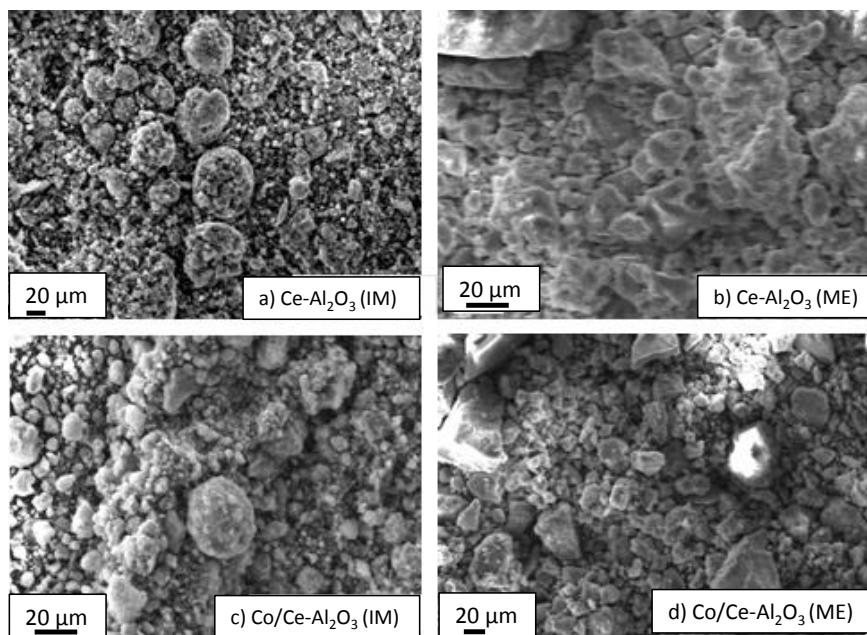


**Figure 7.2:** SEM pictures for a)  $\text{Ce-Al}_2\text{O}_3(\text{IM})$ , b)  $\text{Ce-Al}_2\text{O}_3(\text{ME})$ , c)  $\text{Co/Ce-Al}_2\text{O}_3(\text{IM})$  and d)  $\text{Co/Ce-Al}_2\text{O}_3(\text{ME})$ .

TEM pictures of  $\text{Co/Al}_2\text{O}_3(\text{IM})$  and  $\text{Ce-Al}_2\text{O}_3(\text{ME})$ 550 are shown in **Figure 7.3**. These pictures exemplify the different morphologies of the commercial alumina and of the ME materials. The commercial alumina appears to be composed of needle-like alumina crystallites in random directions (see **Figure 7.3a**), while the ME material shows a more repetitive pattern of agglomerated nanoparticles (see **Figure 7.3b**). The average nanoparticle size of the ME material is around 4-7 nm, while that of the commercial alumina is around 3 nm according to the manufacturer.

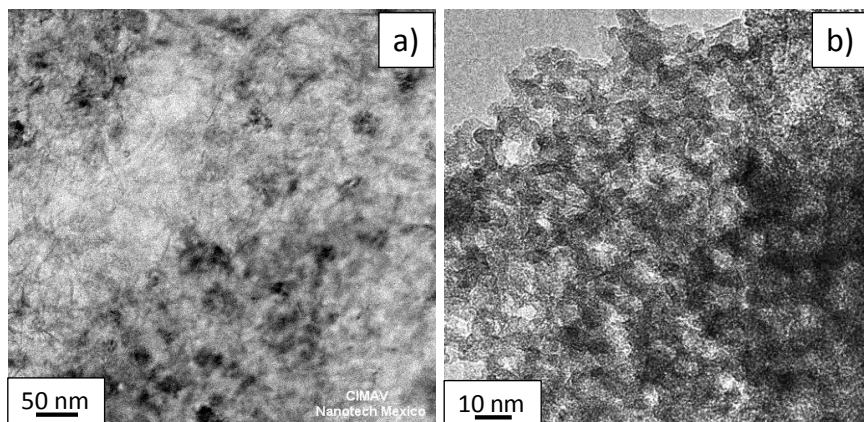


**Figure 7.3:** TEM pictures for a) Co/Al<sub>2</sub>O<sub>3</sub>(IM), b) Ce-Al<sub>2</sub>O<sub>3</sub>(ME)550.

**Figures 7.4** and **7.5** show the results from X-ray diffraction technique and leads to the following conclusions:

First of all,  $\gamma$ -Al<sub>2</sub>O<sub>3</sub> starts to be form at 550 °C by the ME method. These data are interesting since the gamma alumina structure is normally formed at temperatures between 720 °C and 1050 °C. Second, the promoters in the Zr-Al<sub>2</sub>O<sub>3</sub>(ME) and Ce-Al<sub>2</sub>O<sub>3</sub>(ME) materials are very well dispersed since no peaks corresponding to CeO<sub>2</sub> and ZrO<sub>2</sub> are present when the materials are calcined at 550 °C. Furthermore, the promoters seemingly hinder the formation of crystalline  $\gamma$ -Al<sub>2</sub>O<sub>3</sub>, possibly by forming amorphous mixed oxides. Third, when the ME material Ce-Al<sub>2</sub>O<sub>3</sub>(ME) is calcined at 800 °C, crystalline CeO<sub>2</sub> is formed. This result is very interesting since the ME method permits particle growth control of the promoter with an easily adjustable parameter such as the temperature. Fourth, crystalline CeO<sub>2</sub> is present in the Ce-promoted IM material, while a less crystalline metastable ZrO<sub>2</sub> is formed in the Zr-promoted counterpart. Fifth, crystalline Co<sub>3</sub>O<sub>4</sub> is formed in all of the samples except for in Co/Al<sub>2</sub>O<sub>3</sub>(ME). The crystallite sizes of Co<sub>3</sub>O<sub>4</sub> depend on the nature of the support, which will be discussed later on. Possibly, the introduction of promoters in the ME materials decreases the cobalt-support interaction,

prevents the formation of cobalt aluminate and, hence, brings about the formation of  $\text{Co}_3\text{O}_4$ .

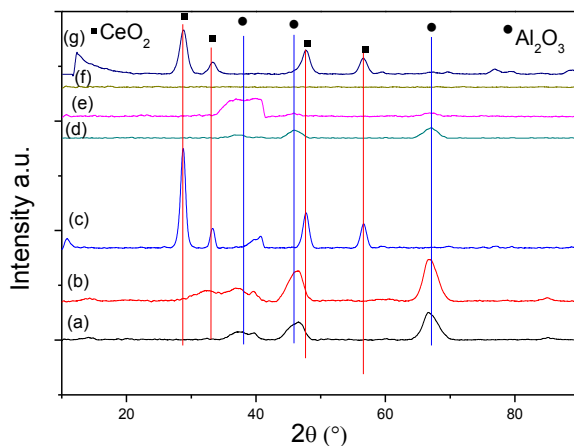


**Figure 7.4:** X-ray diffractograms for the impregnated and co-precipitated supports a)  $\text{Y-Al}_2\text{O}_3$ , b)  $\text{Zr-Al}_2\text{O}_3(\text{IM})$ , c)  $\text{Ce-Al}_2\text{O}_3(\text{IM})$ , d)  $\text{Al}_2\text{O}_3(\text{ME})$ , e)  $\text{Zr-Al}_2\text{O}_3(\text{ME})$ , f)  $\text{Ce-Al}_2\text{O}_3(\text{ME})550$ , and g)  $\text{Ce-Al}_2\text{O}_3(\text{ME})800$ .

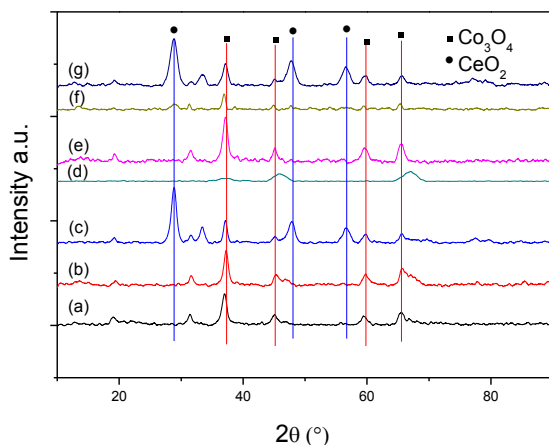


**Figure 7.5:** X-ray diffractograms for the cobalt catalysts.

a)  $\text{Co/Y-Al}_2\text{O}_3(\text{IM})$ , b)  $\text{Co/Zr-Al}_2\text{O}_3(\text{IM})$ , c)  $\text{Co/Ce-Al}_2\text{O}_3(\text{IM})$ , d)  $\text{Co/Al}_2\text{O}_3(\text{ME})$ , e)  $\text{Co/Zr-Al}_2\text{O}_3(\text{ME})$ , f)  $\text{Co/Ce-Al}_2\text{O}_3(\text{ME})550$ , and g)  $\text{Co/Ce-Al}_2\text{O}_3(\text{ME})800$ .

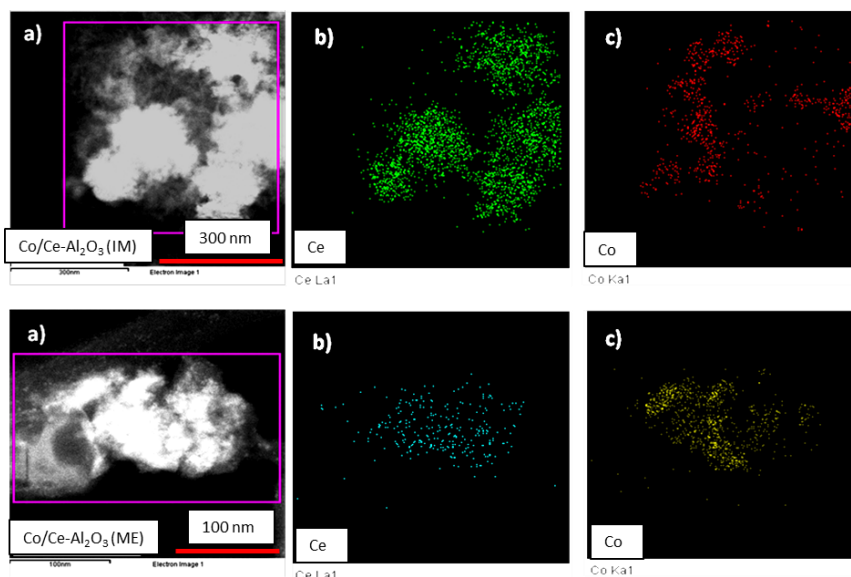


**Figure 7.6:** EDX elemental mapping for  $\text{Co/Ce-Al}_2\text{O}_3(\text{IM})$  and  $\text{Co/Ce-Al}_2\text{O}_3(\text{ME})550$  samples (a) bright field image; (b) Ce mapping; (c) Co mapping.

The EDX spectra for Al and Ce or Zr show an Al/Ce/Co atomic ratio similar to the initial values of Al/Ce and Al/Zr close to 8. Furthermore, the distribution of the promoters on  $\text{Al}_2\text{O}_3$  analysed by EDX elemental mapping in **Figure 7.6** is heterogeneous for the impregnated material and very homogeneous for the microemulsion materials. The mapping for Zr and Ce look similar, thus just Ce is taken as an example. Cerium seems to form large islands rich in  $\text{CeO}_2$  in the  $\text{Co/Ce-Al}_2\text{O}_3(\text{IM})$  which is expected, due to the used preparation method. On the other hand, the microemulsion method disperses the cerium promoter very well. This is the reason why it was not detected by XRD when the material was calcined at  $550\text{ }^\circ\text{C}$ .

The  $\text{N}_2$  physisorption results are presented in **Table 7.1**. The most obvious difference between the samples prepared from commercial alumina and the ME materials are the significantly smaller pore diameters and lower pore volumes of the latter. This, together with the TEM picture (**Figure 7.3b**), suggests that in the ME samples, the primary oxide nanoparticles are

tightly packed together into larger aggregates, and the porosity is probably caused by the interstices between these aggregates (textural porosity). According to the manufacturer, the commercial alumina consists of 3 nm crystallites fused together to a secondary porous structure (structural porosity). The incorporation of a promoter on commercial alumina (by impregnation) leads to a decrease in BET surface area and pore volume (**Table 7.1**), due to partial pore blockage with metal oxides inside the small pores<sup>100, 101</sup>, while the BET and pore volumes are rather increased in the ME materials. For all supports, incorporation of Co reduces the BET and pore volume.

**Table 7.1** N<sub>2</sub> physisorption results for the supports and catalysts.

N <sub>2</sub> Physisorption						
Support	BET		Total		Average	
	Surface area (m <sup>2</sup> /g)	Pore volume <sup>a</sup> (cm <sup>3</sup> /g)	Pore volume <sup>a</sup> (cm <sup>3</sup> /g)	Pore diameter <sup>b</sup> (nm)	Surface area (m <sup>2</sup> /g)	Pore diameter <sup>b</sup> (nm)
Al <sub>2</sub> O <sub>3</sub> (ME)	174	0.2	0.2	3.5	151	3.0
Zr-Al <sub>2</sub> O <sub>3</sub> (ME)	211	0.3	0.3	6.5	191	5.8
Ce-	235	0.4	0.4	6.0	199	4.0
Al <sub>2</sub> O <sub>3</sub> 500(ME)						
Ce-	206	0.3	0.3	3.8	175	3.8
Al <sub>2</sub> O <sub>3</sub> 800(ME)						
Al <sub>2</sub> O <sub>3</sub> (IM)	283	1.1	1.1	14.7	248	14.0
Zr-Al <sub>2</sub> O <sub>3</sub> (IM)	239	0.8	0.8	14.0	227	12.7
Ce-Al <sub>2</sub> O <sub>3</sub> (IM)	198	0.7	0.7	14.7	168	14.1

<sup>a</sup> Determined from a single point of adsorption at P/P<sup>0</sup>=0.998.

<sup>b</sup> Estimated by BJH formalism (adsorption branch).

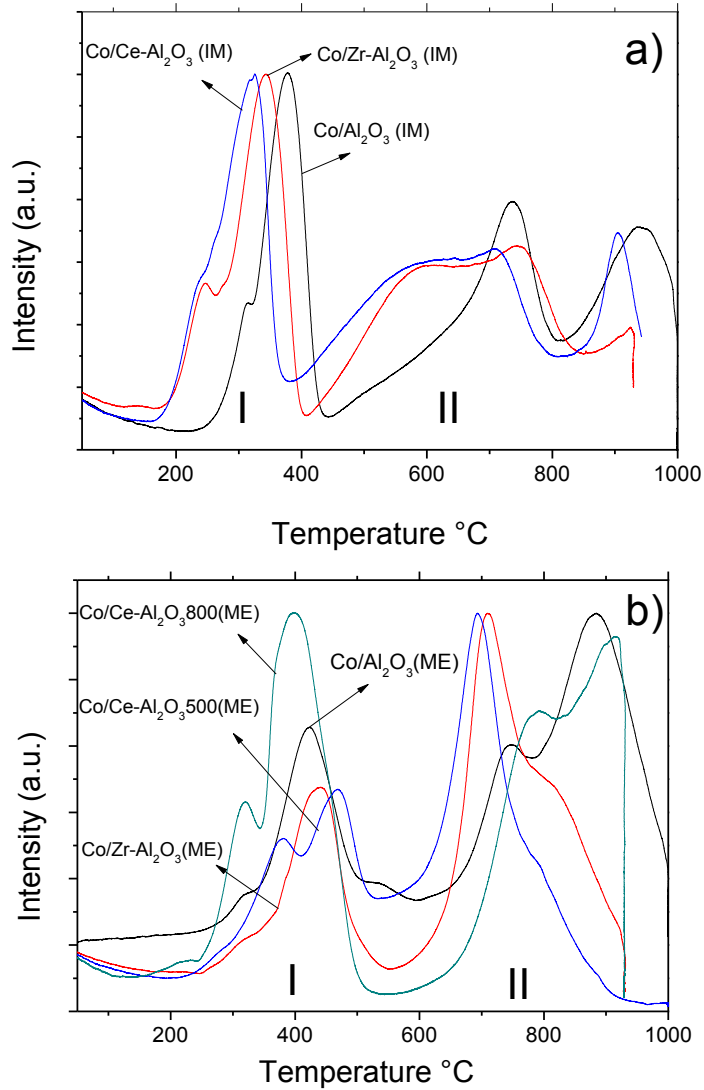


**Figure 7.7:** H<sub>2</sub> TPR profiles of the cobalt catalysts calcined at 350 °C for 10 h) a) supports prepared by impregnation and b) supports prepared by microemulsion.

A comparison of the reduction temperature profiles for the final catalysts is shown in **Figure 7.7**. It is generally accepted that  $\text{Co}_3\text{O}_4$  is reduced in two steps: the first one ( $\text{Co}_3\text{O}_4 + \text{H}_2 \rightarrow 3\text{CoO} + \text{H}_2\text{O}$ ) corresponds to the peak near  $300^\circ\text{C}$ , which is not affected by external factors such as morphology,  $\text{Co}_3\text{O}_4$  particle size and surface area of the catalyst<sup>102</sup>. The second step at temperatures higher than  $\sim 400^\circ\text{C}$  ( $3\text{CoO} + 3\text{H}_2 \rightarrow 3\text{Co}^0 + 3\text{H}_2\text{O}$ ) is more sensitive to the support, particle size, particle-support interaction, reductant flow (rate and composition) and heating rate<sup>103, 104</sup>. It may extend up to around  $800^\circ\text{C}$  for small CoO particles strongly interacting with the support, e.g. when using traditional  $\text{Y-Al}_2\text{O}_3$  supports<sup>103, 104</sup>. However, hydrogen uptake above  $500 - 600^\circ\text{C}$  may also be attributed to the presence of  $\text{Co}^{3+}$  ions in crystallites with a probable stoichiometry of  $\text{Co}_3\text{AlO}_6$  ( $\text{Co}_3\text{O}_4\text{-AlO}_2$ ) or non-stoichiometric spinel structures like  $\text{CoO-Al}_2\text{O}_3$  or spinel structure  $\text{CoAl}_2\text{O}_4$ <sup>105-107</sup>.

The main conclusions derived from **Figure 7.7** are:

- The IM catalysts have reduction profiles typical of Co-based catalysts with conventional supports<sup>103, 104</sup>, where the hydrogen uptakes marked with I and II represent the two-step reduction of  $\text{Co}_3\text{O}_4$ .
- The addition of promoters by the impregnation method to the commercial alumina decreases the reduction temperature of the first step by more than  $50^\circ\text{C}$ . This is believed to be caused by a spill-over effect<sup>108, 109</sup>.
- This is not observed with the ME catalysts calcined at  $550^\circ\text{C}$ , and it is therefore speculated that crystalline phases of  $\text{CeO}_2$  and metastable  $\text{ZrO}_2$  are responsible for the effect.
- Also, in the IM catalysts the promoters shift the second step to lower temperatures. This is attributed to the promoter being mostly deposited on the alumina surface. In this way, cobalt has limited interaction with alumina which led to the formation of larger  $\text{Co}_3\text{O}_4$  crystallites as shown by XRD measurements (**Table 7.2**).

- It appears as if the first reduction step ( $\text{Co}_3\text{O}_4 \rightarrow \text{CoO}$ ) in the ME materials takes place at somewhat higher temperatures than in the IM counterparts. Also, the hydrogen uptake above 600 °C is significantly higher in the former. The lower reducibility of the ME catalysts is attributed to the support nanoparticles being amorphous and the diffusion of cobalt ions into amorphous structures being higher.
- An alternative interpretation of the TPR profiles of the ME catalysts is that both step 1 and 2 of  $\text{Co}_3\text{O}_4$  reduction are completed by 500 °C. In fact, two distinct peaks are visible in this temperature range for the Ce-promoted materials. This interpretation implies that the complete hydrogen uptake up to 500 °C is due to reduction of  $\text{Co}_3\text{O}_4$  to  $\text{Co}^0$ , while the hydrogen uptake above 500 °C is due to reduction of cobalt-support species present in the calcined catalyst. The relative ease of reduction of  $\text{Co}_3\text{O}_4$  to  $\text{Co}^0$  is explained by large  $\text{Co}_3\text{O}_4$  particles on the external surface of the support “pellets” as seen in **Figure 7.8** (see also **Table 7.2**, discussed below), while the low overall reducibility (see DOR in **Table 7.2**) is explained by a large amount of the cobalt in the calcined catalysts being present in compounds others than  $\text{Co}_3\text{O}_4$  (e.g. cobalt aluminates inside the “pellets”).
- The presence of crystalline  $\text{CeO}_2$  micro-domains seems more important than high cerium dispersion for avoiding the formation of cobalt-aluminate species in ME materials. This is seen from the significantly larger hydrogen uptake at temperatures below 500 °C for the  $\text{Co/Ce-Al}_2\text{O}_3(\text{ME})800$  compared with the  $\text{Co/Ce-Al}_2\text{O}_3(\text{ME})550$ . Furthermore, the first peak is shifted to lower temperatures when crystalline  $\text{CeO}_2$  is present, possibly due to a spill-over effect<sup>109</sup>.

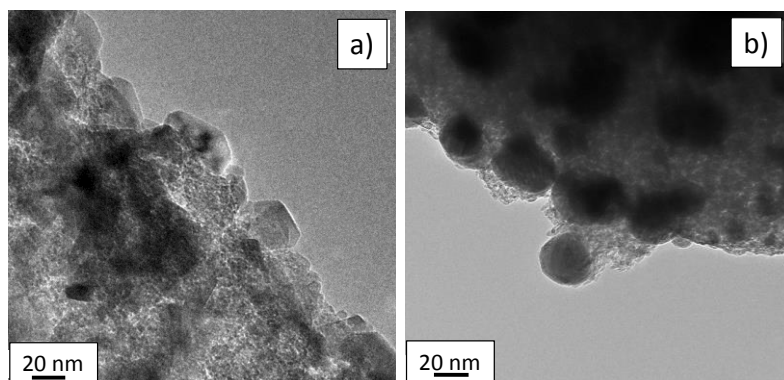


**Figure 7.8:** TEM pictures for a) Co/Ce-Al<sub>2</sub>O<sub>3</sub>(ME)550, b) reduced and passivated Co/Ce-Al<sub>2</sub>O<sub>3</sub>(ME)550.

**Table 7.2** Physicochemical characteristics of the cobalt catalysts.

Catalyst	XRD		Chemisorption		TPR
	Particle size Co <sub>3</sub> O <sub>4</sub> (nm) <sup>a</sup>	Particle size Co <sup>0</sup> (nm) <sup>b</sup>	Particle size Co <sup>0</sup> (nm) <sup>c</sup>	Metal Dispersion %D <sup>d</sup>	DOR <sup>e</sup>
Co/Zr-Al <sub>2</sub> O <sub>3</sub> (ME)	11.3	8.5	14	0.8	11
Co/Ce-Al <sub>2</sub> O <sub>3</sub> 500(ME)	16.2	12	32	0.3	10
Co/Ce-Al <sub>2</sub> O <sub>3</sub> 800(ME)	23.3	17.5	33	1.0	34
Co/Al <sub>2</sub> O <sub>3</sub> (IM)	9.9	7.4	10	3.2	33
Co/Zr-Al <sub>2</sub> O <sub>3</sub> (IM)	11.3	8.5	12	3.8	47
Co/Ce-Al <sub>2</sub> O <sub>3</sub> (IM)	24	18	25	2.3	59

<sup>a</sup> Co<sub>3</sub>O<sub>4</sub> particle size calculated by the Scherrer equation from the X-ray data. <sup>b</sup> According to:  $d(\text{Co}^0) = 0.75 \cdot d(\text{Co}_3\text{O}_4)$ . <sup>c</sup> Calculated from chemisorption and DOR data after reduction at 350 °C for 16h in H<sub>2</sub> according to:  $d(\text{Co}^0)_H = \frac{96}{D} * \text{DOR}$ . <sup>d</sup> Metal dispersion, after reduction at 350 °C for 16h in H<sub>2</sub>. <sup>e</sup> DOR from TPR of reduced catalysts.

The estimated degrees of reduction (DOR) and cobalt dispersion after 16 h at 350 °C in pure H<sub>2</sub> flow are presented in **Table 7.2**. The catalysts using the impregnated promoter presented the highest DOR (59% for Co/Ce-Al<sub>2</sub>O<sub>3</sub>(IM) and 47% for Co/Zr-Al<sub>2</sub>O<sub>3</sub>(IM)) which was expected since the TPR profiles pointed out that the presence of promoters decreased the Co<sub>3</sub>O<sub>4</sub> reduction temperatures. The ME catalysts presented the lowest DOR results supported by the TPR results. These results were improved when the CeO<sub>2</sub> particle size increased as is the case of Co/Ce-Al<sub>2</sub>O<sub>3</sub>(ME)800. The dispersion of Co<sup>0</sup> calculated from H<sub>2</sub> chemisorption in **Table 7.2** is very low for all three ME catalysts due to low DOR and relatively large average cobalt particle size compared to the IM counterparts. The large cobalt particles should logically be located at the external surface of the “pellets” made up of lumped-together support nanoparticle-aggregates, as the pores are very small (4 nm). This preferential deposition of cobalt on the external surface might be the result of an excess amount of aqueous cobalt salt solution used during impregnation. This was necessary since the pore volumes of the supports were smaller than what was required for dissolution of the cobalt precursor.

#### **7.4 Catalytic activity in the Fischer-Tropsch reaction**

The Co/Al<sub>2</sub>O<sub>3</sub>(ME) catalyst results have been excluded from the reported data due to very poor activity and selectivity. These poor results are believed to be due to the absence of Co<sub>3</sub>O<sub>4</sub> in the calcined catalyst and, hence, to the absence of Co<sup>0</sup> in the reduced catalyst. The CO conversion, selectivity to methane (S<sub>CH<sub>4</sub></sub>), selectivity to hydrocarbons with five or more carbon atoms (S<sub>C<sub>5</sub>+</sub>) and selectivity to carbon dioxide (S<sub>CO<sub>2</sub></sub>) for the remaining investigated cobalt catalysts are presented in **Table 7.3**. The catalytic experiments involved two periods. First, the catalysts were tested at a gas hourly space velocity (GHSV) of 6000 cm<sup>3</sup>/h<sub>g</sub> catalyst in order to compare the CO conversion between all the catalysts. The second period the GHSV was adjusted in order to reach 30 ± 4% CO conversion.

**Table 7.3** Conversion levels and selectivity data for the various catalysts

GHSV cm <sup>3</sup> /h,g	Catalysts	X <sub>CO</sub> (%)	S <sup>a</sup> <sub>CH4</sub> (%)	S <sup>a</sup> <sub>C5+</sub> (%)	S <sub>CO2</sub> (%)
6000	Co/Al <sub>2</sub> O <sub>3</sub> (IM)	5.4	12.2	76.3	1.4
1500		27.3	8.6	83.5	1.0
6000	Co/Ce-Al <sub>2</sub> O <sub>3</sub> (IM)	21.7	10.1	80.0	0.7
4900		29.1	8.7	84.6	0.4
6000	Co/Zr-Al <sub>2</sub> O <sub>3</sub> (IM)	12	10	81	1.0
2350		31	7.6	86.0	0.4
6000	Co/Ce-Al <sub>2</sub> O <sub>3</sub> (ME)550	2.3	18.1	62.3	2.2
1000		28.0	13.6	74.4	1.8
6000	Co/Ce-Al <sub>2</sub> O <sub>3</sub> (ME)800	6.5	11.1	73.6	1.2
1800		28.5	9.2	85.2	0.8
6000	Co/Zr-Al <sub>2</sub> O <sub>3</sub> (ME)	4.0	20.0	61.0	3.0
1000		27.	17	67	1.0

<sup>a</sup>Selectivities are CO<sub>2-free</sub>

The CO conversions at 6000 GHSV decrease in the following order: Co/Ce-Al<sub>2</sub>O<sub>3</sub>(IM) > Co/Zr-Al<sub>2</sub>O<sub>3</sub>(IM) > Co/Ce-Al<sub>2</sub>O<sub>3</sub>(ME)800 > Co/Al<sub>2</sub>O<sub>3</sub>(IM) > Co/Zr-Al<sub>2</sub>O<sub>3</sub>(ME) > Co/Ce-Al<sub>2</sub>O<sub>3</sub>(ME)550. From these data the following conclusions can be derived:

- Promoted catalysts prepared by impregnation of the promoter, show a better catalytic performance than the unpromoted Co/Al<sub>2</sub>O<sub>3</sub>(IM) catalyst. This behaviour is mainly related to the enhanced DOR, possibly due to the surface deposition of the promoters resulting in crystalline (or metastable) promoter oxides enabling spill-over of hydrogen.
- The catalysts that used supports prepared by microemulsion have the lowest CO conversion. This is mainly related to the lower DOR as a result of higher cobalt-support interaction and of the lack of crystalline phases of promoter oxides. However, the presence of

promoters improved the FT performance of the ME catalysts, as the Co/Al<sub>2</sub>O<sub>3</sub>(ME) was completely inactive.

- The increase of crystalline micro-domains of CeO<sub>2</sub> in Co/Ce-Al<sub>2</sub>O<sub>3</sub>(ME)800 increased the CO conversion of the catalyst. This result is attributed to the improved DOR as a result of stabilization of the alumina matrix by calcining at higher temperature, i.e. 800 °C, which results in less cobalt-aluminate formation, and of the improved spill-over effect.

The selectivity of the main products from the FT reaction at around 30 % CO conversion is shown in **Table 7.3**. From these results it can be concluded that the S<sub>C5+</sub> increases when the CO conversion increases. This is mainly ascribed to  $\alpha$ -olefin re-adsorption known as a secondary reaction in the FT reaction. It might also be due to the water formation in the FT reaction which is reported to be beneficial for the S<sub>C5+</sub>. This effect is also related to the decrease of methane selectivity, S<sub>CH<sub>4</sub></sub>, which suggests that there is a common intermediate for the FT products formation such as (-CH<sub>2</sub>-). In addition, the selectivity to methane appears higher for the ME-catalysts. This might be attributed to part of the cobalt being present inside the small pores. Previous studies have shown that small pores may provoke the increase of the initial H<sub>2</sub>/CO ratio, i.e. 2.1, due to faster diffusion of H<sub>2</sub><sup>110</sup>. It could also be explained by the tininess of such Co particles (smaller than 6 nm), as it has been shown that such particles have a higher surface coverage of hydrogen<sup>111</sup>.

It is also observed that Co/Zr-Al<sub>2</sub>O<sub>3</sub>(ME) forms more products with lower molecular weight. This result is attributed to the fact that highly dispersed Zr favours the H<sub>2</sub> dissociation, which might favour the easier H insertion into the product intermediates.

A lower selectivity to CO<sub>2</sub> is observed when CeO<sub>2</sub> is present in the catalyst support (see **Table 7.3**). This is explained by the cerium capacity of storing oxygen. In other words, the CO dissociation on the metallic cobalt will lead to active oxygens atoms (O\*) on the surface ready to react, which might react with CO and form CO<sub>2</sub>. In the presence of Ce, the CO<sub>2</sub> might

be caught by the oxygen vacancies in the  $\text{CeO}_{2-x}$  and form  $\text{CeO}_2$  and the  $\text{CO}_2$  concentration might decrease.<sup>112</sup>

## 7.5 Conclusions

The main conclusions of this work can be summarized in the following points:

About the supports:

- To our knowledge, this is the first time Ce- and Zr-alumina nanoparticles have been successfully synthesized by co-precipitation in water-in-oil microemulsion.
- The ME supports have more homogeneous morphology and particle sizes than the IM supports. In addition, STEM-EDX mapping prove good dispersions of the promoters in the ME supports.
- By using the ME preparation technique,  $\gamma\text{-Al}_2\text{O}_3$  apparently is formed at lower temperatures than normally required.
- The promoted ME materials calcined at 550 °C seemingly consist of amorphous mixed oxides, while the IM supports have segregated phases of crystalline  $\text{CeO}_2$  and metastable  $\text{ZrO}_2$ .
- The ME method permits promoter particle size control with the calcination temperature as adjustable parameter.
- The ME supports present a textural porosity formed by the interstices between nanoparticle aggregates. They have low pore volumes and small pores compared with the IM supports.

About the cobalt catalysts:

- In general, the ME catalysts have stronger cobalt-support interactions than their IM counterparts, possibly due to their low-crystalline/amorphous supports, which result in low DOR and low catalytic activities compared to their IM counterparts.
- The presence of promoters in the IM materials decreases the reduction temperature of  $\text{Co}_3\text{O}_4 \rightarrow \text{CoO}$  due to a spill-over effect. In addition, the presence of promoter on the surface of the alumina (as opposed to inside the alumina structure) decreases the cobalt-

support interaction and therefore favours the formation of larger  $\text{Co}_3\text{O}_4$  particles which are easier to reduce. The improved DOR enhances the catalytic activity and selectivity ( $S_{\text{C}5+}$ ).

- The presence of crystalline  $\text{CeO}_2$  in the ME material calcined at 800 °C decreases the formation of cobalt-aluminate, possibly by the segregated  $\text{CeO}_2$  phase being present on the surface of the alumina (as opposed to inside the alumina structure), and introduces a spill-over effect. The improved DOR, as compared to  $\text{Co/Ce-Al}_2\text{O}_3(\text{ME})550$ , is reflected in the increased catalytic activity and  $S_{\text{C}5+}$ .
- ME catalysts present low dispersion of  $\text{Co}^0$  due to low DOR and relatively large average cobalt particle size compared to the IM counterparts. These large cobalt particles are located at the external surface of the support “pellets”. The internal of the “pellets” are believed to be occupied by cobalt-aluminate and, possibly, by very small cobalt particles. The latter is concluded from the high relative  $S_{\text{CH}_4}$  for the ME catalysts<sup>98</sup>, indicating either a higher  $\text{H}_2/\text{CO}$  ratio in the gas phase in the pores (due to diffusion limitations) or a preferential adsorption of  $\text{H}_2$  on the cobalt surface (e.g. due to Co particles smaller than 6 nm).



## Chapter 8

### Ordered mesoporous silicas as support for cobalt Fischer-Tropsch catalyst (Paper IV)

This chapter summarizes the results from paper IV. As explained in chapter 3, mesoporous materials have been reported as promising candidates for cobalt supports in Fischer-Tropsch synthesis. This chapter focuses on the effect of the silica pore structure in the cobalt catalyst and its application in the Fischer-Tropsch synthesis. Four supports were prepared by a relatively new synthesis method referred to as “the atrane route”, as explained in chapters 3 and 4. Two of the supports were typical ordered mesoporous silicas (MCM-41 and SBA-15), and the other two supports were pore-expanded (PE) versions of the same. The modification consisted in expanding the pores in MCM-41 and SBA-15 from 2.6 and 7.5 nm, to 6.3 and 29 nm, respectively. This was possible by the help of a swelling agent added at mild conditions. The final products, i.e. MCM-41, SBA-15, PE-MCM-41 and PE-SBA-15 silicas, were impregnated with cobalt, calcined and activated in hydrogen to be tested in Fischer-Tropsch synthesis at close to industrial conditions, as explained in chapters 4 and 6.

#### 8.1 Synthesis approach

A generalized synthesis strategy for the preparation of mesoporous silicas with 1D, 2D and 3D structures using the *atrane route* is presented for the first time. The *atrane route*, which was explained in chapters 3 and 4, is the formation of atrane complex precursors for the preparation of ordered mesoporous silicas. The main advantage is the delay of the hydrolysis and condensation processes of the silica which results in a homogeneously ordered mesoporous material.

This route uses a complex reactant, i.e. triethanolamine  $\text{N}(\text{CH}_2\text{-CH}_2\text{-OH})_3$ , which reacts with tetraortosilicate  $\text{Si}(\text{OC}_2\text{H}_5)_4$  and replaces its four alcohols in order to form a stable silatrane complex (see **Figure 3.6**)<sup>113-115</sup>.

Thereafter, the silatrane species react with water and hydrolyse in order to form the oxo-hydroxo silica polymers with negative charge. The hydrolysis can take place in a basic or acidic medium. This will depend on the used surfactant, i.e. CTAB for MCM-41 and P123 for SBA-15.

In the synthesis of MCM-41 silica, the  $\text{CTA}^+$  ions (from the surfactant) form hexagonal micellar aggregations (see **Figure 8.1**). The silica polymers with negative charge previously formed will be attracted by strong electrostatic interaction to the surfactant micelles that are positively charged. Afterwards, the final product is silica coating the surfactant micelles. The surfactant is eliminated by thermal decomposition and thereafter a ordered mesoporous silica is formed<sup>116</sup>. A more detailed explanation of the synthesis process can be found in the appended Paper IV. However, the interesting part is related to the increase of the silica pore size which was achieved by the  $\text{CTA}^+$  micelle expansion. In the case of PE-MCM-41, the addition of a swelling agent, TIPB, self-organizes inside the  $\text{CTA}^+$  micelles and expands its diameter<sup>117, 118</sup>.

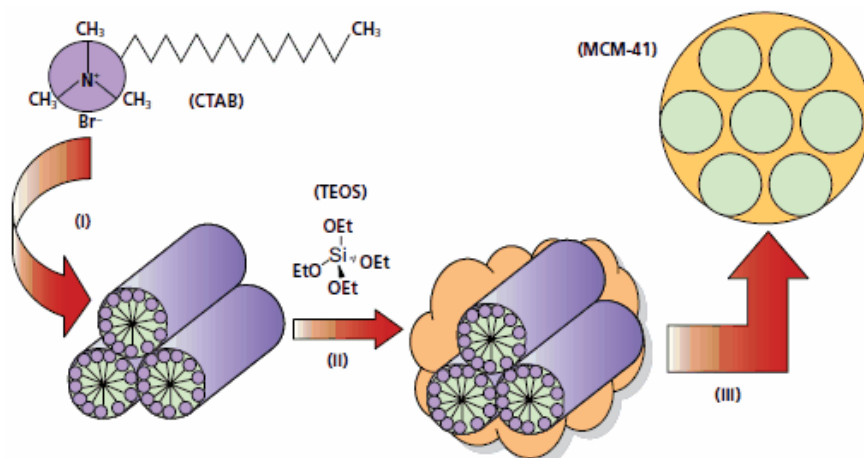


**Figure 8.1:** CTAB cetyltrimethyl ammonium bromide and MCM-41 formation (adapted from<sup>119</sup>)

In the case of the synthesis of silica type SBA-15, the surfactant is P123 which is a mixture of a triblock copolymer: polyethylene

oxide/polypropylene oxide / polyethylene oxide (EO/PO/EO). The micellization of the polymers is driven by the hydrophobic polyethylene oxide (PO) block with a core consisting of PO blocks and a corona of EO blocks<sup>120-123</sup>. The hydrophilic part EO will attract the anionic oxo-hydroxo-Si oligomers forming the inorganic siliceous condensation on the micelles. When the TMB is added to the synthesis, it prefers to be self-assembled in the hydrophobic core of PO and thereafter the micelles swell.

In both silica types, MCM-41 and SBA-15, the pore expansion caused by the swelling agent, either TIPB or TMB may affect the equilibrium of the surfactant micelles and disorganize their structure, which might produce non-ordered mesoporous silica. For this reason it is suggested to use the atrane route. In addition, the silica synthesis was performed at soft conditions, while other methods make use of an autoclave in a post-synthesis process in order to expand the pores.

## 8.2 Characterization of the materials

The textural properties of the supports and cobalt catalysts are listed in **Table 8.1**. Both MCM-41 and SBA-15 silicas (see **Figure 8.2**) present narrow pore size distributions. SBA-15 has almost twice the average pore size diameter of MCM-41. PE-MCM-41 presents a physisorption isotherm with two hystereses, the first one related to the structural pores of the silica similar to MCM-41 and the second one ascribed to N<sub>2</sub> condensation in the inter-particle pores with a pore size distribution around 30 nm. Consequently it is assumed that this material has structural and textural porosity. PE-SBA-15, in **Figure 8.3**, presents a hysteresis loop type corresponding to a 3D spherical cell structure with interconnected pores (windows)<sup>124</sup>, as schematically illustrated in **Figure 8.4**.

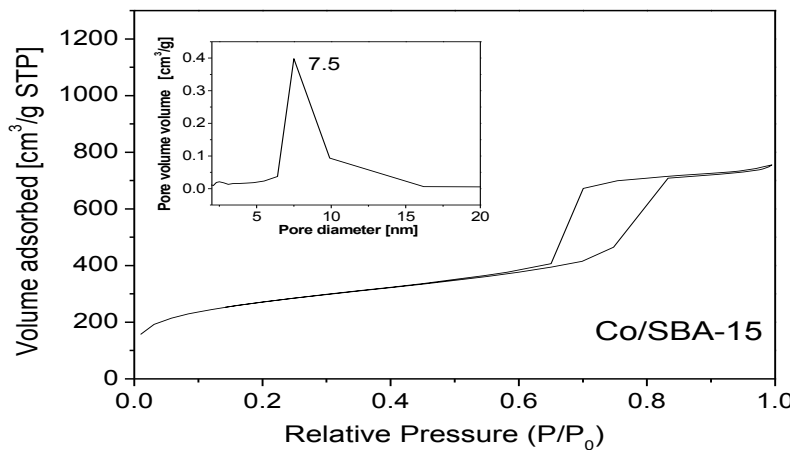
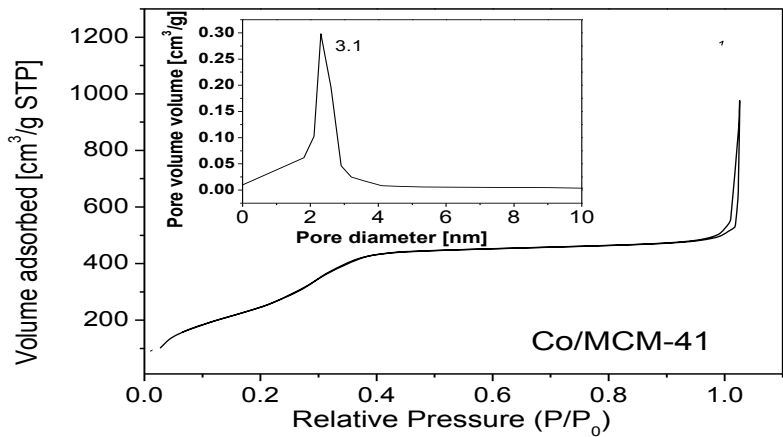


**Figure 8.2:** N<sub>2</sub> sorption isotherms and pore size distribution curves for Co-mesoporous silica catalysts.

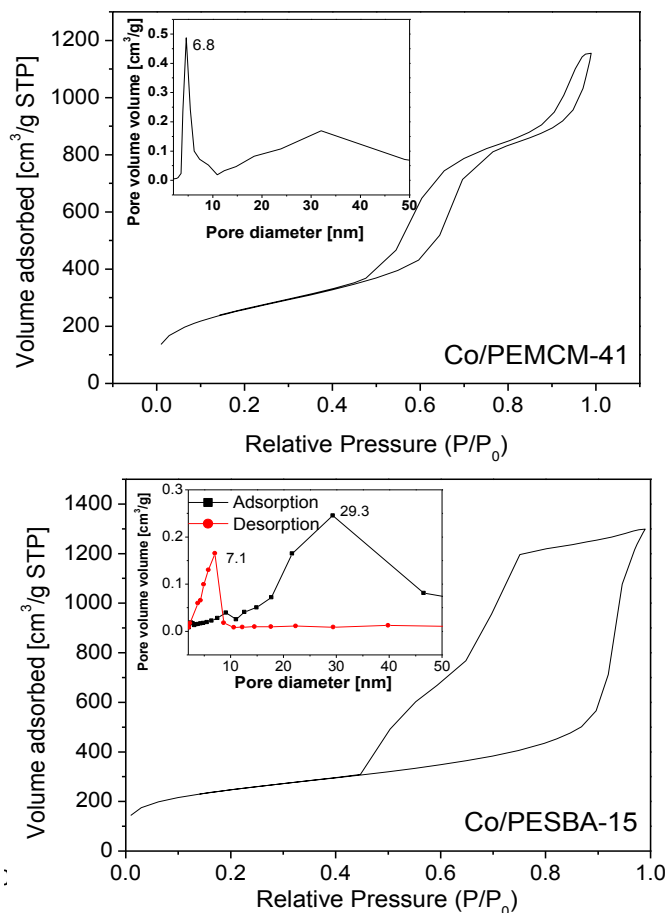


**Figure 8.3:** N<sub>2</sub> sorption isotherms and pore size distribution curves for pore-expanded Co-mesoporous silica catalysts.

The diameter of the cell and window structure is obtained from the isotherm adsorption and desorption branches, (see **Figure 8.3** and **Table 8.1**). **Figure 8.5** shows SEM pictures of the supports. MCM-41 shows a perfect hexagonal structure extrapolated from its nano-scale structure. The SBA-15 morphology is fiber-like with different sizes<sup>125</sup>. These hexagonal and cylindrical morphologies changed to agglomerated spherical

particles after the pore size expansion. This suggests that the swelling agent is located inside and outside the surfactant micelles (CTAB and P123), which might prevent the formation of large and long particles.

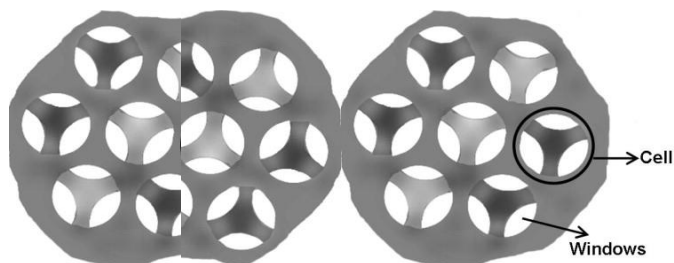


**Figure 8.4:** Mesocellular foam silica representation (adapted <sup>126</sup>)

**Table 8.1** N<sub>2</sub> physisorption results for the supports and catalysts.

Sample	BET Surface area (m <sup>2</sup> /g)	Total pore volume <sup>a</sup> (cm <sup>3</sup> /g)	Mesopore diameter <sup>b</sup> (nm)
MCM-41	1200	0.9	2.6
PE-MCM-41	900	1.8	6.3
SBA-15	940	1.1	7.5
PE-SBA-15	860	1.9	*29.3/5.0
Co/MCM-41	990	0.8	3.1
Co/PE-MCM-41	633	1.4	6.8
Co/SBA-15	721	0.8	7.9
Co/PE-SBA-15	576	1.8	*29.0/7.1

<sup>a</sup> Determined from a single point of adsorption at P/P<sub>0</sub>=0.998.

<sup>b</sup> Estimated by BJH formalism (desorption branch).

\*The two values represent the cell diameter and window diameter of the cell from BJH adsorption and desorption

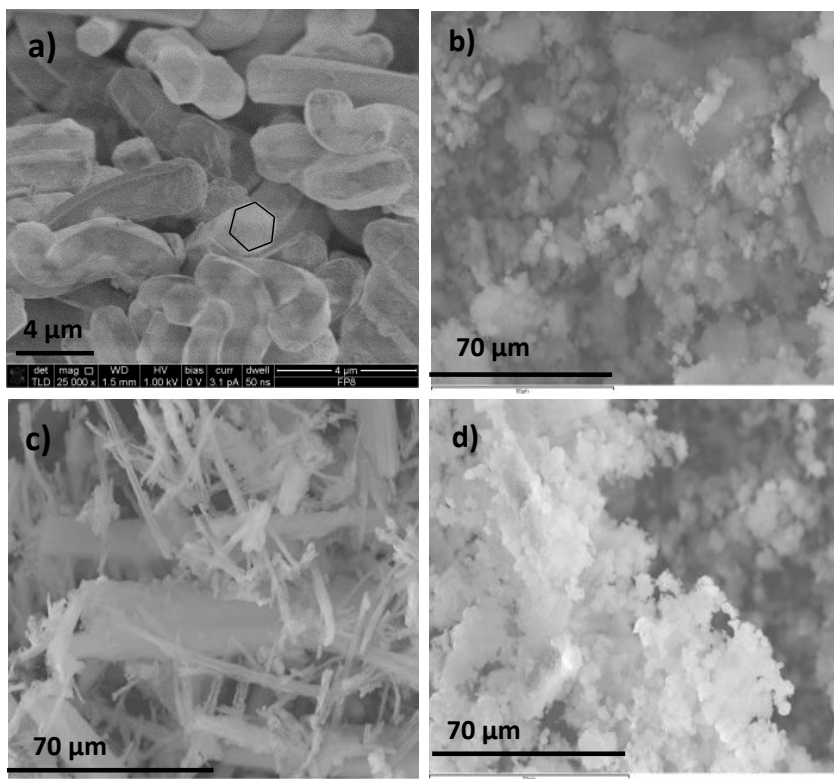


**Figure 8.5:** Representative SEM images of a) MCM-41, b) PE-MCM-41, c) SBA-15 and d) PE-SBA-15 calcined at 550 °C for 6 h.

TEM pictures (**Figure 8.6**) show that the channel structure is kept in PE-MCM-41 but the parallel channels changed in the perpendicular direction (from 1D to 2D). The mesostructured 2D formation in SBA-15 changed to 3D in PE-SBA-15, which is consistent with N<sub>2</sub> physisorption results. The network was formed for pore cells with a main pore diameter of 30 nm and interconnected windows of 7 nm (see the schematic representation in **Figure 8.4**).

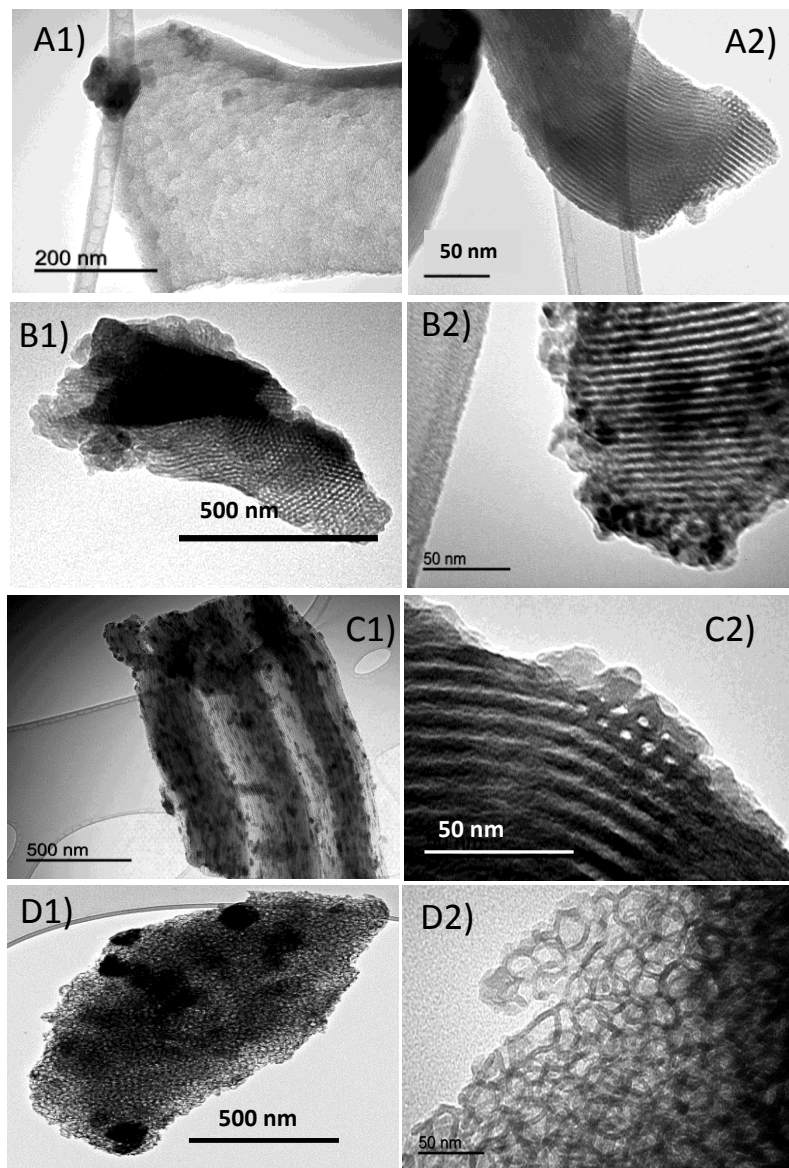


**Figure 8.6:** Representative TEM images of A) Co/MCM-41, B) Co/PE-MCM-41, C) Co/SBA-15, D) Co/PE-SBA-15 after cobalt deposition, calcined at 350 °C for 10 h. The right column shows higher resolution of the catalysts.

After cobalt deposition on the silicas,  $\text{Co}_3\text{O}_4$  species are identified in all the catalysts by X-ray diffractograms. The average particle size using Scherrer's equation is presented in **Table 8.2**. Also, the  $\text{Co}^0$  particle sizes as estimated from chemisorption and DOR are presented and increase with the pore diameter of the supports.

**Table 8.2** Physicochemical characteristics

Sample	XRD		H <sub>2</sub> Chemisorption		
	$d(\text{Co}_3\text{O}_4)^a$ (nm)	$d(\text{Co}^0)^b$ (nm)	$d(\text{Co}^0)^c$ (nm)	$D^d$ (%)	$DOR^e$ (%)
<b>Co/MCM-41</b>	7.0	5.3	4.7	7.2	35
<b>Co/PEMCM-41</b>	9.4	7.0	6.1	6.8	43
<b>Co/SBA-15</b>	15.1	11.3	7.2	8.0	60
<b>Co/PESBA-15</b>	14.7	11.1	7.5	7.4	58

<sup>a</sup> Calculated from Scherrer equation

<sup>b</sup> According to:  $d(\text{Co}^0) = 0.75 \cdot d(\text{Co}_3\text{O}_4)$

<sup>c</sup> Particle size calculated after reduction at 350 °C for 16 h in H<sub>2</sub>

<sup>d</sup> Metal dispersion, after reduction at 350 °C for 16 h in H<sub>2</sub>

<sup>e</sup> Degree of reduction from TPR of reduced catalysts

The temperature programmed reduction profiles of the catalysts are shown in **Figure 8.7**. The profile of Co/SBA-15 is most similar to those of cobalt catalysts with conventional supports<sup>103, 104</sup>, where the first peak around 330 °C probably represents the reduction of  $\text{Co}_3\text{O}_4$  to CoO (theoretically 25% of total hydrogen uptake if all cobalt is present as  $\text{Co}_3\text{O}_4$  in the calcined catalyst), and the second peak with maximum at 360 °C probably represents the reduction of CoO to  $\text{Co}^0$  (theoretically 75% of total

hydrogen uptake). The hydrogen uptake above 600 °C is very small for this catalyst and indicates that the cobalt-support interactions are weak. This explains why this catalyst has the highest DOR (see **Table 8.2**).

The TPR profiles of the other catalysts are more difficult to interpret, probably due to overlapping peaks of the first ( $\text{Co}_3\text{O}_4 \rightarrow \text{CoO}$ ) and second ( $\text{CoO} \rightarrow \text{Co}^0$ ) reduction steps of  $\text{Co}_3\text{O}_4$ , and possibly due to that part of the formed CoO during TPR is interacting strongly with the support and not reduced to  $\text{Co}^0$  until temperatures above 600 °C. It is, however, easily understood that they all have strong cobalt-support interactions. Especially Co/MCM-41, which has the highest hydrogen uptake above 600 °C. This is ascribed to the very small  $\text{Co}_3\text{O}_4$  particles in this catalyst (see **Table 8.2**), as a result of the high surface area and small pore size (see **Table 8.1**). The small particles interact strongly with surface –OH species from MCM-41 silica and results in the lowest DOR of all catalysts.

It is seen that the cobalt-support interactions in Co/PE-SBA-15 are stronger than in Co/SBA-15, at least during TPR, even though the former has larger average pores. This could maybe be related to the cobalt present in the narrower window pores interacting with the silanol groups. However, the DOR of Co/PE-SBA-15 is almost as high as that of Co/SBA-15 (see **Table 8.2**). This is ascribed to the large 3D spherical pores, in combination with the reduced pore length (as evidenced from **Figure 8.5**). The large pores have many advantages in this application. For example, when  $\text{Co}_3\text{O}_4$  is reduced with  $\text{H}_2$ , water is produced and might oxidize the formed  $\text{Co}^0$ . This is especially pronounced when the support has long and small pores. In contrast, the Co/PE-SBA-15 catalysts might not have this problem.

It should be mentioned here that cobalt-support interactions in ordered mesoporous silicas have also been attributed to the difference in the arrangement of surface –OH groups between different silicas<sup>127</sup>. For instance, it has been reported that in MCM-41, isolated –OH groups exist in an ordered way without much interactions with other –OH groups. On the contrary, the inner surface of SBA-15 contains both isolated and interacting –OH groups able to form hydrogen bonds with other –OH groups<sup>127</sup>.

Therefore it is reasonable to think that due to the inner surface of the SBA-15 support, there is less interaction of cobalt with the surface –OH groups.

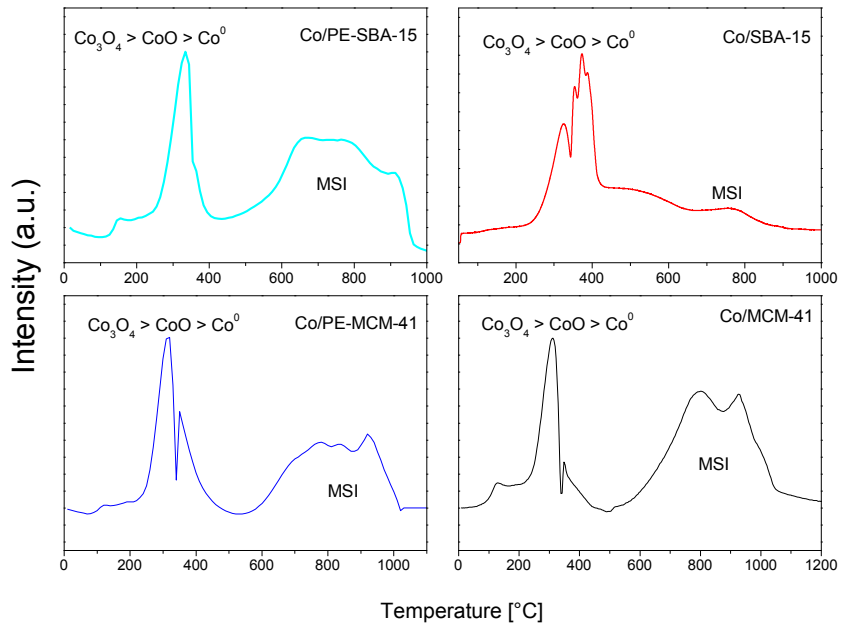


**Figure 8.7:** H<sub>2</sub> TPR profiles of the cobalt catalysts calcined at 350 °C for 10 h. (MSI = metal-support interaction)

### 8.3 Catalytic activity

**Table 8.3** Conversion levels and selectivity data for the different catalysts

GHSV cm <sup>3</sup> /h,g	Catalysts	X <sub>CO</sub> (%)	S <sub>CH<sub>4</sub></sub> <sup>a</sup> (%)	S <sub>C<sub>5</sub>+<sup>a</sup></sub> (%)	S <sub>CO<sub>2</sub></sub> (%)
6000	Co/MCM-41	4.4	12.2	76.3	1.4
1500		27.0	8.6	83.5	1.0
6000	Co/PE-MCM-41	5.7	10.1	80.0	0.7
1600		29.1	8.7	84.6	0.4
6000	Co/SBA-15	10.0	18.3	62.1	2.2
2550		28.0	13.5	74.5	1.8
6000	Co/PE-SBA-15	18.5	11.1	73.6	1.2
4800		28.5	7.2	85.2	1.8

<sup>a</sup>Selectivities are CO<sub>2</sub>-free

The experiments were performed in the same manner as for the catalysts supported on nanoparticles. The first experiment concerns the comparison between the catalysts' activity at GHSV 6000 cm<sup>3</sup>/h,g (see **Table 8.3**).

The activity decreases in the following order: Co/PE-SBA-15 > Co/SBA-15 > Co/PE-MCM-41 > Co/MCM-41. The lower activities of the Co/MCM-41 and Co/PE-MCM-41 are mainly explained by low DOR, and most probably not by diffusional limitations on reactant arrival (deduced from their high S<sub>C<sub>5</sub>+<sup>a</sup></sub>). It was deduced from the physicochemical characteristics that the best candidates for the Fischer-Tropsch reaction were Co/SBA-15 and Co/PE-SBA-15. These catalysts were comparable since both had similar Co<sup>0</sup> particle size, degree of reduction and dispersion. However, the catalyst Co/PE-SBA-15 had the best catalytic results showing almost double CO conversion (**Table 8.3**). The difference between these two catalysts is attributed to the existence of a 3D pore structure and large pore diameter in Co/PE-SBA-15. The open network of this support favours the reactants and products diffusion, while in the long (as evidenced from the SEM picture (**Figure 8.5**)) and small pores in Co/SBA-15 the diffusion becomes rate limiting.

At CO conversion around 30%, the selectivity to C<sub>5+</sub> decreases in the order: Co/PE-SBA-15 > Co/PE-MCM-41 > Co/MCM-41 > Co/SBA-15. Again, this might be attributed to the support pore characteristics. The Co/PE-SBA-15 catalyst has cell spheres structures where the growth of longer hydrocarbons chains are favoured, maybe due to the steric effect of the chains are less pronounced and can grow more freely. This last comment could be interesting to study in further investigations. The very poor S<sub>C<sub>5+</sub></sub> of Co/SBA-15 is most probably caused by diffusion limitations increasing the H<sub>2</sub>/CO ratio inside the pores. This, in turn, is caused by long length of the mesopores, in agreement with literature<sup>128</sup>.

## 8.4 Conclusions

The following conclusions can be drawn from this study:

- To our knowledge, this is the first time the atrane route has been used as a generalized synthesis strategy for the preparation of mesoporous materials with 1D, 2D and 3D structures.
- On the micro-meter scale, MCM-41 has hexagonal structure, while SBA-15 presents a fiber-like morphology with various sizes and widths of the particles. These morphologies change to agglomerated spherical particles in the pore-expanded materials.
- MCM-41 and SBA-15 silicas present narrow pore size distributions (2.6 and 7.5 nm, respectively) and structural porosity (1D and 2D, respectively). PE-MCM-41 presents structural and textural porosity, with the main mesopores having increased to 6 nm due to the pore expansion. PE-SBA-15 presents a 3D cell structure pore (29 nm in diameter) with interconnected pores (windows, 5 nm).
- In all cases, Co<sub>3</sub>O<sub>4</sub> particles are formed on both the external and internal surface of the materials.
- The cobalt-support interaction is highest in Co/MCM-41, due to the smallest pore size and the smallest Co<sub>3</sub>O<sub>4</sub> particles. Also Co/PE-MCM-41 has a strong cobalt-support interaction and

both catalysts show relatively low DOR and possess the lowest catalytic activities.

- Despite their small pore diameters and their 1D and 2D for Co/MCM-41 and Co/PE-MCM-41, respectively, these catalysts show normal relative  $S_{CH_4}$ <sup>98</sup> and actually rather high  $S_{C_5+}$ , which indicates that they are not under the influence of diffusion limitations on reactant arrival. This is probably due to relatively short pore lengths<sup>128</sup>.
- Co/SBA-15 and Co/PE-SBA-15 have higher DOR, mainly due to larger  $Co_3O_4$  particles. In the case of Co/PE-SBA-15, also its large 3D spherical pores might help in the reduction process, as the TPR profile of this catalyst actually suggested a strong cobalt-support interaction.
- The Co/PE-SBA-15 catalyst shows the highest catalytic activity and  $S_{C_5+}$ . This is ascribed to its high DOR and its large 3D pore structure. The Co/SBA-15 has poor  $S_{C_5+}$  and a high relative  $S_{CH_4}$ <sup>98</sup>, which suggests that it is under the influence of diffusion limitations on reactant arrival. This is ascribed to its fiber-like morphology with seemingly long pores, in combination with the lack of a 3D porous structure<sup>128</sup>.

## Chapter 9

### **Mesoporous silicas promoted with Zr as potential support for cobalt Fischer-Tropsch catalysts (Paper V)**

This chapter summarizes the results from paper V. In the previous chapter, the synthesis of the pore size expansion of SBA-15 silica type has been discussed. The structure of this silica was interesting since a cellular structure of approx. 30 nm and interconnected window pores of 5 nm was obtained. The cobalt catalyst using this silica had the best catalytic behaviour among the studied catalysts in that catalyst series. Those results were ascribed to the silica 3D pore structure and to the relatively high degree of reduction of the cobalt. However, TPR indicated the presence of cobalt-silicate species, possibly due to the small window pore. In order to further increase the DOR and, accordingly, the catalyst activity, we suggested to increase the window pore diameter of the PE-SBA-15 by the addition of a  $\text{NH}_4\text{F}$  salt during the silica synthesis. This modified silica was named mesocellular foam MCF in order to differentiate it from the previous PE-SBA-15 silica. Also, the addition of Zr during the synthesis of the support was studied as a measure to prevent the cobalt-silicate formation. The results are compared with those of SBA-15 and those of a Zr-promoted SBA-15.

The supports were impregnated with cobalt. However, evaluation in the Fischer-Tropsch synthesis remains to be done.

## 9.1 Characterization of the materials

First of all, a test experiment was performed in order to understand the differences between the synthesis methods of the silica MCF and SBA-15. A comparison of two pairs of silica was first performed, one MCF and SBA-15 synthesized by the atrane route denoted (A) and the second one synthesized by a conventional sol-gel synthesis denoted (D). **Figure 9.1** shows that the materials obtained by the atrane route MCF(A) have homogeneous particles in the range of 1-3  $\mu\text{m}$ . On the contrary MCF(D) forms heterogeneous agglomerations of particles with several sizes. In **Figure 9.2**, SEM pictures of SBA-15 with and without Zr are shown. The support SBA-15 has fibrous-like structure morphology. However, the incorporation of Zr during the synthesis changed the typical SBA-15 morphology to spherical particles of smaller size. This effect is ascribed to the fact that Zr tends to agglomerate during the hydrolysis and condensation process. Since the materials (MCF and SBA-15 with and without Zr) synthesized by the atrane route (A) seems novel and more attractive it was the chosen form for further studies, while the silicas synthesized by sol-gel were excluded. TEM images of MCF(A), from now on just named MCF, are shown in **Figure 9.3**.

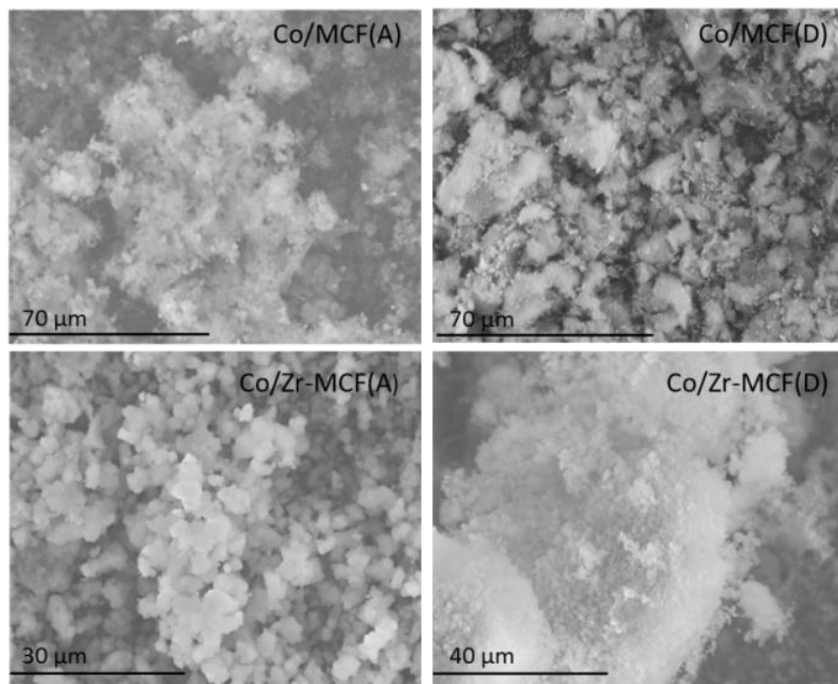


**Figure 9.1:** SEM pictures for cobalt catalysts in MCF silicas.

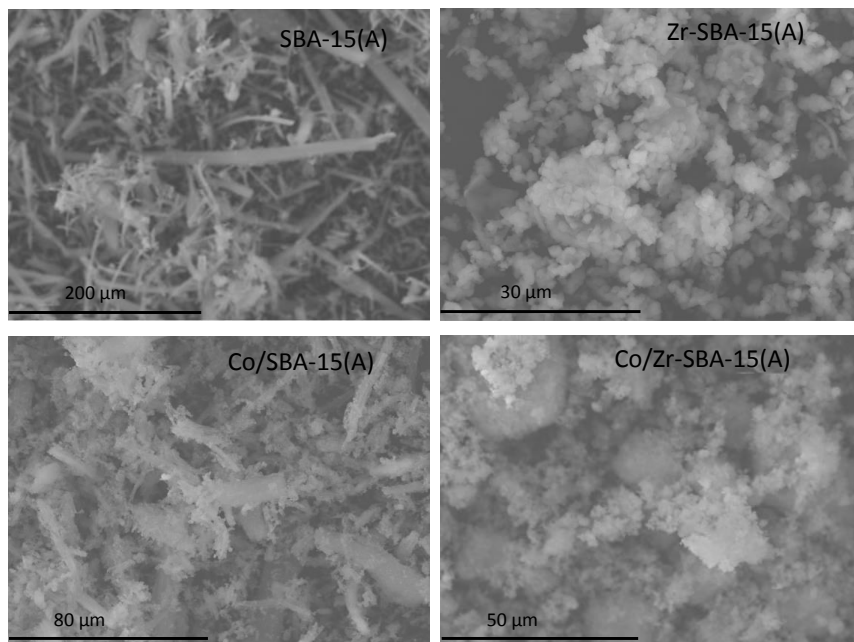


**Figure 9.2:** Representative SEM images for the supports SBA-15, Zr-SBA-15 (calcined at 550 °C for 6 h) and for the catalysts Co/SBA-15 and Co/Zr-SBA-15 (calcined at 350°C for 10 h)

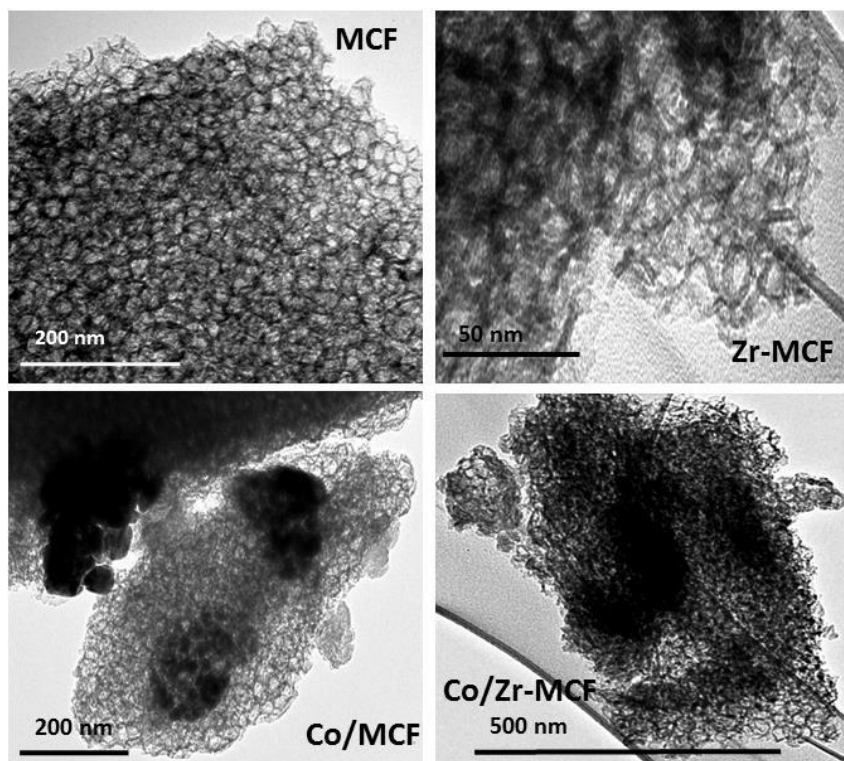


**Figure 9.3:** TEM images for the supports MCF, Zr-MCF and catalysts Co/MCF and Co/Zr-MCF synthesized by the atrane route.

The MCF silica shows spherical pores with an average pore diameter of 30 nm, these spheres are interconnected in 3D directions. The case of Zr-MCF is different; the material shows a disordered and distorted foamy amorphous material with thicker walls in comparison to MCF silica without Zr. SBA-15 and Zr-SBA15 have tubular channels structure in 1D direction with pores of 7-8 nm. The picture is not shown here since it was presented in the previous chapter. The textural properties of the supports are listed in **Table 9.1**. However, just the N<sub>2</sub> adsorption-desorption isotherms and pore size distribution of MCF silica types are presented in **Figure 9.4**. According to the **IUPAC** nomenclature, all the silicas have type IV(a)

isotherms correspondent to mesoporous materials with pore diameter in the range of 2–50 nm<sup>124, 129</sup>.

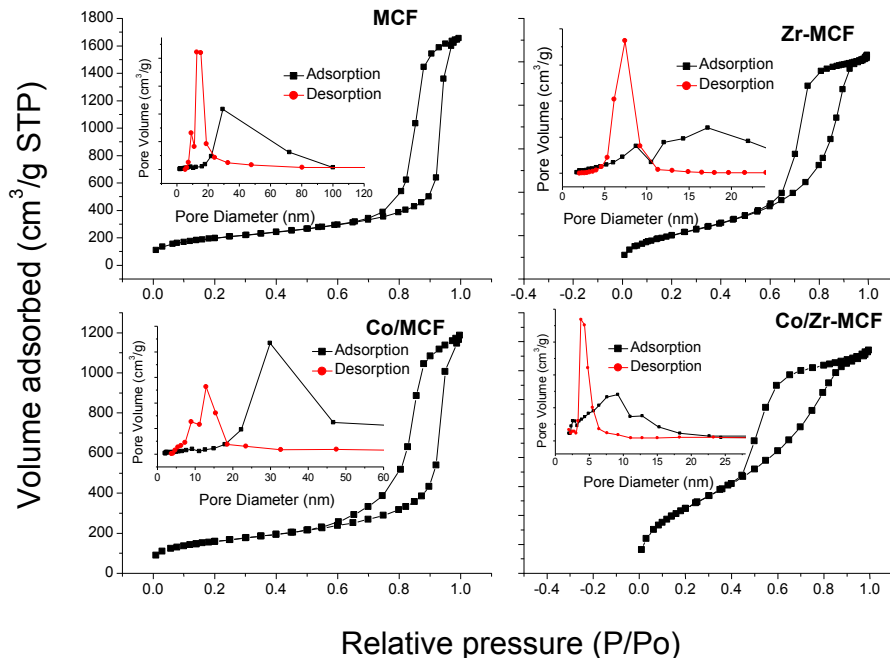


**Figure 9.4:** N<sub>2</sub> physisorption for the supports MCF, Zr-MCF and catalysts Co/MCF and Co/Zr-MCF synthesized by the atrane route

The hysteresis for Co/MCF presents a characteristic hysteresis loop for 3D structure, i.e. mesocellular silica foam<sup>124</sup>. A typical mesocellular foam structure is a 3D cell with interconnected window pores. The diameters of the cell and the window are obtained from the adsorption and desorption branches of the isotherms, (see **Figure 9.4** and **Table 9.1**). Zr is seen to reduce the pore diameter of both SBA-15 and MCF.

**Table 9.1** N<sub>2</sub> physisorption results for the supports and catalysts.

Sample	BET Surface Area <sup>a</sup> (m <sup>2</sup> /g)	Total pore volume <sup>b</sup> (cm <sup>3</sup> /g)	Av. pore diam. <sup>c</sup> (nm)	BJH Ads. <sup>d</sup> (nm)	BJH Des. <sup>e</sup> (nm)
SBA-15	940	1.1	7.5	-	-
Zr-SBA-15	674	0.7	7.3	-	-
MCF	689	2.5	-	29.2	13.8
Zr-MCF	726	1.6	-	17.2	7.2
Co/SBA-15	721	0.8	7.9	-	-
Co/Zr-SBA-15	536	0.6	7.1	-	-
Co/MCF	550	1.8	-	29.8	12.9
Co/Zr-MCF	563	0.7	-	9.2	3.8

<sup>a</sup> Determined from a single point of adsorption at P/P<sub>0</sub>=0.998.

<sup>b</sup> Estimated by BJH formalism (desorption branch)

<sup>c</sup> Estimated by BJH formalism (adsorption branch)

<sup>d</sup> Cell pore size determined from the adsorption branches of the isotherms

<sup>e</sup> Window pore size determined from the desorption branches of the isotherms

**Table 9.2** and **Figure 9.5** show the results from XRD diffractograms. Co<sub>3</sub>O<sub>4</sub> is identified for all the catalysts. The particle size for Co<sub>3</sub>O<sub>4</sub> was calculated with Scherrer's equation. Within each group of supports (SBA and MCF), the Co<sub>3</sub>O<sub>4</sub> particle size increases with the support pore diameter (see **Table 9.1**). The Co<sup>0</sup> particle size and dispersion are calculated from H<sub>2</sub> chemisorption after catalyst activation and reported in **Table 9.2**. The dispersion is quite similar for all the cases; however Co/Zr-SBA-15 shows the highest value. The DOR is highest for Co/MCF.

**Table 9.2** Physicochemical characteristics

Sample	XRD		H <sub>2</sub> Chemisorption		
	$d(\text{Co}_3\text{O}_4)^a$	$d(\text{Co}^0)^b$	$d(\text{Co}^0)^c$	$D^d$	$DOR^e$
	(nm)	(nm)	(nm)	(%)	(%)
Co/SBA-15	15.1	11.3	7.2	8.0	60
Co/Zr-SBA-15	8.8	6.6	3.8	8.4	33
Co/MCF	13.5	10.1	9.2	7.1	68
Co/Zr-MCF	11.9	8.9	5.9	7.8	48

<sup>a</sup> Calculated from Scherrer equation

<sup>b</sup> According to:  $d(\text{Co}^0) = 0.75 \cdot d(\text{Co}_3\text{O}_4)$

<sup>c</sup> Particle size calculated after reduction at 350 °C for 16 h in H<sub>2</sub>

<sup>d</sup> Metal dispersion, after reduction at 350 °C for 16 h in H<sub>2</sub>

<sup>e</sup> Degree of reduction from TPR of reduced catalysts

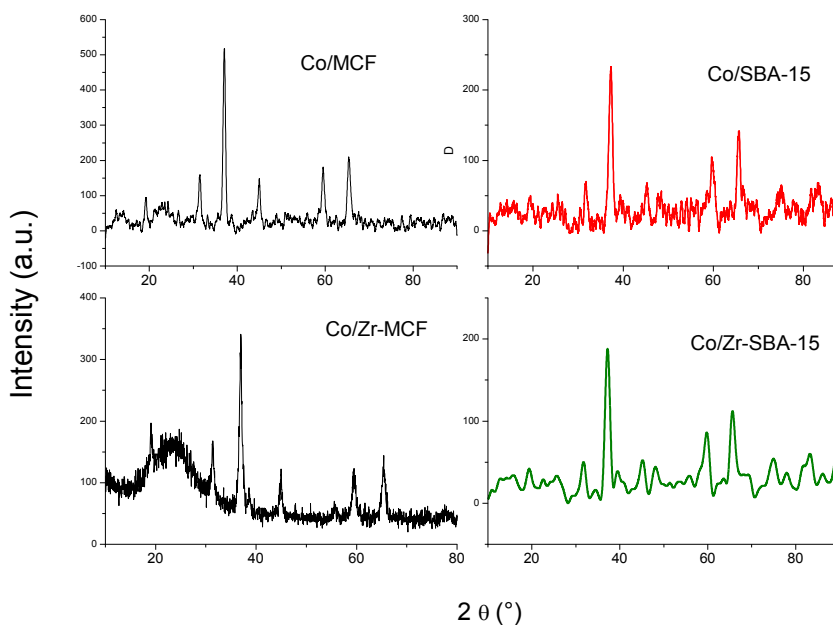


**Figure 9.5:** X-Ray patterns for the studied catalysts calcined at 350 °C for 10 h.

A comparison of the temperature programmed reduction profiles for the final catalysts is shown in **Figure 9.6**. Two main regions of H<sub>2</sub> uptakes are considered, one at temperatures lower than 500 °C corresponding to the reduction of Co<sub>3</sub>O<sub>4</sub> and CoO and the second one at temperatures higher than 500-600 °C corresponding to the reduction of cobalt-silicates species. The most interesting TPR profile comes from Co/MCF, when comparing this result with Co/PE-SBA-15 from the previous chapter. Apparently, the amount of Co-silicate species has been reduced, which was one of the goals. This reduction is attributed to the increase of the window pore diameter of the silica support from 5 to 13.8 nm. The Zr addition seemingly increases the cobalt-support interaction in both MCF and SBA-15. This might be the result of the small pore sizes and, accordingly, smaller cobalt particles.

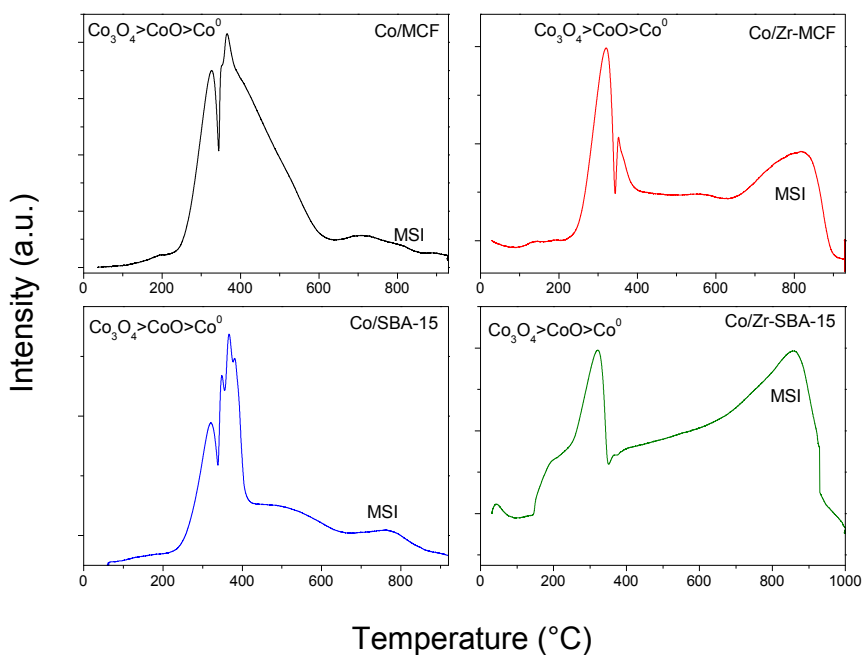


**Figure 9.6:** H<sub>2</sub> Temperature profile for the catalysts Co/MCF, Co/Zr-MCF, Co/SBA-15 and Co/Zr-SBA-15

## 9.2 Conclusions

The addition of the  $\text{NH}_4\text{F}$  salt during the MCF silica synthesis resulted in a material that has a window pore diameter of 13.8 nm, compared to 5.0 nm in the PE-SBA-15 material (see chapter 8), while the cell pore size was more or less identical in the two materials. The  $\text{Co}^0$  particle size in Co/MCF (9.2 nm) is somewhat larger than in Co/PE-SBA-15 (7.5 nm), and the DOR is 68 and 58%, respectively. Hence, it is concluded that the addition of the  $\text{NH}_4\text{F}$  salt during the silica synthesis had the expected effect. However, as the cobalt dispersion is slightly lower in Co/MCF (7.1%) due to the larger cobalt particles compared with Co/PE-SBA-15 (7.4%), the catalysts need to be evaluated in the Fischer-Tropsch in order to find out which one has the highest activity.

The addition of Zr reduces the pore size of the SBA-15 and MCF silicas and, accordingly, also the  $\text{Co}_3\text{O}_4$  particle size. This results in strong cobalt-support interactions and low DOR. However, the cobalt dispersions reach higher values than the Zr-free counterparts due to the tiny Co particle sizes. The Zr addition to the SBA-15 and MCF is believed not to hinder the original 2D and 3D structures. However, some distortion of the 3D structure in MCF is seen, and both the cell pore size and the window pore size are almost halved compared to the Zr-free MCF.

## Chapter 10

### Final conclusions

Natural gas is an energy resource used for the conversion of gas-to-liquid "GTL" through the Fischer-Tropsch reaction. Cobalt Fischer-Tropsch catalysts are commonly used for the production of long-chain hydrocarbons in GTL process. The support for the cobalt catalyst has a large influence on the physicochemical properties of the catalyst. For this reason, the design of the support, its chemical composition and method of synthesis are important for obtaining a highly active and selective catalyst. In this respect, the objective of the thesis is the evaluation of the synthesis and characterization of Si and Al oxides with non-conventional morphology (alumina nanoparticles and mesoporous silica) and their modification with Ce and Zr promoters. Additionally, non-conventional synthesis methods have been used for this purpose, such as water-in-oil microemulsion for the preparation of alumina nanoparticles, and the atrane route for ordered mesoporous silicas.

The main conclusions of this work are summarized as follows:

In relation to the use of alumina nanoparticles as cobalt catalyst supports, the following can be concluded:

To our knowledge, for the first time it has been shown that Ce- and Zr-alumina nanoparticles can be successfully synthesized by co-precipitation in water-in-oil microemulsion (ME). It has been found that by using the ME preparation technique,  $\gamma$ -Al<sub>2</sub>O<sub>3</sub> starts to form at lower temperatures than normally required. However, upon introduction of the Ce and Zr promoters, the material becomes amorphous. The ME materials are composed of non-porous amorphous nanoparticles lumped together to larger aggregates. They possess textural porosities created by the voids between these aggregates, with pore sizes of around 4-7 nm.

The interaction of cobalt with these ME materials was significantly higher in comparison to commercial alumina that presents a similar surface area but has structural porosity with an average pore diameter of 15 nm. Ce and Zr promoters were added to the alumina supports in order to reduce the interactions of the support with the cobalt. The deposition of the promoters was performed by two methods: co-precipitation of the promoter and aluminium oxides in water-in-oil microemulsion system; and impregnation of the commercial alumina with the promoter salts. The ME method allowed the formation of mixed oxide nanoparticles with highly homogeneous distribution. An interesting point of view of this method was that the particle size of the promoter in the alumina support can be tuned by changing the calcination temperature.

The presence of the promoters increased the reducibility of the cobalt catalysts, and decreased the strong cobalt-support interactions. However, after calcination of the support materials at 550 °C, the promoted ME catalysts still had very much lower degrees of reduction compared to the promoted commercial alumina catalysts. This was attributed to the non-crystalline well dispersed CeO<sub>2</sub> and ZrO<sub>2</sub>.

It is believed that the promoters added to the commercial alumina by impregnation decreased the reduction temperature of Co<sub>3</sub>O<sub>4</sub> → CoO due to a spill-over effect. In addition, the presence of promoter on the surface of the alumina (as opposed to inside the alumina structure as observed with the ME materials) decreased the cobalt-support interaction and therefore favoured the formation of larger Co<sub>3</sub>O<sub>4</sub> particles which are easier to reduce. The improved reducibility enhanced the catalytic activity and selectivity to long-chain hydrocarbons.

By calcining the Ce-promoted ME material at 800 °C, crystalline CeO<sub>2</sub> was formed and the reducibility of the corresponding cobalt catalyst was significantly increased, as well as the catalytic activity and selectivity to long-chain hydrocarbons. The presence of crystalline CeO<sub>2</sub> decreased the formation of cobalt-aluminate, possibly by the segregated CeO<sub>2</sub> phase being

present on the surface of the alumina (as opposed to inside the alumina structure), and introduced a spill-over effect.

The selectivities of the ME catalysts in the Fischer-Tropsch reaction indicated either a higher H<sub>2</sub>/CO ratio in the gas phase in the pores (due to diffusion limitations) or a preferential adsorption of H<sub>2</sub> on the cobalt surface (e.g. due to Co particles smaller than 6 nm). This is explained by part of the cobalt being present inside the small (4-7 nm) pores, while a great part of the cobalt was also deposited on the external surface of the ME-support “pellets”.

A highly dispersed Zr favours the H<sub>2</sub> dissociation which might promote the easier H atom insertion into the intermediates product. As a consequence, the Zr-promoted ME catalyst showed the highest selectivity to products with lower molecular weight.

In relation to the use of mesoporous silicas as cobalt catalyst supports for Fischer-Tropsch reaction, the following can be concluded:

To our knowledge, for the first time it has been shown that it is possible to synthesize pore expanded mesoporous silicas with 1D, 2D and 3D pore structures via the atrane route combined with the addition of swelling agents. The advantage of this method is that due to the slowed-down hydrolysis and condensation reactions, pore expansion can be achieved by the addition of swelling agents at mild conditions and there is therefore no need to perform the pore expansion in a post-synthesis process using an autoclave system.

In the Fischer-Tropsch synthesis, the support materials with the smallest pore sizes (MCM-41 and its pore expanded counterpart) resulted in small cobalt particles interacting strongly with the support. This led to low reducibility of the cobalt and therefore poor catalytic activities. The SBA-15 had larger pores and the cobalt on this support was more easily reduced. However, the morphology of this support (long fibre-like particles) induced

diffusion limitations on reactant arrival, thereby resulting in a very poor selectivity to long-chain hydrocarbons.

The 3D spherical structure silica, obtained by pore expansion of the SBA-15, had cell pore diameters up to 30 nm and interconnected window pores of 5 nm. The cobalt catalyst with this support showed the highest Fischer-Tropsch activity and selectivity to long-chain hydrocarbons, where the results were attributed to the higher reducibility of cobalt, the 3D pore structure and the shorter pore lengths (as compared with SBA-15).

This 3D spherical structure silica showed a relatively high interaction degree of the cobalt and silica. It was found that by widening of the pore window from 5 nm to 14 nm, by the addition of a  $\text{NH}_4\text{F}$  salt during the silica synthesis, the cobalt-silica interaction was decreased and the degree of reduction was further increased. The catalytic performance of this catalyst remains to be evaluated.

Finally, it has been shown that it is possible to obtain silicas promoted with Zr with high 3D porosity and, thus avoiding the separation of phases.

Positive side effects of this thesis work have been the introduction to the Bolivian academia of the following topics: Gas-to-liquids, Fischer-Tropsch synthesis, cobalt catalysts for Fischer-Tropsch reaction, nanoparticles and mesocellular foam silica types. As a result, projects on these topics involving bachelor and master students in Bolivia, have followed. In this way this thesis work has contributed to widen the academic research in Bolivia.

## Acknowledgements

First of all I would like to thank SIDA for the financial support, without it this work would not have been possible. Further, I gratefully acknowledge the funding received for my short research stays and conferences from: The European cooperation in Science and Technology, COST-STSM-CM1101-14172 and COST-STSM-CM0903-12323, The Latin American network in nanoscience NanoAndes and POKE.

I feel very grateful to my supervisors at KTH, Ass. Prof. Magali Boutonnet and Prof. Emeritus Sven Järås for giving me the opportunity to carry out doctoral studies at the division of Chemical Technology. I appreciate the possibilities you gave me to travel, participate in conferences and your confidence in me and my work. Special thanks to Prof. Magali for your kindness and patience. I want to thank Ass. Prof. Henrik Kusar for his interest and supervision during these years. Many thanks to my supervisor Prof. Lars Pettersson, for the great help in the end of this process, all your patience, support, and dedication in my thesis, made me feel confident, supported and stronger. Thank you very much Lars, for all!

Warm thanks to my Bolivian supervisor Prof. Saúl Cabrera at UMSA University in La Paz, Bolivia. Saul, you were not just my supervisor, you are a person to whom I admire in all the senses of life, you are not just one of the best Bolivian scientists, but also you are a great person, a great human being that cares about people and push them to improve. I feel very fortunate to have you as mentor, close friend and colleague.

Many thanks to Prof. Margarita Sanchez-Dominguez, for hosting me at CIMAV, Monterrey, Mexico and giving me the possibility to learn more and furthermore, to introduce me amazing people like Andrea V., R2D2 and Maya (you are very chido guys <3). Thanks Margarita for all your kindness! I hope we will collaborate more together in the future.

Thousand thanks to Alberto Prof. Marinas for being a great host for me at UCO University, Cordoba, Spain. Especial thanks to PhD. Vicente Montez, for being a great scientist from whom I have learn a lot. Thank you Chentito for all the help and warm friendship.

I am very grateful to Christina Hörnell for improving the linguistic quality of this thesis and the appended papers. Especially, for having such an alive feeling of life and passion for chemistry.

Very warm thanks to Matteo L, Francesco R. and Javier B. for all the help with the reactor and characterization equipment. You all have saved me many times guys; thank you very much my dears!

I would like to express my special gratitude to all professors, researchers, both former and present, at Chemical Technology for making the department a stimulating and great workplace. Especially to Yohannes K. for showing always a smile to me. I will particularly remember the camaraderie between the PhD students and all nice social activities we have had together, all coffees, barbeques, beers, conferences, trips etc.

I am very thankful to my colleagues at the Natural Gas Institute (IGN-UMSA) and Chemical Research Institute (IIQ-UMSA) in La Paz, Bolivia, for their support and friendship. Thanks to all the people I have work with all these years, for sharing not only work, but also nice social activities.

Thanks to the great friends that were always for me when needed in Bolivia, making every stay there amazing during these years. Especially thanks to (Claudia A., Soledad Ch., Eve Luz Y., Shirley H., Lizangela H., Esther V. Pamela C., Mauricio P., Fabian, B., Daniel B., Oscar R., Miguel. M, Juan Manuel M. and Willmar P.)

I want to thank my great friend Orlando P., who introduced me to the exotic world of chemistry! I have started this road thanks to you Orli, and here it is the result, thanks a lot!

My deep gratitude goes to my friends that I met in Sweden; great people that I always want to have in my life. First, to Sara for all the especial moments together, and for the extreme help with the thesis' correction the last weeks. Without you Sara, this thesis wouldn't be what it is now. Especially I want to thank you for being such an amazing and real person who I always know will be there for me! Huge thanks to Zari, for the everyday support, thanks for giving me so much energy and love when needed. I have done many simple crazy things with you and I love it.

Thanks to my amazing Spanish-Italian friends: to Francesco M. for all the fun, cool time together and support, to Rodrigo S. for letting me know

that I can count with you always, to Silvia T. for making me start a training life which I love. Love you guys! Huge thanks to my best ones outside the academia: Sofie S., Sadia S., Jaime J. Janice and Annu, for all the amazing brunches and so much fun we always have. To Cristiani and Valentina for being so sweet and great friends. To my great friends Stano J., Elin T., and Rahif Z. friends with whom I spent great moments, without you guys my stays would be even harder.

My deepest and warm thanks go for Robert, my heart, which shows me all his love in so many ways. Thanks, for all the laughs together, all the patience, all the help with the thesis, all the understanding and all the magic we have. Love you amor! Thanks to my family from Umeå, for all the love, for making me feel at home every Christmas and holidays. Especially to G. Marie and Ove for treating me like a daughter, and most important for raising such a super human being.

Finalmente, quiero agradecer a mi familia: mi madre Rosaura (Gogo), por su infinito amor, por mimarme en todos los sentidos, por ser tan fuerte, por ser mi padre y madre siempre, por haber renunciado a tantas cosa por mí, eres una madre increíble, mamá! Espero ser por lo menos la mitad de buena que tú algún día. Te amo mucho! A mi abuela Rosa (Rosita) porque no he conocido mujer más trabajadora que tú, aún a tus 75 años sigues teniendo largos días laborales, por el simple placer de trabajar. Porque nunca te visto débil y especialmente gracias por haber criado a seis maravillosas personas sola, aún más, porque siempre estas velado por todos nosotros. Nos has enseñado mucho mamá! Y por la persona que eres te amo mucho!

Finalmente agradecer a todos mis tíos, primos, y en general a toda mi familia por su infinito amor, apoyo, por entenderme y dejarme SER, aunque vaya en contra de sus principios y pensamientos, gracias familia, los amo! También quiero expresar mi inmensa gratitud a mi familia de Lima limón que quiero tanto y vino desde tan lejos a mostrar su amor! Gracias Silvia y Mabel por estar aquí conmigo!

All these people mention here, are very important for me, because I have learn a lot from them and I would not be the person I´m, without them in my life. INFINITE THANKS TO ALL OF YOU!



## Nomenclature

1D	1-dimensional
2D	2-dimensional
3D	3-dimensional
a.u.	Arbitrary unit
ASF	Anderson-Schulz-Flory
BET	Brunauer-Emmett-Teller
CTAB	Cetyltrimethylammonium bromide
FID	Flame ionization detector
FT	Fischer-Tropsch
FTS	Fischer-Tropsch Synthesis
GC	Gas chromatograph
GHSV	Gas hourly space velocity
GTL	Gas to Liquids
HTFT	High Temperature Fischer-Tropsch
LTFT	Low Temperature Fischer-Tropsch
$M_{av}$	Molecular average weight
MCF	Mesocellular foam
MCM-41	Mobil Composition of Matter No. 41
MFC	Mass flow controller
SBA-15	Santa Barbara Amorphous type material
SNG	Synthetic natural gas
TCD	Thermal conductivity detector
TEA	Triethanolamine
TEM	Transmission electron microscopy
TEOS	Tetraethyl orthosilicate
TPR	Temperature programmed reduction
WGS	Water-gas shift
WGSR	Water-gas shift reaction
wt. %	Percentage in terms of mass
XRD	X-ray diffraction



## References

1. N. Abas, A. Kalair and N. Khan, *Futures*, 2015, **69**, 31-49.
2. BP, *Statistical Review of world energy*, 2014.
3. S. H. Mohr, J. Wang, G. Ellem, J. Ward and D. Giurco, *Fuel*, 2015, **141**, 120-135.
4. A. P. Steynberg and H. G. Nel, *Fuel*, 2004, **83**, 765-770.
5. L. P. Dancuart and A. P. Steynberg, in *Studies in Surface Science and Catalysis*, eds. B. H. Davis and M. L. Occelli, Elsevier, 2007, vol. Volume 163, pp. 379-399.
6. R. Rauch, A. Kiennemann and A. Sauciuc, in *The Role of Catalysis for the Sustainable Production of Bio-fuels and Bio-chemicals*, ed. K. S. T. A. L. Stöcker, Elsevier, Amsterdam, 2013, pp. 397-443.
7. A. P. Steynberg, in *Studies in Surface Science and Catalysis*, eds. S. André and D. Mark, Elsevier, 2004, vol. Volume 152, pp. 1-63.
8. A. de Klerk, in *Fischer-Tropsch Refining*, Wiley-VCH Verlag GmbH & Co. KGaA, 2011, pp. 1-20.
9. P. F. Schubert, C. A. Bayens, L. Weick and M. O. Haid, *Studies in Surface Science and Catalysis*, 2001, **136**, 459-464.
10. J. Rostrup-Nielsen and L. J. Christiansen, *Concepts in syngas manufacture: Catalytic science series 10*, World Scientific Pub Co Pte, 2011.
11. P. M. Maitlis, in *Greener Fischer-Tropsch Processes for Fuels and Feedstocks*, Wiley-VCH Verlag GmbH & Co. KGaA, 2013, pp. 1-15.
12. B. H. Davis, in *Greener Fischer-Tropsch Processes for Fuels and Feedstocks*, Wiley-VCH Verlag GmbH & Co. KGaA, 2013, pp. 193-207.
13. A. de Klerk, Y.-W. Li and R. Zennaro, in *Greener Fischer-Tropsch Processes for Fuels and Feedstocks*, Wiley-VCH Verlag GmbH & Co. KGaA, 2013, pp. 53-79.
14. L. Yang and X. Ge, *Advances in Bioenergy*, 2016, **1**, 125-188.
15. J. van de Loosdrecht and J. W. Niemantsverdriet, in *Chemical Energy Storage*, ed. R. Schlögl, De Gruyter, Berlin, 2013.
16. P. M. Maitlis, in *Greener Fischer-Tropsch Processes for Fuels and Feedstocks*, Wiley-VCH Verlag GmbH & Co. KGaA, 2013, pp. 237-265.

17. H. Schulz, *Applied Catalysis A: General*, 1999, **186**, 3-12.
18. H. Schulz, E. vein Steen and M. Claeys, *Studies in Surface Science and Catalysis*, 1994, **81**, 455-460.
19. J. Barrientos, PhD Thesis, Deactivation of cobalt and nickel catalysts in Fischer-Tropsch synthesis and methanation. Royal Institute of Technology, 2016.
20. C. Chen, Q. Wang, R. Zhang, B. Hou, D. Li, L. Jia and B. Wang, *Applied Catalysis A: General*, 2016, **523**, 209-220.
21. J. van de Loosdrecht, F. G. Botes, I. M. Ciobica, A. Ferreira, P. Gibson, D. J. Moodley, A. M. Saib, J. L. Visagie, C. J. Weststrate and J. W. Niemantsverdriet, in *Comprehensive Inorganic Chemistry II (Second Edition)*, ed. K. Poeppelmeier, Elsevier, Amsterdam, 2013, pp. 525-557.
22. S. Ali, M. J. Al-Marri, A. G. Abdelmoneim, A. Kumar and M. M. Khader, *International Journal of Hydrogen Energy*, 2016, **41**, 22876-22885.
23. H. Schulz, *Studies in Surface Science and Catalysis*, 2007, **163**, 177-199.
24. M. Steinberg, *Coal Science and Technology*, 1995, **24**, 1507-1510.
25. M. Rahman, D. Pudasainee and R. Gupta, *Fuel Processing Technology*, 2017, **158**, 35-56.
26. G. F. Botes, T. C. Bromfield, R. L. J. Coetzer, R. Crous, P. Gibson and A. C. Ferreira, *Catalysis Today*, 2016, **275**, 40-48.
27. R. Suarez Paris, L. Lopez, J. Barrientos, F. Pardo, M. Boutonnet and S. Jaras, in *Catalysis: Volume 27*, The Royal Society of Chemistry, 2015, vol. 27, pp. 62-143.
28. A. P. Steynberg, M. E. Dry, B. H. Davis and B. B. Breman, *Studies in Surface Science and Catalysis*, 2004, **152**, 64-195.
29. E. Rytter and A. Holmen, *Catalysis Today*, 2016, **275**, 11-19.
30. M. K. Gnanamani, G. Jacobs, W. D. Shafer and B. H. Davis, *Catalysis Today*, 2013, **215**, 13-17.
31. A. P. Vogel, B. van Dyk and A. M. Saib, *Catalysis Today*, 2016, **259**, 323-330.
32. O. A. Kungurova, A. A. Khassin, S. V. Cherepanova, A. A. Saraev, V. V. Kaichev, N. V. Shtertser, G. K. Chermashentseva, E. Y. Gerasimov, E. A. Paukshtis, O. V. Vodyankina, T. P. Minyukova and G. Abou-Jaoudé, *Applied Catalysis A: General*, 2017, **539**, 48-58.

33. M. E. Dry, *Catalysis Today*, 2002, **71**, 227-241.
34. D. Reinalda and J. Kars, Google Patents, 1991.
35. R. J. Dogterom, C. M. A. M. Mesters and M. J. Reynhout, Google Patents, 2011.
36. S. Storsæter, B. Tøtdal, J. C. Walmsley, B. S. Tanem and A. Holmen, *Journal of Catalysis*, 2005, **236**, 139-152.
37. C. H. Bartholomew and R. J. Farrauto, *Journal of Catalysis*, 1976, **45**, 41-53.
38. A. F. Costa, H. S. Cerqueira, E. Falabella, S. Aguiar, J. Rollán and A. Martínez, *Studies in Surface Science and Catalysis*, 2007, **167**, 141-146.
39. Q. Zhang, W. Deng and Y. Wang, *Journal of Energy Chemistry*, 2013, **22**, 27-38.
40. G. R. Johnson and A. T. Bell, *Journal of Catalysis*, 2016, **338**, 250-264.
41. A. P. Dral, C. Lievens and J. E. ten Elshof, *Langmuir*, 2017, **33**, 5527-5536.
42. F. A. Wigzell and S. D. Jackson, *Applied Petrochemical Research*, 2017, **7**, 9-21.
43. H. Wu, Y. Yang, H. Suo, M. Qing, L. Yan, B. Wu, J. Xu, H. Xiang and Y. Li, *Journal of Molecular Catalysis A: Chemical*, 2015, **396**, 108-119.
44. X. Zhang, H. Su and X. Yang, *Journal of Molecular Catalysis A: Chemical*, 2012, **360**, 16-25.
45. J. Gaube and H. F. Klein, *Applied Catalysis A: General*, 2008, **350**, 126-132.
46. E. Rytter, A. u. R. Salman, N. E. Tsakoumis, R. Myrstad, J. Yang, S. Lögdberg, A. Holmen and M. Rønning, *Catalysis Today*, 2017.
47. J. Hong, W. Chu, P. A. Chernavskii and A. Y. Khodakov, *Applied Catalysis A: General*, 2010, **382**, 28-35.
48. H. Sukkathanyawat, S. Tungkamani, M. Phongaksorn, T. Rattana, P. Narataruksa and B. Yoosuk, *Energy Procedia*, 2015, **79**, 372-377.
49. G. Prieto, M. I. S. De Mello, P. Concepción, R. Murciano, S. B. C. Pergher and A. n. Martínez, *ACS Catalysis*, 2015, **5**, 3323-3335.
50. V. Vosoughi, A. K. Dalai, N. Abatzoglou and Y. Hu, *Applied Catalysis A: General*, 2017, **547**, 155-163.

51. G. R. Johnson and A. T. Bell, *Journal of Catalysis*, 2016, **338**, 250-264.
52. S. Iqbal, T. E. Davies, J. S. Hayward, D. J. Morgan, K. Karim, J. K. Bartley, S. H. Taylor and G. J. Hutchings, *Catalysis Today*, 2016, **272**, 74-79.
53. J. Chandradass, J. H. Yoon and D.-s. Bae, *Materials Science and Engineering: A*, 2008, **473**, 360-364.
54. D. I. Enache, M. Roy-Aubergier and R. Revel, *Applied Catalysis A: General*, 2004, **268**, 51-60.
55. B. Jongsomjit, J. Panpranot and J. G. Goodwin Jr, *Journal of Catalysis*, 2003, **215**, 66-77.
56. Z. Li, J. Wu, J. Yu, D. Han, L. Wu and J. Li, *Journal of Molecular Catalysis A: Chemical*, 2016, **424**, 384-392.
57. Y. Liu, J. Chen, K. Fang, Y. Wang and Y. Sun, *Catalysis Communications*, 2007, **8**, 945-949.
58. T. Miyazawa, T. Hanaoka, K. Shimura and S. Hirata, *Catalysis Communications*, 2014, **57**, 36-39.
59. X. Zhang, H. Su, Y. Zhang and X. Gu, *Fuel*, 2016, **184**, 162-168.
60. A. E. P. de Lima and D. C. de Oliveira, *Catalysis Today*, 2017, **283**, 104-109.
61. M. Arsalanfar, A. A. Mirzaei, H. R. Bozorgzadeh, H. Atashi, S. Shahriari and A. Pourdolat, *Journal of Natural Gas Science and Engineering*, 2012, **9**, 119-129.
62. L. He, BotaoTeng, Y. Zhang and M. Fan, *Applied Catalysis A: General*, 2015, **505**, 276-283.
63. E. Iglesia, *Applied Catalysis A: General*, 1997, **161**, 59-78.
64. H. Xiong, Y. Zhang, K. Liew and J. Li, *Journal of Molecular Catalysis A: Chemical*, 2008, **295**, 68-76.
65. E. J. Gibson and C. C. Hall, *Journal of Applied Chemistry*, 1954, **4**, 49-61.
66. V. Vosoughi, S. Badoga, A. Dalai and N. Abatzoglou, *Ind. Eng. Chem. Res.*, 2016, **55**, 6049-6059.
67. M. Luaidi, PhD thesis. Fischer-Tropsch Synthesis over Cobalt-based catalysts for BTL application, KTH, 2012.
68. J. Hong, W. Chu, P. A. Chernavskii and A. Y. Khodakov, *Journal of Catalysis*, 2010, **273**, 9-17.

69. W. Chu, P. A. Chernavskii, L. Gengembre, G. A. Pankina, P. Fongarland and A. Y. Khodakov, *Journal of Catalysis*, 2007, **252**, 215-230.
70. J. S. Girardon, E. Quinet, A. Griboval-Constant, P. A. Chernavskii, L. Gengembre and A. Y. Khodakov, *Journal of Catalysis*, 2007, **248**, 143-157.
71. C. García-Sancho, R. Moreno-Tost, J. Mérida-Robles, J. Santamaría-González, A. Jiménez-López and P. Maireles-Torres, *Applied Catalysis A: General*, 2012, **433–434**, 179-187.
72. G. R. Moradi, M. M. Basir, A. Taeb and A. Kiennemann, *Catalysis Communications*, 2003, **4**, 27-32.
73. K. Azzam, G. Jacobs, W. Ma and B. H. Davis, *Catalysis Letters*, 2014, **144**, 389-394.
74. R. Bechara, D. Balloy, J.-Y. Dauphin and J. Grimblot, *Chemistry of Materials*, 1999, **11**, 1703-1711.
75. A. K. Dalai and B. H. Davis, *Applied Catalysis A: General*, 2008, **348**, 1-15.
76. A. Y. Khodakov, R. Bechara and A. Griboval-Constant, in *Studies in Surface Science and Catalysis*, 2002, vol. 142 B, pp. 1133-1140.
77. E. Van Steen, M. Claeys, M. E. Dry, J. Van De Loosdrecht, E. L. Viljoen and J. L. Visagie, *Journal of Physical Chemistry B*, 2005, **109**, 3575-3577.
78. L. Wei, Y. Zhao, Y. Zhang, C. Liu, J. Hong, H. Xiong and J. Li, *Journal of Catalysis*, 2016, **340**, 205-218.
79. J.-S. Jung, S. W. Kim and D. J. Moon, *Catalysis Today*, 2012, **185**, 168-174.
80. I. T. Ghampson, C. Newman, L. Kong, E. Pier, K. D. Hurley, R. A. Pollock, B. R. Walsh, B. Goundie, J. Wright, M. C. Wheeler, R. W. Meulenberg, W. J. DeSisto, B. G. Frederick and R. N. Austin, *Applied Catalysis A: General*, 2010, **388**, 57-67.
81. A. M. Saib, M. Claeys and E. van Steen, *Catalysis Today*, 2002, **71**, 395-402.
82. C. Lesaint, W. R. Glomm, Ø. Borg, S. Eri, E. Rytter and G. Øye, *Applied Catalysis A: General*, 2008, **351**, 131-135.
83. M. Kruk, M. Jaroniec, R. Ryoo and J. Sang Hoon, *Chemistry of Materials*, 2000, **12**, 1414-1421.

84. K.-C. Kao and C.-Y. Mou, *Microporous and Mesoporous Materials*, 2013, **169**, 7-15.
85. P. Schmidt-Winkel, W. W. Lukens, D. Zhao, P. Yang, B. F. Chmelka and G. D. Stucky, *Journal of the American Chemical Society*, 1999, **121**, 254-255.
86. R. Amin, B. Liu, S. Ullah and H. Z. Biao, *International Journal of Hydrogen Energy*, 2017, **42**, 21607-21616.
87. L. Wei, Y. Zhao, Y. Zhang, C. Liu, J. Hong, H. Xiong and J. Li, *Journal of Catalysis*, 2016, **340**, 205-218.
88. A. Vinu, T. Mori and K. Ariga, *Science and Technology of Advanced Materials*, 2006, **7**, 753-771.
89. S. Cabrera, PhD tesis, Mesoporous oxides synthesized by the atrane route, Universitat de Valencia, 1999.
90. S. Cabrera, J. El Haskouri, C. Guillem, J. Latorre, A. Beltrán-Porter, D. Beltrán-Porter, M. D. Marcos and P. Amorós, *Solid State Sci*, 2000, **2**, 405-420.
91. J. El Haskouri, S. Cabrera, C. Guillem, J. Latorre, A. Beltrán, D. Beltrán, M. D. Marcos and P. Amorós, *Chemistry of Materials*, 2002, **14**, 5015-5022.
92. P. R. A. F. Garcia, R. N. Bicev, C. L. P. Oliveira, O. A. Sant'Anna and M. C. A. Fantini, *Microporous and Mesoporous Materials*, 2016, **235**, 59-68.
93. M. J. Sprague, *Chemie Ingenieur Technik*, 1985, **57**, 430-430.
94. P. G. J.L. Lemaitre, F. Delannay, *Characterization of Heterogeneous Catalysts*, Denker, New York, 1984.
95. D. Schanke, S. Vada, E. A. Blekkan, A. M. Hilmen, A. Hoff and A. Holmen, *Journal of Catalysis*, 1995, **156**, 85-95.
96. S. Bhatia, J. Beltramini and D. D. Do, *Catalysis Today*, 1990, **7**, 309-438.
97. M. Lualdi, S. Lögdberg, F. Regali, M. Boutonnet and S. Järås, *Topics in Catalysis*, 2011, **54**, 977-985.
98. S. Lögdberg, M. Lualdi, S. Järås, J. C. Walmsley, E. A. Blekkan, E. Rytter and A. Holmen, *Journal of Catalysis*, 2010, **274**, 84-98.
99. M. Sanchez-Dominguez, *Nanotechnology and Nanomaterials* ed. D. A. Hashim, (2012).
100. A. Martínez, G. Prieto and J. Rollán, *Journal of Catalysis*, 2009, **263**, 292-305.

101. C. Liu, J. Li, Y. Zhang, S. Chen, J. Zhu and K. Liew, *Journal of Molecular Catalysis A: Chemical*, 2012, **363–364**, 335-342.
102. D. G. Castner, P. R. Watson and I. Y. Chan, *The Journal of Physical Chemistry*, 1990, **94**, 819-828.
103. Ø. Borg, M. Rønning, S. Storslter, W. van Beek and A. Holmen, in *Studies in Surface Science and Catalysis*, eds. B. H. Davis and M. L. Occelli, Elsevier, 2007, vol. Volume 163, pp. 255-272.
104. S. Lögdberg, J. Yang, M. Lualdi, J. C. Walmsley, S. Järås, M. Boutonnet, E. A. Blekkan, E. Rytter and A. Holmen, *Journal of Catalysis*, 2017, **352**, 515-531.
105. N.-Y. Topsøe and H. Topsøe, *Journal of Catalysis*, 1982, **75**, 354-374.
106. M. A. Simionato, Elisabete Moreira, *Materials Research*, 2003, **6**, 535-539.
107. J. van de Loosdrecht, M. van der Haar, A. M. van der Kraan, A. J. van Dillen and J. W. Geus, *Applied Catalysis A: General*, 1997, **150**, 365-376.
108. S. Schaefer, V. Fierro, A. Szczurek, M. T. Izquierdo and A. Celzard, *International Journal of Hydrogen Energy*, 2016, **41**, 17442-17452.
109. D. Nabaho, J. W. Niemantsverdriet, M. Claeys and E. v. Steen, *Catalysis Today*, 2016, **275**, 27-34.
110. R. J. Madon and E. Iglesia, *Journal of Catalysis*, 1994, **149**, 428-437.
111. J. P. den Breejen, P. B. Radstake, G. L. Bezemer, J. H. Bitter, V. Frøseth, A. Holmen and K. P. d. Jong, *Journal of the American Chemical Society*, 2009, **131**, 7197-7203.
112. N. Kumari, M. A. Haider, M. Agarwal, N. Sinha and S. Basu, *The Journal of Physical Chemistry C*, 2016, **120**, 16626-16635.
113. S. Cabrera, Haskouri, Jamal El Alamo, Jaime, A. AU - Beltrán, D. AU - Beltrán, , *Adv. Mater*, 1999, **11**, 379-381.
114. Y. Kondratenko, V. Fundamensky, I. Ignatyev, A. A. Zolotarev, T. Kochina and V. L. Ugolkov, *Polyhedron*.
115. J. El Haskouri, S. Cabrera, M. Caldés, J. Alamo, A. Beltrán-Porter, M. D. Marcos, P. Amorós and D. Beltrán-Porter, *International Journal of Inorganic Materials*, 2001, **3**, 1157-1163.
116. D. Ortiz de Zárate, L. Fernández, A. Beltrán, C. Guillem, J. Latorre, D. Beltrán and P. Amorós, *Solid State Sci*, 2008, **10**, 587-601.

117. A. Sayari, Y. Yang, M. Kruk and M. Jaroniec, *The Journal of Physical Chemistry B*, 1999, **103**, 3651-3658.
118. A. Sayari, D. Shee, N. Al-Yassir and Y. Yang, *Topics in Catalysis*, 2010, **53**, 154-167.
119. S. Ray, M. Brown, A. Bhaumik, A. Dutta and C. Mukhopadhyay, *Green Chemistry*, 2013, **15**, 1910-1924.
120. Wang Wendong, PhD thesis 2011.
121. M. Bartolini, J. Molina, J. Alvarez, M. Goldwasser, P. Pereira Almaso and M. J. P. Zurita, *Journal of Power Sources*, 2015, **285**, 1-11.
122. R. Sanz, G. Calleja, A. Arencibia and E. S. Sanz-Pérez, *Microporous and Mesoporous Materials*, 2015, **209**, 165-171.
123. R. Sanz, G. Calleja, A. Arencibia and E. S. Sanz-Pérez, *Energy & Fuels*, 2013, **27**, 7637-7644.
124. M. Thommes, K. Kaneko, A. V. Neimark, J. P. Olivier, F. Rodriguez-Reinoso, J. Rouquerol and K. S. W. Sing, *Pure and Applied Chemistry*, 2015, **87**, 1051-1069.
125. H. P. Lin, C. Y. Tang and C. Y. Lin, *Journal of the Chinese Chemical Society*, 2002, **49**, 981-988.
126. L. Qian, X. Lv, Y. Ren, H. Wang, G. Chen, Y. Wang and J. Shen, *Journal of Chromatography A*, 2013, **1322**, 81-89.
127. J. Hukkamäki, S. Suvanto, M. Suvanto and T. T. Pakkanen, *Langmuir*, 2004, **20**, 10288-10295.
128. M. Lualdi, S. Lögdberg, G. Di Carlo, S. Järås, M. Boutonnet, A. M. Venezia, E. A. Blekkan and A. Holmen, *Topics in Catalysis*, 2011, **54**, 1175.
129. S. Brunauer, L. S. Deming, W. E. Deming and E. Teller, *Journal of the American Chemical Society*, 1940, **62**, 1723-1732.